



HAL
open science

Characterization of neocortical networks from high-resolution EEG: application to disorders of consciousness

Jennifer Rizkallah

► **To cite this version:**

Jennifer Rizkallah. Characterization of neocortical networks from high-resolution EEG: application to disorders of consciousness. Signal and Image processing. Université de Rennes 1 [UR1], 2019. English. NNT: . tel-02372280

HAL Id: tel-02372280

<https://hal.science/tel-02372280v1>

Submitted on 20 Nov 2019

HAL is a multi-disciplinary open access archive for the deposit and dissemination of scientific research documents, whether they are published or not. The documents may come from teaching and research institutions in France or abroad, or from public or private research centers.

L'archive ouverte pluridisciplinaire **HAL**, est destinée au dépôt et à la diffusion de documents scientifiques de niveau recherche, publiés ou non, émanant des établissements d'enseignement et de recherche français ou étrangers, des laboratoires publics ou privés.

THESE DE DOCTORAT DE

L'UNIVERSITE DE RENNES 1
COMUE UNIVERSITE BRETAGNE LOIRE

ECOLE DOCTORALE N° 601
*Mathématiques et Sciences et Technologies
de l'Information et de la Communication*
Spécialité : *Signal, Image et Vision*

Par

Jennifer RIZKALLAH

Characterization of neocortical networks from high-resolution EEG: application to disorders of consciousness

Thèse présentée et soutenue à Rennes, le 08/11/2019

Unité de recherche : Laboratoire Traitement de Signal et de l'Image LTSI – INSERM UMR1099

Rapporteurs avant soutenance :

Silvia Casarotto Research Fellow at the Università degli Studi di Milano
Fadi Karamah Associate Professor at the American university of Beirut

Composition du Jury :

Examineurs :	Catherine Marque Mohamad Khalil Nicolas Farrugia	Professeure à l'Université de Technologie de Compiègne Professeur à l'Université Libanaise Maitre de conférences à IMT Atlantique
Dir. de thèse :	Fabrice Wendling Hassan Amoud	Directeur de recherche INSERM Professeur à l'Université Libanaise
Co-dir. de thèse :	Mahmoud Hassan	Postdoctorant au LTSI, Université de Rennes 1

Invité(s)

Naji Riachi Associate Professor at the Lebanese American University

ACKNOWLEDGMENTS

This work was carried out in the context of the European project LUMINOUS at Laboratoire Traitement du Signal et de l'image (LTSI), Rennes- France and at AZM center for research in biotechnology, Tripoli-Lebanon and was financed by the Institut national de la santé et de la recherche médicale (INSERM, France) and the AZM and SAADE Association (Tripoli, Lebanon).

I owe my deepest gratitude to my advisors: prof. Fabrice Wendling, prof. Hassan Amoud and Dr. Mahmoud Hassan. Without their invaluable advices, continuous support and encouragements this work would never been completed.

Besides my advisors, I would like to thank the rest of my thesis committee: prof. Silvia Casarotto, prof. Fadi Karamah, prof. Catherine Marque, prof. Mohamad Khalil, Dr. Nicolas Farrugia and prof. Naji Riachi for being a part of my thesis defense jury.

I would like to thank prof. Lotfi Senhadji for welcoming me in LTSI and the secretaries: Soizic, Patricia and Muriel for their logistical support and sympathy.

I want to thank prof. Christian Benar and prof. Jean-Louis Dillenseger for accepting to be part of my Individual Monitoring Committee (comité de suivi de thèse).

I would like to express my special thanks to Prof. Julien Modolo and Dr. Pascal Benquet for their contribution in enriching this thesis with their experiences and suggestions.

I would like to thank all the LUMINOUS project partners with whom I had the pleasure to share memorable moments and scientific collaborations during all our meetings.

Many thanks go to all the colleagues I had the opportunity to meet during these years of thesis whether in France or in Lebanon.

Finally, it is a privilege to express my sincere appreciation to all my parents, sisters and my husband for their continuous support, sacrifices and unconditional love.

TABLE OF CONTENTS

Acknowledgments	3
Table of contents	5
List of figures	9
List of tables	11
List of abbreviations	13
Résumé en français.....	15
Summary in english.....	21
Chapter 1: General introduction.....	27
Chapter 2. Background and problem statement	31
2.1. Brain connectivity and graphs	31
2.2. Graph measures.....	33
2.2.1. Segregation (local)	33
2.2.2. Integration (global).....	34
2.2.3. Hubness	34
2.3. Neuroimaging techniques	37
2.3.1. Functional magnetic resonance imaging (fMRI)	37
2.3.2. Magneto-encephalography (MEG)	37
2.3.3. Electroencephalography (EEG).....	37
2.4. EEG source connectivity	38

2.5. Thesis objectives.....	39
2.5.1. Methodological development.....	39
2.5.2. Clinical application	41
chapter 3. Materials and methods.....	45
3.1. Database.....	45
3.1.1. Study 1: BrainGraph database (picture naming).....	45
3.1.2. Study 2: BrainGraph database (resting state).....	47
3.1.3. Study 3 and 4: DoC database	48
3.2. EEG source connectivity	51
3.2.1. Inverse problem.....	52
3.2.2. Functional connectivity (FC)	55
3.3. Orthogonalisation approach.....	57
3.4. Modularity	58
3.5. Modular states algorithm	60
Chapter 4. Results	63
Study 1: Dynamic reshaping of functional brain networks during visual object recognition	63
Study 2: The effect of removing zero-lag functional connections on EEG-source space networks at rest.....	83
Study 3: Decreased integration of EEG source-space networks in disorders of consciousness	117
Chapter 5. Discussion and future work	137

5.1. Dynamic functional networks at rest and task.....	138
5.2. EEG source connectivity	139
5.3. Methodological considerations	140
5.3.1. Ill-posed inverse problem solution.....	140
5.3.2. Template brain.....	141
5.3.3. Number of Regions of interests.....	141
5.3.4. Sliding window length	141
5.3.5. Connectivity matrix threshold.....	142
5.4. Future directions	142
List of publications.....	145
References	147

LIST OF FIGURES

Figure 1: Brain connectivity. A) Structural connectivity refers to anatomical connections between neural elements such as fiber tracts connecting brain regions. B) Functional connectivity presents statistical dependencies between brain regions. C) Effective connectivity consists of directed causal influences one brain region produces in another.	32
Figure 2: Graphs and adjacency matrices. A) Binary directed network. B) Weighted directed network. C) Binary undirected network. D) Weighted undirected network.	33
Figure 3: Illustration of some graph measures: degree, clustering coefficient, path length, modularity, participation coefficient and hubs (provincial and connector).	36
Figure 4: Neuroimaging techniques. A) Functional magnetic resonance imaging (fMRI). B) Magneto-encephalography (MEG). C) Electro-encephalography (EEG).	38
Figure 5: Volume conduction problem. A) Ideally, each electrode measures brain activity from the source below it. (b) In reality, signals recorded at each electrode are generated from several sources.	38
Figure 6: States of consciousness according to the level of awareness and arousal.	42
Figure 7: The meaningful (left) and meaningless (right) images used in the study.	46
Figure 8: Picture naming experimental setup. The cognitive task consisted in naming visual stimuli of two categories: meaningful and meaningless pictures.	47
Figure 9: CRS-R response profile (Giacino et al., 2004).	49
Figure 10: EEG source connectivity pipeline. EEG recorded at the scalp level are preprocessed before solving the inverse problem to obtain the regional time series. Finally, functional connectivity matrices are computed.	52
Figure 11: Symmetric orthogonalisation approach. The correlations between ROIs introduced during source reconstruction can be removed by mutually orthogonalising the ROI time-series, illustrated here for two vectors in two dimensions. An optimal set of corrected time-series is	

reconstructed by iterating towards the closest set of orthogonal vectors to the starting time-series. The process is initialized with the closest orthonormal matrix to the uncorrected vectors, then adjusts in turn the vector magnitudes and orientations to minimize the Euclidean distance between the corrected and uncorrected time-series, adapted from (Colclough et al., 2015). .. 58

Figure 12: Multislice modularity approach. A coupling parameter that links nodes across time windows is introduced before performing the modularity maximization procedure to dynamically track modules changes during time. 59

Figure 13: Modular states algorithm pipeline. (A) Computing the modules for the dynamic networks using multislice modularity method then (B) computing the similarity between the dynamic modular structures and clustering the similarity matrix into “categorical modules (adapted from by (Kabbara et al., 2019)). 61

LIST OF TABLES

Table 1: Patients demographic information: age, gender, days since injury, traumatic (T) or non-traumatic (NT) etiology and clinical best diagnosis.	50
Table 2 : Summary of the 68 ROIs derived from the Desikan-Killiany atlas.....	54

LIST OF ABBREVIATIONS

AEC: Amplitude Envelope Correlation

AEC_{Col}: Colclough orthogonalisation approach combined with AEC

AEC_{Pas}: Pascual-Marqui orthogonalisation approach combined with AEC

BEM: Boundary Element Model

BOLD: Blood Oxygen Level Dependent

Coh: Coherence

CRS: Coma Recovery Scale

CRS-R: Coma Recovery Scale Revised

DMN: Default Mode Network

DoC: Disorders of Consciousness

DSN: Dorsal Somatomotor Network

EEG: Electro-Encephalography

EMCS: Emergence from Minimally Conscious State

FC: Functional Connectivity

FDR: False Discovery Rate

FEM: Finite Element Model

fMRI: functional Magnetic Resonance Imaging

GSP: Graph Signal Processing

ICA: Independent Component Analysis

ImCoh: Imaginary Coherence

LORETA: Low resolution brain electromagnetic tomography

MCS: Minimally Conscious State

MCS+: Minimally Conscious State Plus

MCS-: Minimally Conscious State Minus

MEG: Magneto-Encephalography

MI: Mutual Information

MNE: Minimum Norm Estimate

PC: Partial Coherence

PLI: Phase Lag Index

PLV: Phase Locking Value

PLV_{Col}: Colclough orthogonalisation approach combined with PLV

PLV_{Pas}: Pascual-Marqui orthogonalisation approach combined with PLV

ROIs: Regions Of Interests

RSNs: Resting States Networks

sLORETA: Standardized low resolution brain electromagnetic tomography

TMS: Transcranial Magnetic Stimulation

UWS: Unresponsive Wakefulness Syndrome

wMNE: weighted Minimum Norm Estimate

wPLI: weighted Phase Lag

RESUME EN FRANÇAIS

Le cerveau humain est un réseau complexe et les connexions entre les régions cérébrales sont cruciales pour le traitement de l'information. Une fonction cognitive efficace est garantie lorsque le cerveau reconfigure d'une manière dynamique l'organisation de son réseau durant le temps (Bola and Sabel, 2015). Il n'est donc pas surprenant que la science des réseaux ait contribué aux domaines des neurosciences et de la neurologie au cours de la dernière décennie (Bassett and Sporns, 2017).

La neuroscience des réseaux ('Network Neuroscience') a été développée récemment pour mieux comprendre les systèmes neuronaux en adoptant des outils de la théorie des graphes. Ce domaine de recherche a fourni aux chercheurs une nouvelle opportunité d'évaluer, de quantifier et de caractériser les réseaux cérébraux complexes. Les études ont montré aussi que la plupart des troubles cérébraux, y compris les maladies neuro-dégénératives et mentales, sont également considérés comme des « maladies de réseau », c'est-à-dire qu'elles se caractérisent par des altérations du réseau cérébral structurel et/ou fonctionnel (Fornito et al., 2015; Stam, 2014). Du point de vue clinique, il existe donc une forte demande pour des nouvelles méthodes non invasives, basées sur les réseaux et faciles à utiliser, permettant d'identifier ces réseaux pathologiques dans la perspective de proposer de nouveaux outils de diagnostic et suivi thérapeutique.

Les techniques de neuro-imagerie peuvent être utilisées pour identifier les réseaux cérébraux impliqués dans les fonctions cérébrales normales ainsi que dans les troubles neurologiques. Dans ce contexte, l'imagerie par résonance magnétique fonctionnelle (IRMf) s'est considérablement développée au cours des trois dernières décennies et est maintenant couramment utilisée pour caractériser la connectivité cérébrale fonctionnelle (Rogers et al., 2007). Cependant, plusieurs fonctions cérébrales (normales ou pathologiques) sont très rapides et se produisent sur des périodes de temps très courtes (<1 seconde). De tels changements ne peuvent pas être suivis avec l'IRMf en raison de sa résolution temporelle intrinsèque faible (de l'ordre de 1 seconde).

L'électroencéphalographie (EEG) est une technique non invasive unique (en plus de la magnétoencéphalographie MEG), qui permet de suivre la dynamique de l'activité cérébrale à

la milliseconde. Des études antérieures sur les analyses de la connectivité fonctionnelle à partir de l'EEG ont été principalement réalisées au niveau des électrodes, c'est-à-dire calculer le couplage statistique entre les signaux enregistrés par les capteurs au niveau du scalp. Cependant, l'interprétation des réseaux EEG obtenus au niveau scalp (au niveau des électrodes) n'est pas simple, car les signaux sont altérés par le « volume de conduction » (Brunner et al., 2016; Van de Steen et al., 2016). La méthode appelée « connectivité de sources en EEG » est une des solutions potentielles qui réduit l'effet de ce problème et permet de suivre la dynamique des réseaux cérébraux large échelle tout en conservant l'excellente résolution temporelle de l'EEG (Hassan and Wendling, 2018; O'Neill et al., 2018).

C'est dans ce contexte que s'inscrivent mes travaux de thèse qui prolongent les développements méthodologiques et cliniques de notre équipe de recherche sur la connectivité fonctionnelle au niveau des sources cérébrales. L'objectif de mes travaux de thèse est double : i) progresser sur les aspects méthodologiques de la méthode connectivité de sources en EEG et ii) utiliser cette méthode dans une application clinique en lien avec les troubles de la conscience. Ma thèse se divise donc en deux grandes parties, avec deux études réalisées dans chaque partie. Dans la première partie (aspects méthodologiques), j'ai abordé, dans une première étude, la capacité de la méthode connectivité de sources en EEG à suivre les altérations dynamiques des réseaux cérébraux durant une tâche cognitive rapide. Puis dans une seconde étude, j'ai testé l'effet du problème de l'étalement spatial des sources sur la reconstruction des réseaux fonctionnels. Dans la deuxième partie (applications cliniques), j'ai analysé les altérations dans les réseaux cérébraux chez les patients souffrant d'un désordre de la conscience.

Aspects méthodologiques

Dans la première étude de la partie méthodologique, j'ai testé la capacité de la méthode connectivité de sources en EEG à suivre les modifications de la dynamique cérébrale durant une tâche cognitive. Nous avons choisi la tâche bien définie de dénomination d'objets visuels (DiCarlo et al., 2012), qui implique des processus cognitifs rapides (quelques centaines de ms, du début du stimulus à l'articulation) et j'ai déterminé la différence dans les réseaux fonctionnels dynamiques lors de la reconnaissance d'images significatives ('meaningful') et non significatives ('meaningless'). De plus, j'ai proposé une nouvelle mesure appelée « occurrence » qui présente la probabilité que deux régions cérébrales quelconques tombent dans le même module (où les régions fortement interconnectés mais mal connectés à d'autres régions

sont groupées ensemble) au fil du temps, afin de suivre les changements modulaires des régions cérébrales.

Dans ce but, des données EEG haute résolution (256 électrodes) ont été collectées de 20 sujets sains. J'ai estimé les réseaux cérébraux fonctionnels en utilisant la méthode connectivité de sources en EEG. Ensuite, en utilisant des algorithmes de modularité, j'ai suivi la reconfiguration de réseaux fonctionnels lors de la reconnaissance d'images significatives ('meaningful') et non significatives ('meaningless'). Les résultats ont montré une différence dans les caractéristiques des modules concernant les deux conditions en termes d'intégration (interactions entre modules) et d'occurrence (la probabilité que deux régions du cerveau soient dans le même module durant une tâche). L'intégration et l'occurrence étaient plus importantes pour les images non significatives que pour les images significatives. Ces résultats, rapportés dans un article publié dans le « Journal of neural engineering » (Rizkallah et al., 2018), ont également révélé que l'occurrence dans les régions frontales droites et occipito-temporelle gauche peuvent prédire la capacité du cerveau à reconnaître et à nommer rapidement les stimuli visuels.

Bien que la méthode connectivité de sources en EEG soit une technique prometteuse, elle reste perfectible et plusieurs problèmes méthodologiques restent ouverts (Palva and Palva, 2012; Schoffelen and Gross, 2009; Van Diessen et al., 2015) dont l'« étalement spatial des sources » ('spatial leakage') qui induit des connexions parasites entre sources proches correspondant à des régions adjacentes. Pour traiter ce problème, la plupart des approches existantes reposent sur l'hypothèse que l'« étalement spatial des sources » génère une connectivité exagérée ce qui se traduit par des corrélations à décalage de phase nul. Ainsi, ces méthodes ont résolu ce problème en supprimant les connexions à décalage nul (Nolte et al., 2004; Stam et al., 2007) ou en adoptant une approche fondée sur l'orthogonalisation (Brookes et al., 2012; Hipp et al., 2012; Pascual-Marqui et al., 2017). D'où le deuxième but de cette partie méthodologique, comparer plusieurs méthodes permettant de corriger le problème de l'étalement spatial des sources et d'autres qui ne le corrigent pas afin de déterminer l'effet de la correction de fuite sur les réseaux reconstruits.

Dans cette deuxième étude méthodologique, des signaux EEG à haute résolution (256 électrodes) ont été collectés de 30 sujets sains à l'état de repos. J'ai estimé les réseaux cérébraux en utilisant la méthode connectivité de sources en EEG en adoptant plusieurs techniques (divisées en 2 familles) pour le calcul de la connectivité. La première famille, qui ne corrige

pas le problème de l'étalement spatial, comprend les méthodes appelées « indice de verrouillage de phase » ('Phase Locking Value' PLV) et « corrélation de l'amplitude de l'enveloppe » ('Amplitude Envelope Correlation' AEC). La deuxième famille qui le corrige en supprimant les connexions à décalage nul compris l' « indice de décalage de phase » ('Phase Lag Index' PLI) et deux méthodes d'orthogonalisation combinées avec les méthodes PLV et AEC. J'ai comparé les réseaux obtenus par chaque méthode de connectivité fonctionnelle avec le réseau IRMf obtenu au repos (du Human Connectome Project -HCP-, N = 487). Les résultats montrent de faibles corrélations pour tous les réseaux EEG obtenus, cependant les réseaux PLV et AEC sont significativement corrélés avec le réseau IRMf ($\rho = 0.11$, $p = 1.93 \times 10^{-8}$ et $\rho = 0.06$, $p = 0.007$, respectivement), alors que les autres méthodes ne le sont pas. Ces résultats, rapportés dans un article (en révision) dans « Brain Topography » (Rizkallah et al., 2019a), suggèrent que les méthodes qui corrigent le problème d'étalement spatial des sources (en supprimant les connexions à décalage nul) estiment des réseaux plus loin de ceux estimés à partir de l'IRMf.

Aspects cliniques

La deuxième partie de ma thèse s'inscrit dans le contexte du projet européen LUMINOUS (H2020 FET-Open) dont l'objectif général est d'étudier, de modéliser et de quantifier la conscience. Plusieurs études ont associé les désordres de conscience à des altérations des réseaux cérébraux fonctionnels et/ou structurels (Amico et al., 2017; Annen et al., 2018). Les désordres de conscience englobent une variété d'états de conscience, tels que l'état d'éveil sans réponse ou l'état végétatif (EV, le patient est éveillé avec seulement des mouvements réflexes (Laureys et al., 2010)), l'état de conscience minimale (ECM, le patient fait des comportements reproductibles et intentionnels (Giacino et al., 2002)) et l'émergence de l'état de conscience minimale (EECM, caractérisé par une récupération de la communication fonctionnelle et / ou de l'utilisation d'objets (Giacino et al., 2002)). Nous manquons à ce jour des méthodes fiables pour évaluer objectivement le niveau de conscience chez les patients présentant des troubles de la conscience (Laureys et al., 2004). Plusieurs techniques de neuro-imagerie ont récemment révélé des résultats importants concernant les perturbations dans les réseaux cérébraux correspondant à ces états de perte de conscience, notamment l'IRMf (Demertzi et al., 2015; Di Perri et al., 2014; Di Perri et al., 2017), la tomographie par émission de positrons (Stender et al., 2014; Thibaut et al., 2012) et EEG obtenus au niveau du scalp (Chennu et al., 2017; Sitt et al., 2014). Plusieurs patients considérés comme inconscients ont présenté des signes de suivi

des commandes avec des études basées sur l'IRMf (Bardin et al., 2012; Monti et al., 2010b; Owen et al., 2006) et des paradigmes actifs (Cruse et al., 2012; Goldfine et al., 2011).

Dans ce contexte, j'ai étudié l'apport de la connectivité fonctionnelle estimée à partir de l'EEG. J'ai analysé les altérations dans les réseaux cérébraux dans les désordres de conscience en utilisant la méthode connectivité de sources en EEG. Dans cette partie clinique, je me suis concentrées sur deux caractéristiques principales de réseau : l'intégration (traitement global de l'information) et la ségrégation (traitement local de l'information). Deux études ont été réalisées dans ce contexte: i) une analyse statique, dont l'objectif était de voir s'il existait un (des)équilibre entre l'intégration et la ségrégation du réseau chez les patients atteints de désordres de conscience et ii) une étude dynamique permettant de suivre les altérations dynamiques dans les réseaux cérébraux corticaux en fonction des états de conscience.

Les données EEG haute résolution ont été collectées à Liège par le « coma science group » de 82 participants à l'état de repos: 61 patients (EECM (n = 6), ECM (n = 46), et EV (n = 9)) et 21 sujets sains. J'ai estimé les réseaux cérébraux fonctionnels dans cinq bandes de fréquence différentes (delta, thêta, alpha, bêta et gamma) à l'aide de la méthode connectivité de sources en EEG. J'ai utilisé des analyses basées sur la théorie des graphes pour évaluer leur relation avec les niveaux de conscience ainsi que les différences entre les groupes de volontaires sains et les groupes de patients. Les résultats sont rapportés dans un article publié dans « Neuroimage Clinical » (Rizkallah et al., 2019b). Ils ont montré que les réseaux de patients souffrant des désordres de conscience sont caractérisés par un traitement global de l'information altéré (l'intégration des réseaux cérébraux fonctionnels diminuait avec un niveau de conscience inférieur). En outre, j'ai pu identifier deux régions cérébrales à intégration réduite impliquées entre les groupes: le précuneus gauche (impliqué dans le traitement de soi, la prise de conscience et le traitement de l'information consciente) et le cortex orbitofrontal gauche (impliqué dans la sélection d'action en fonction de contextes sensoriels et dans la perception de la douleur).

Finalement, j'ai exploré les changements dynamiques des structures modulaires du cerveau chez les patients qui ont des désordres de conscience en appliquant une nouvelle méthode développée dans l'équipe (Kabbara et al., 2019). Cette méthode consiste à évaluer la similitude entre les structures modulaires durant le temps et extraire les structures les plus représentatives de chaque group étudié. Les résultats ont montré que dans la bande gamma, les réseaux qui sont

les plus présents chez les sujets sains et ECM sont les réseaux cognitifs et moteurs (régions cingulate, préfrontales et centrales). Tandis que chez les sujets à l'état végétatif, j'ai trouvé le réseau visuel sensoriel. De même dans la bande beta, j'ai trouvé non seulement les réseaux cognitifs et moteurs, mais aussi le réseau responsable du langage (les régions supramarginales associées avec les régions supérieures temporelles et précentrales à gauche) chez les sujets sains et ECM et qui disparaissent pour les sujets EV. Enfin, dans la bande alpha, les résultats montrent que les connexions fronto-pariétales (réseau attentionnel) présentes chez les sujets sains et ECM disparaissent chez les patients EV.

SUMMARY IN ENGLISH

The human brain is a complex network and the connections between the brain regions are crucial for information processing. Cognitive function is guaranteed when the brain dynamically reconfigures its network organization over time (Bola and Sabel, 2015). It is then unsurprising that, in the last decade, network science has contributed to neuroscience and neurology (Bassett and Sporns, 2017).

Network Neuroscience has recently been developed to better understand neural systems by adopting graph theory tools. This area of research has provided researchers with a new opportunity to evaluate, quantify and characterize complex brain networks. Studies have also showed that most brain disorders, including neurodegenerative and mental diseases, are considered as network diseases. They are characterized by changes in the structural and/or functional brain networks (Fornito et al., 2015; Stam, 2014). Thus, from a clinical point of view, there is a strong demand for new, non-invasive, network-based and easy-to-use methods to identify these pathological networks, in order to propose new diagnostic and therapeutic monitoring tools.

Neuroimaging techniques can be used to identify brain networks involved in normal brain functions as well as in neurological disorders. In this context, functional magnetic resonance imaging (fMRI) has considerably developed during the last three decades and is now commonly used to characterize functional brain connectivity (Rogers et al., 2007). However, several brain functions (normal or pathological) are very fast and occur over very short time periods (<1 second). Such changes cannot be tracked with fMRI due to its intrinsic low temporal resolution (on the order of 1 second).

Electroencephalography (EEG) is a unique noninvasive technique (in addition to magnetoencephalography MEG), which tracks the dynamics of brain activity at millisecond time-scale. Previous studies on EEG functional connectivity have mainly been performed at the scalp level by computing the statistical coupling between the signals recorded by the sensors. However, the interpretation of the EEG networks obtained at the scalp (sensors) level is not simple, since the signals are altered by the volume conduction problem (Brunner et al., 2016; Van de Steen et al., 2016). EEG source connectivity is a potential solution which reduces the

effect of this problem and enables the tracking of large scale brain networks dynamics while maintaining the EEG excellent temporal resolution (Hassan and Wendling, 2018; O'Neill et al., 2018).

It is in this context that my thesis was carried out. My work here extends the methodological and clinical developments of our research team on functional connectivity at cortical level. The aim of my thesis work is twofold: i) to progress on the methodological aspects of the EEG source connectivity method and ii) to use this method in a clinical application related to the disorders of consciousness. My thesis is divided into two main parts, with two studies realized in each part. In the first part (methodological aspects), I approached, in a first study, the capacity of the EEG source connectivity method to track the brain network dynamic alterations during a fast cognitive task. Then in a second study, I tested the effect of the spatial leakage problem on the reconstructed functional brain networks. In the second part (clinical applications), I analyzed brain networks alterations in patients with disorders of consciousness, using static analysis in the first study and dynamic analysis in the second one.

Methodological aspects

In the first study of the methodological part, I tested the ability of the EEG source connectivity method to track brain dynamic changes during a cognitive task. We chose the well-defined visual object recognition and naming task (DiCarlo et al., 2012) which involves fast cognitive processes (a few hundred of ms, from stimulus onset to reaction) and I determined the differences in dynamic functional networks when recognizing meaningful and meaningless images. In addition, I proposed a new measure called "occurrence" which presents the probability of any two brain regions to fall into the same module (where highly interconnected regions and poorly connected to other regions are grouped together) over time, in order to track the brain regions' modular changes.

For this purpose, high resolution EEG data (256 electrodes) were collected from 20 healthy subjects. I estimated the functional brain networks using the EEG source connectivity method. Then, using modularity algorithms, I followed the reconfiguration of functional brain networks during the recognition of meaningful and meaningless images. The results showed a difference in the characteristics of the modules concerning the two conditions in terms of integration (interactions between modules) and occurrence (the probability of two brain regions to be in

the same module during a task). Integration and occurrence values were higher for non-significant images than for meaningful images. These findings, reported in an article published in the “Journal of Neural Engineering” (Rizkallah et al., 2018), have also revealed that right frontal and left occipito-temporal regions occurrence can predict the brain's ability to recognize and to quickly name visual stimuli.

Although EEG source connectivity method is a promising technique, it remains immature and several methodological questions remain open (Palva and Palva, 2012; Schoffelen and Gross, 2009; Van Diessen et al., 2015). One of these methodological issues is the spatial leakage which induces spurious connections between adjacent brain regions. Most of the existing approaches to deal with this problem are based on the hypothesis that source leakage generates inflated connectivity manifesting as zero-phase-lag correlations. Thus, these methods solved this problem by removing zero-lag connections (Nolte et al., 2004; Stam et al., 2007) or by adopting an orthogonalisation-based approach (Brookes et al., 2012; Hipp et al., 2012; Pascual-Marqui et al., 2017). Hence, the second purpose of this methodological part is to compare several methods that correct the spatial leakage problem and others that don't in order to test the effect of leakage correction on the reconstructed networks.

In this second methodological study, resting state high-resolution EEG signals (256 electrodes) were collected from 30 healthy subjects then I estimated brain networks using EEG source connectivity by adopting several functional connectivity techniques (divided into 2 families). The first family that does not correct the leakage problem includes the Phase Locking Value (PLV) and the Amplitude Envelope Correlation (AEC). The second family that corrects this problem by removing zero-lag correlations includes the Phase Lag Index (PLI) and two orthogonalisation methods combined with PLV and AEC techniques. I compared the networks obtained by each functional connectivity method with resting fMRI network (collected from Human Connectome Project -HCP-, $N = 487$). Results showed weak correlations for all the EEG networks obtained. However the PLV and AEC networks were significantly correlated with the fMRI network ($\rho = 0.11$, $p = 1.93 \times 10^{-8}$ and $\rho = 0.06$, $p = 0.007$, respectively), while all other methods were not. These results, reported in an article (in revision) in "Brain Topography" (Rizkallah et al., 2019a), suggest that methods that correct the spatial leakage problem (by removing zero-lag correlations) estimate networks very differently from those estimated from fMRI. These results were also validated on MEG data collected in the context of the HCP.

Clinical aspects

The second part of my thesis is in the context of the European project LUMINOUS (H2020 FET-Open) whose general objective is to study, model and quantify consciousness. Several studies have associated disorders of consciousness with functional and/or structural brain networks alterations (Amico et al., 2017; Annen et al., 2018). Disorders of consciousness encompass a variety of consciousness states, such as the unresponsive wakefulness syndrome (UWS, the patient is awake with only reflex movements (Laureys et al., 2010)), the minimally conscious state (MCS, the patient does reproducible and purposeful behaviors (Giacino et al., 2002)) and the emergence from the minimally conscious state (EMCS, characterized by a recovered functional communication and/or object use (Giacino et al., 2002)). We lack to date reliable methods to objectively assess the level of consciousness in patients with disorders of consciousness (Laureys et al., 2004). Several neuroimaging techniques have recently revealed important results regarding brain network perturbations underlying these states of unconsciousness, notably fMRI (Demertzi et al., 2015; Di Perri et al., 2014; Di Perri et al., 2017), positron emission tomography (Stender et al., 2014; Thibaut et al., 2012) and scalp EEG (Chennu et al., 2017; Sitt et al., 2014). Several patients considered unconscious showed signs of command-following with fMRI (Bardin et al., 2012; Monti et al., 2010b; Owen et al., 2006) and EEG active paradigms (Cruse et al., 2012; Goldfine et al., 2011).

In this context, I studied the contribution of functional connectivity estimated from EEG signals. I analyzed the brain network alterations in patients with disorders of consciousness using the EEG source connectivity method. In this clinical part, I focused on two main network features: integration (global information processing) and segregation (local information processing). Two studies were performed: i) a static analysis, where the objective was to investigate if there is a balance between network integration and segregation in patients with disorders of consciousness and ii) a dynamic study to track the dynamic alterations in cortical brain networks according to states of consciousness.

The high-resolution EEG data were collected in Liège by the “coma science group” from 82 participants at rest: 61 patients (EMCS (n = 6), MCS (n = 46), and UWS (n = 9)) and 21 healthy subjects. I estimated functional brain networks in five different frequency bands (delta, theta, alpha, beta, and gamma) using the EEG source connectivity method. I used graph theory-based analyzes to assess their relationship to the level of consciousness as well as the differences

between groups of healthy volunteers and patients. These results are reported in an article published in "Neuroimage Clinical" (Rizkallah et al., 2019b). They showed that networks of patients with disorders of consciousness were characterized by impaired global information processing (the functional brain networks integration decreased with lower level of consciousness). Moreover, I was able to identify two common anatomical brain regions with decreased integration that were involved between groups: the left precuneus (engaged in self-related processing, awareness and conscious information processing) and the left orbitofrontal cortex (engaged in action selection depending on emotional and sensory contexts and in pain perception).

Finally, I applied a new method developed very recently by our team (Kabbara et al., 2019) to explore the brain modular states dynamic changes in healthy subjects and patients with disorders of consciousness. This method consists of assessing the similarity between the modular states over time and extracting the most representative states for each group. Results in the gamma band were mostly seen in the cognitive and motor networks (cingulate, prefrontal and central regions) in healthy subjects and MCS patients, whereas in UWS patients, they were found mostly in the sensory visual network. As for the beta band, they were not only located in the cognitive and motor networks, but also in the language network (the supramarginal regions associated with the super-temporal and pre-central regions on the left) in healthy subjects and MCS, but not in the UWS patients. Finally, in the alpha band, states were found in the fronto-parietal regions (attentional network) in healthy subjects and MCS patients but not in UWS patients.

CHAPTER 1: GENERAL INTRODUCTION

The human brain is a network by nature: connections between neurons are crucial for information processing. An efficient cognitive function is guaranteed when the brain dynamically reconfigures its network organization at multiple time scales (Bola and Sabel, 2015; Braun et al., 2015). It is therefore unsurprising that network science has contributed to the fields of neuroscience and neurology in the last decade (Bassett and Sporns, 2017). A relatively new research field, referred to as **network neuroscience has provided researchers with an extraordinary opportunity to assess, quantify and understand the multifaceted features of complex brain networks, using graph theoretical analysis**. On the other hand, emergent evidence shows that most brain disorders, including neurodegenerative diseases and mental illnesses, are also currently considered as network diseases, i.e. they are characterized by alterations in the structural/functional brain network (Fornito et al., 2015; Stam, 2014). Thus, the demand is high for non-invasive, network-based and easy-to-use methods to identify these pathological networks in the perspective of proposing new diagnostic and therapeutic follow-up tools.

Neuroimaging techniques can be used to identify brain networks involved in normal brain functions (picture naming, learning, etc.) as well as in neurological disorders. In this context, functional Magnetic Resonance Imaging (fMRI) has considerably developed during the past three decades and is now commonly used to characterize brain connectivity (Rogers et al., 2007). However, several brain functions (normal or pathological) are very fast and occur over very short time periods (< 1 second). Such changes cannot be tracked with fMRI due to intrinsic low time resolution (in the order of 1 s).

Magneto/ Electro-encephalography (M/EEG) are unique non-invasive techniques which enable the tracking of brain dynamics on a millisecond time-scale. Most previous studies on M/EEG functional connectivity analyses were mainly performed at the sensor level, i.e. computing correlation between recorded signals from the sensors.

However, the interpretation of M/EEG networks obtained at the scalp level is not straightforward, since scalp/sensor M/EEG signals are corrupted by the volume conduction due to the head electrical conduction properties (Brunner et al., 2016; Van de Steen et al., 2016). EEG source-space connectivity is a potential solution which reduces the aforementioned volume conduction and enables the tracking of large-scale brain network dynamics on a sub-second time-scale (Hassan and Wendling, 2018; O'Neill et al., 2018). In our first study, **we tested the ability of this method to track brain dynamic changes during a cognitive task. We chose the well-defined visual object recognition and naming task (DiCarlo et al., 2012) which involves fast cognitive processes (a few hundred ms from stimulus onset to reaction). Moreover, we proposed a new graph measure called ‘occurrence’ which consists of measuring the probability of any two nodes to fall in the same module over time, to track the brain regions’ modular changes during time.**

Although EEG source connectivity is a promising technique, it is still immature and methodological aspects should be carefully accounted for to avoid pitfalls (Palva and Palva, 2012; Schoffelen and Gross, 2009; Van Diessen et al., 2015). One of these methodological considerations is the spatial leakage problem (i.e. presence of spurious connections between adjacent regions). To deal with this problem, most existing approaches are based on the hypothesis that leakage generates inflated connectivity between estimated sources, which manifests as zero-phase-lag correlations. Thus, these methods dealt with the leakage problem by removing the zero lag connections (Nolte et al., 2004; Stam et al., 2007) or adopting orthogonalisation-based approach (Brookes et al., 2012; Hipp et al., 2012; Pascual-Marqui et al., 2017). **In our second analysis, we presented a comparative study to test the effect of leakage correction on the reconstructed networks by comparing methods that correct the source leakage problem and those that do not.**

On the other hand, emerging evidence associates disorders of consciousness (DoC) with alterations in functional and/or structural brain networks (Amico et al., 2017; Annen et al., 2018). DoC encompass a variety of consciousness states, such as the unresponsive wakefulness syndrome (UWS; wakefulness with only reflex movements) (Laureys et al., 2010; Monti et al., 2010a), the minimally conscious state (MCS; reproducible and purposeful behavior) (Giacino et al., 2002), and emergence from the minimally conscious state (EMCS; characterized by recovered functional communication and/or object use) (Giacino et al., 2002). To date, we lack

reliable methods to objectively assess consciousness level in patients with disorders of consciousness (Laureys et al., 2004).

Significant discoveries regarding the neural correlates underlying these states of unconsciousness have recently been made by several neuroimaging techniques including functional MRI (fMRI) (Demertzi et al., 2015; Di Perri et al., 2014; Di Perri et al., 2017), positron emission tomography (PET) (Stender et al., 2014; Thibaut et al., 2012) and scalp EEG (Chennu et al., 2014; Chennu et al., 2017; Sitt et al., 2014). Several patients considered unconscious showed signs of command-following with fMRI (Bardin et al., 2012; Monti et al., 2010b; Owen et al., 2006) and EEG active paradigms (Cruse et al., 2012; Goldfine et al., 2011). In our study, we tackled the brain alterations in DOC using EEG source connectivity and focused on two network characteristics: integration (global information processing) and segregation (local information processing). **Two studies were performed: i) A static analysis, where the objective was to investigate if a balance between network integration and segregation in DOC patients exists and to identify the involved brain regions that differentiate between different groups and ii) a dynamic study to track time-varying alterations in cortical brain networks as a function of clinical consciousness levels.**

This thesis was part of the Future Emerging Technologies (H2020-FETOPEN-2014-2015-RIA under agreement No. 686764, “LUMINOUS”) as part of the European Union’s Horizon 2020 research and training program 2014–2018 (<http://www.luminous-project.eu/>). The general objective of the LUMINOUS project is to study, model, quantify, and alter observable aspects of consciousness. The conceptual framework of the project rests on information theoretic developments that link consciousness to the amount of information that a physical system can represent and generate as an integrated whole, and from the related idea that consciousness can be quantified by metrics reflecting information processing and representation complexity. This thesis was also financed by the AZM and SAADE Association, Tripoli, Lebanon.

This manuscript is organized as follows: In chapter 2, we report the background of the brain networks and disorders of consciousness and we state the problems we aim to tackle. In chapter 3, we describe all the materials and methods. Results are presented in chapter 4, under the form of published or under revision articles. For each article, a synthesis presenting the objectives, methods and results are provided. Finally, conclusions and perspectives are given in chapter 5.

CHAPTER 2.

BACKGROUND AND PROBLEM STATEMENT

In this chapter, we describe the basic notions of the methods and approaches used during the thesis such as brain connectivity, graph theoretical approaches and network measures, in addition to some neuroimaging techniques and the EEG source connectivity method. From the application viewpoint, we introduce the basic notions and the clinical need of the brain disorders of consciousness. Finally, the general and specific objectives of this thesis will be described.

2.1. Brain connectivity and graphs

At the macroscopic scale, emerging evidence shows that brain functions arise from continuous communications between spatially distant brain regions, called brain connectivity (Bullmore and Sporns, 2009). Three main types of brain connectivity can be distinguished: structural, functional and effective connectivity (Bullmore and Sporns, 2009; Rubinov and Sporns, 2010).

The structural connectivity (Fig1.A), also known as anatomical connectivity, refers to a pattern of anatomical connections summarizing synaptic links between neurons at the micro scale or projections between brain regions (measured using diffusion imaging) at the macro scale. This physical organized connection pattern is symmetric and stable at short time range (seconds to minutes) and is subjected to significant morphological change at longer time scales (hours and days) (Dennis et al., 2013). A number of studies examined the structural brain networks at rest (Hagmann et al., 2008; Li et al., 2013; Van Den Heuvel and Sporns, 2011). Moreover, it has been shown that structural connectivity analysis is sensitive and detects alterations of brain networks in neurological diseases (Fornito et al., 2015; Liu et al., 2014; Mallio et al., 2015) and during development or learning (Hagmann et al., 2010; Scholz et al., 2009).

Functional connectivity (FC) (Fig1.B) describes patterns of dynamic interactions, usually computed from time series data (recorded from functional neuroimaging techniques such as electro-encephalography (EEG), magneto-encephalography (MEG) or functional magnetic

resonance imaging (fMRI)) and estimates their statistical couplings. Unlike structural connectivity, FC may change over the sub-second scale. It can be estimated by calculating, for instance, the correlation, spectral coherence, phase-locking value or amplitude envelope correlation of all elements of the brain, regardless if they are directly connected or not (Goñi et al., 2014). In this thesis, we are interested in this type of brain connectivity (several FC methods will be fully described in section 3.2.2). The FC was widely used to study brain information processing at rest (Allen et al., 2014; Baker et al., 2014; Brookes et al., 2014; Kabbara et al., 2017; Yuan et al., 2012), during task (Bassett et al., 2011; Hassan et al., 2015; O’neill et al., 2017) and to detect network disruptions in brain disorders (Chennu et al., 2017; Engels et al., 2017; Hassan et al., 2016; Hassan et al., 2017; Kabbara et al., 2018).

Effective connectivity consists of directed causal influences one brain region produces in another. It can be measured using methods such as Granger causality (Granger, 1969), transfer entropy or methods based on autoregressive models (Friston et al., 2003). Then, it is, like functional connectivity, time varying and can change rapidly (sub-second time scale).

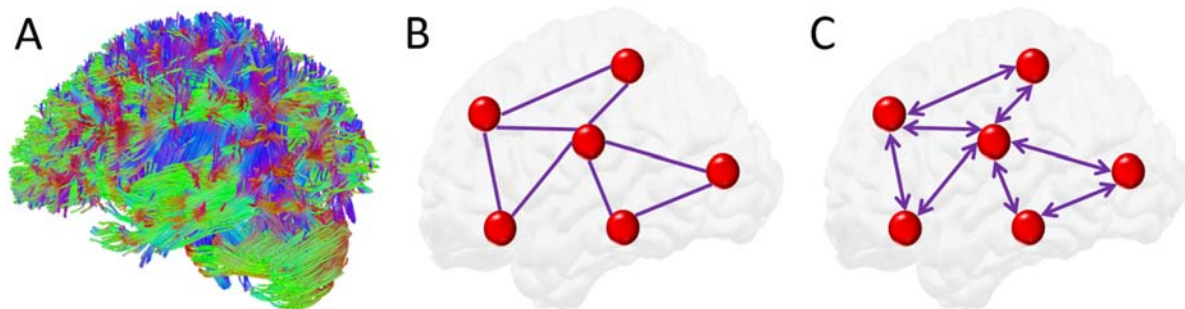


Figure 1: Brain connectivity. A) Structural connectivity refers to anatomical connections between neural elements such as fiber tracts connecting brain regions. B) Functional connectivity presents statistical dependencies between brain regions. C) Effective connectivity consists of directed causal influences one brain region produces in another.

Mapping of brain connectivity is rapidly increasing (Fornito et al., 2016). It consists of presenting the network as graph (Bullmore and Sporns, 2009). Such mapping typically starts by identifying a set of nodes (or vertices), and then attempts to estimate the set of edges (or links) between these nodes. Depending on the nature of edges, graphs can be classified into four types: directed/undirected and weighted/binary graphs (Sporns, 2011). Graph can also be represented by connectivity matrices known as “adjacency matrices”, where nodes are represented by rows or columns, and edges are represented by matrix elements (Fig2). In directed graphs, an edge between two nodes represents the connection from a specific node to the other and the corresponding adjacency matrices are not symmetrical (Fig2.A and B).

However, in undirected graphs, edges do not have any direction and the connectivity matrices are symmetric (Fiedler, 1973) (Fig2.C and D). Binary or un-weighted graphs are obtained by applying a threshold on the adjacency matrices of the weighted graphs. In weighted networks, matrix elements are continuous values often normalized between 0 and 1. In contrast, in binary matrices, elements are either 0 (no connection) or 1 (connection exists).

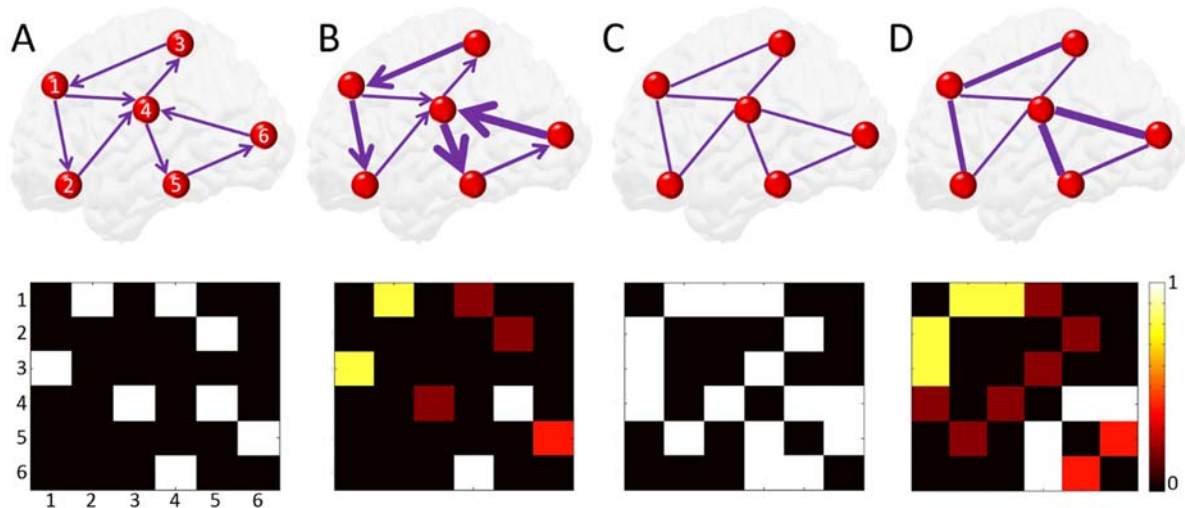


Figure 2: Graphs and adjacency matrices. A) Binary directed network. B) Weighted directed network. C) Binary undirected network. D) Weighted undirected network.

2.2. Graph measures

Once the brain network is modeled by a graph, several metrics can be extracted to describe the network properties at different levels (Rubinov and Sporns, 2010). Here we describe some of the most relevant measures in the context of brain network analysis. Some graph measures are illustrated in Fig3.

2.2.1. Segregation (local)

- **Clustering coefficient:**

Clustering coefficient is one of the main measures used to quantify network segregation. It is defined as the number of existing connections between the neighbors' node divided by all the possible connections between them (Watts and Strogatz, 1998)

- **Modularity**

The modularity consists of partitioning a network into a number of clusters or modules, also called communities, where nodes in the same module are highly interconnected but poorly connected to other groups of nodes (Sporns and Betzel, 2016). Each module can act in parallel and nearly independently to achieve its goals, and the success or failure of each module does not affect other modules (Fornito et al., 2016). The intra-module degree is one of the features that can be extracted from modules to quantify network segregation.

2.2.2. Integration (global)

- **Path length:**

A path length describes how close on average a node is connected to all the other ones. In a binary network, the path length between two nodes is the number of connecting edges. In a weighted network, the length of a path represents the sum of the edge weights (Sporns, 2011).

- **Global efficiency:**

Global efficiency is the average inverse shortest path length (Latora and Marchiori, 2001). It describes how efficiently the network shares information. A network with high global efficiency indicates that, on average, nodes are reached by short communications.

- **Participation coefficient**

The participation coefficient measures the diversity of a node inter-modular connections (Guimera and Amaral, 2005). Nodes with high participation coefficients interconnect multiple modules together.

2.2.3. Hubness

- **Degree and strength:**

The degree is the number of connections of a node. The strength is another measure similar to the degree, but it considers the node weights and uses them in the weighted graphs. These measures provide information about how highly and strongly connected is the node. Generally, highly connected nodes are very influential on their neighbors (Bullmore and Sporns, 2009).

- **Betweenness centrality:**

The betweenness centrality is the percentage of short paths that include the node (the shortest path length is the minimum distance or steps between two nodes) (Freeman, 1977). High betweenness centrality nodes have a large influence on the information flow through the network. It is also used to find hub nodes in a network.

- **Hubs:**

Hubs are nodes that connect communities, usually with a high degree, short average path length and high centrality. They play a key role in establishing and maintaining an efficient communication in a network. In addition, hubs can be classified into provincial (mostly connected to nodes within their own module) and connector hubs (connected to several different modules) (van den Heuvel and Sporns, 2013).

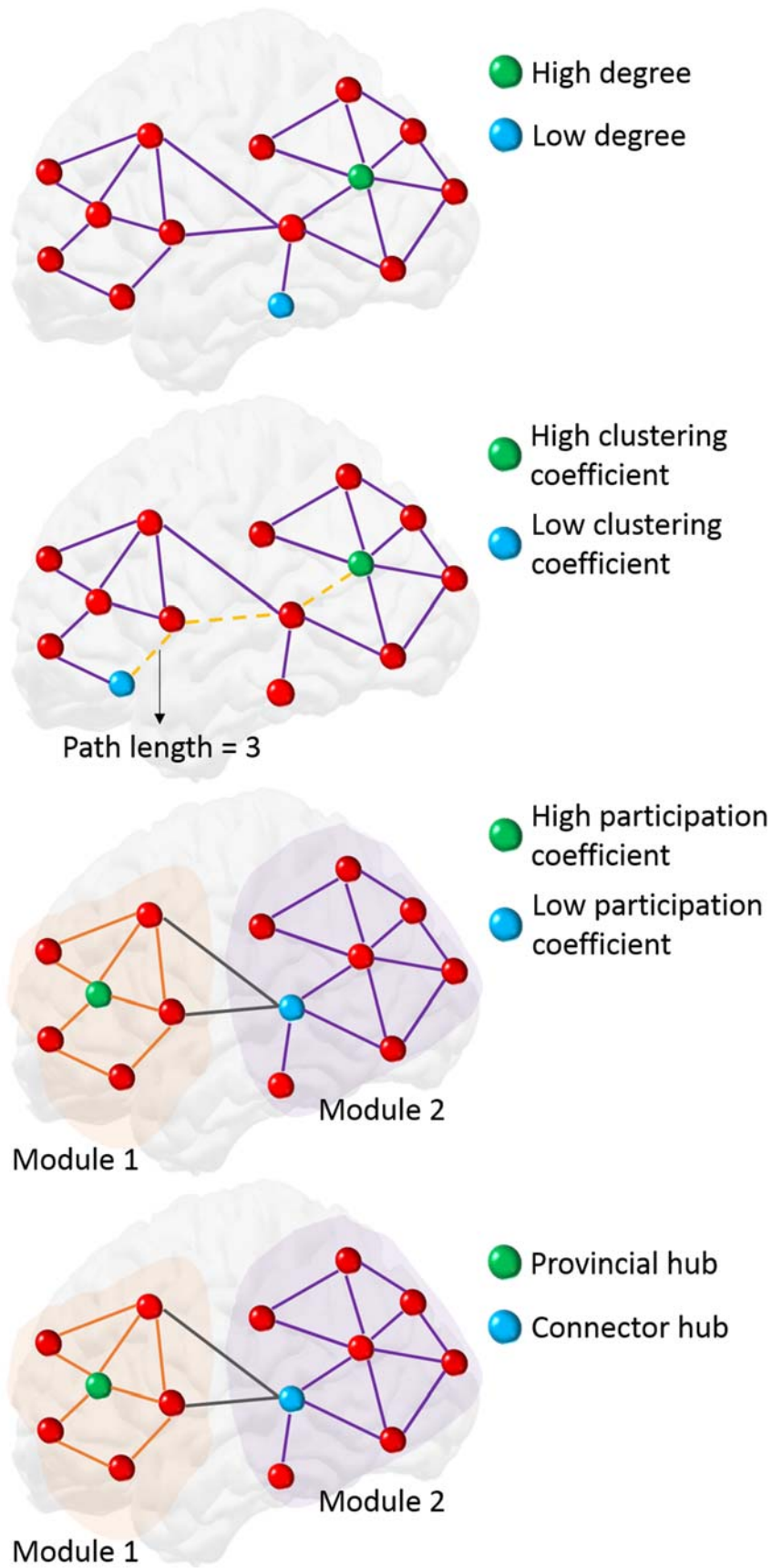


Figure 3: Illustration of some graph measures: degree, clustering coefficient, path length, modularity, participation coefficient and hubs (provincial and connector).

2.3. Neuroimaging techniques

Neuroimaging techniques are used to map the brain activity. They are divided into two parts: structural and functional. As we are interested in the functional brain connectivity, we describe in these sub-sections the three main techniques used to map the functional brain activity at large scale.

2.3.1. Functional magnetic resonance imaging (fMRI)

fMRI (Fig4.A) is a non-invasive technique used to record brain activity by measuring the in vivo blood flow changes (Huettel et al., 2004). It measures the “blood oxygen level dependent” (BOLD) signals, a non-direct measure of the neural activity. Its concept is based on the fact that increased activity in a particular part of the brain increases oxygenated blood flow. This technique provides excellent spatial resolution (about 1-3 mm) but it is limited in temporal resolution since the BOLD response inferred from the hemodynamic changes takes time (1-2 s) (Logothetis et al., 2001). Thus low temporal resolution (about 1second) is not sufficient to tracking the dynamics of brain networks at sub-second time scale, one of the main objectives of my thesis.

2.3.2. Magneto-encephalography (MEG)

The MEG (Fig4.B) detects the magnetic fields associated with the intracellular current flow within neurons. An important advantage of MEG is that magnetic fields are not attenuated or distorted when recorded from the sensor level (Gallen et al., 1995). Moreover, this technique has an excellent time resolution (below 1 ms). On the other hand, MEG involves greater practical difficulties, as it is expensive and its use for long time periods is very complicated as is the case in DoC patients for example.

2.3.3. Electroencephalography (EEG)

EEG (Fig4.C) records the fluctuations of the electric fields generated when neurons communicate, using electrodes placed on the scalp (Buzsaki et al., 2012). EEG consists of a wave that varies in time; it contains frequency components that can be analyzed separately. The main frequencies (rhythms) of the human EEG waves are delta (0.5 - 4.5 Hz), theta (5 - 8 Hz), alpha (8 – 13 Hz), beta (13 – 30 Hz) and gamma (30 – 45 Hz). The main advantage of the EEG technique are the excellent time resolution (in order of milliseconds), the non-invasiveness and

the ease-of-use at the patient's bedside, which makes it very practical for patients with impaired consciousness for instance (Chennu et al., 2014; Chennu et al., 2017; Harrison and Connolly, 2013). In this thesis, we used dense-EEG (256 electrodes).

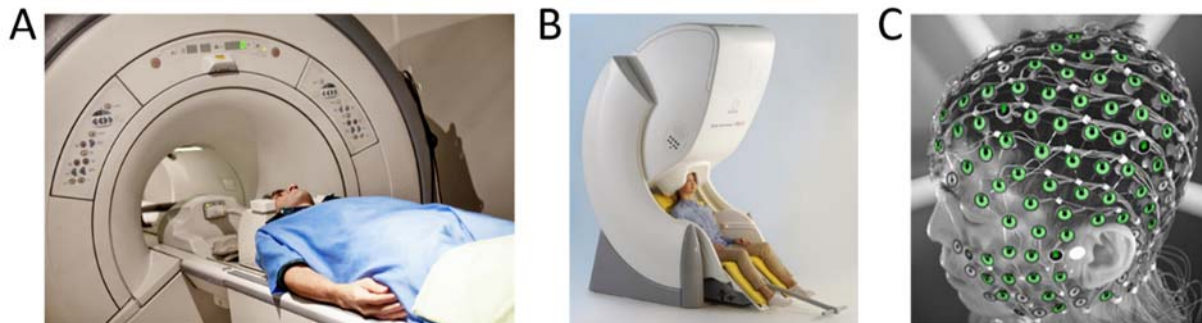


Figure 4: Neuroimaging techniques. A) Functional magnetic resonance imaging (fMRI). B) Magneto-encephalography (MEG). C) Electro-encephalography (EEG).

2.4. EEG source connectivity

Until the last decades, most EEG FC studies were performed at the sensor level by computing the statistical couplings between recorded signals. However, the biological interpretation of corresponding network alterations is not straightforward, since scalp EEG signals can be severely corrupted by the “volume conduction” due to the head electrical conduction properties and the “field spread” since single brain source activity can be collected by multiple sensors (Brunner et al., 2016; Van de Steen et al., 2016; Van Diessen et al., 2015), see Fig5. Several studies have indeed reported the limitations of computing connectivity at the EEG scalp level (see for review (Hassan and Wendling, 2018; Schoffelen and Gross, 2009). Moreover, scalp analysis does not allow making inferences about interacting brain regions.

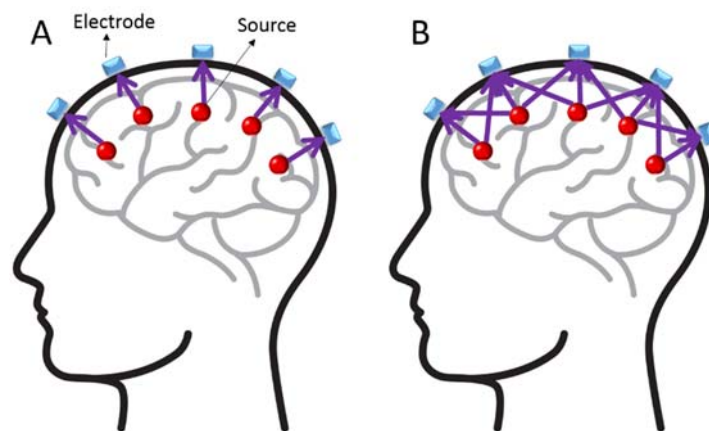


Figure 5: Volume conduction problem. A) Ideally, each electrode measures brain activity from the source below it. (b) In reality, signals recorded at each electrode are generated from several sources.

A potential solution is the emerging technique called “EEG source connectivity” (De Pasquale et al., 2010; Hipp et al., 2012; Mehrkanoon et al., 2014), which is supposed to reduce the aforementioned problems by directly identifying the brain networks at the cortical level with a high time/space resolution (Hassan and Wendling, 2018). This method involves two main steps: i) solve the ill-posed EEG inverse problem to reconstruct the dynamics of brain sources and ii) compute the statistical couplings between the reconstructed sources, which will be described in the next chapter.

2.5. Thesis objectives

2.5.1. Methodological development

The main advantages of the EEG source connectivity method is the possibility to provide high time /space resolution brain networks. On one hand, this method was used to track dynamics of brain networks during sub-second tasks such as press button task (O’neill et al., 2017), motor imagination task of right-hand flexion for instance (Edelman et al., 2015), and finger movements cued by visual stimuli (Babiloni et al., 2005). To what extent this method can differentiate between two conditions (meaningful vs. meaningless pictures) is less explored. Here, we chose the visual object recognition and naming task (DiCarlo et al., 2012) to **test the ability of this method to track the brain dynamics (to assess how functional brain network modules dynamically reconfigure) during the recognition of two object categories (meaningful and meaningless pictures)**. Moreover, we used this technique to see if there is a correlation between network modularity and the reaction time of the participants when meaningful pictures are presented. During this study, we introduced a new parameter called ‘*the occurrence*’ which present the probability of any two nodes to fall in the same module over time. Study details and results will be reported in chapter 4 – study 1.

On the other hand, as this method involves several steps from de-noising the scalp signals to reconstructing the source signals, several methodological aspects should be carefully accounted for to avoid pitfalls. Some of these parameters were analyzed, such as the head model (Liu et al., 2018) and EEG reference choice (Hu et al., 2018; Liu et al., 2015). “Source leakage” or “spatial leakage” is also one of the issue facing the source connectivity method (Hipp et al., 2012) since the functional connectivity at the source level reduces the effect of the field spread but it does not totally suppress its effects (Brookes et al., 2012). Spurious connections can be

created between the estimated time-series of adjacent regions. This effect is called “source leakage” or “spatial leakage”.

To deal with the aforementioned “source leakage” problem, few approaches have been proposed and they are centered on removing the edges between the very close sources (De Pasquale et al., 2010; de Pasquale et al., 2012). More recently, a number of methods were developed to remove zero-lag correlation based on the hypothesis that leakage generates inflated connectivity between estimated sources, which manifests as zero-phase-lag correlations (Brookes et al., 2012; Drakesmith et al., 2015). Un-mixing methods, called ‘leakage correction’, have been reported to force the reconstructed signals to have zero cross-correlation at lag zero. Some of the methods remove zero-lag connections when extracting FC measures as phase lag index (PLI) (Stam et al., 2007) or the imaginary coherence (ImCoh) (Nolte et al., 2004). Others remove the zero-lag connections before performing any connectivity analysis by adopting orthogonalisation-based approach (Brookes et al., 2012; Colclough et al., 2015; Hipp et al., 2012; Pascual-Marqui et al., 2017). However, several studies described the presence of these connections and proved their importance since not all zero-lag connections are spurious (Gollo et al., 2014; Roelfsema et al., 1997). Accordingly, by removing these connections, true near zero-lag connections can still be undetected (Finger et al., 2016; Palva et al., 2018; Pascual-Marqui et al., 2017; Wang et al., 2018).

Here, **our objective is to study the effect of removing zero-lag connections on the reconstructed networks.** Two families of FC methods were tested on rest EEG data: i) the FC metrics that do not remove the zero-lag-phase connectivity including the phase locking value (PLV) and the amplitude envelope correlation (AEC) and ii) the FC metrics that remove the zero-lag connections such as the phase lag index (PLI) and two orthogonalisation approaches combined with PLV (PLV_{Col} – PLV combined with the symmetric orthogonalisation technique (Colclough et al., 2015) and PLV_{Pas} – PLV combined with the innovations orthogonalisation technique (Pascual-Marqui et al., 2017)) and AEC (AEC_{Col} – AEC combined with the symmetric orthogonalisation technique (Colclough et al., 2015) and AEC_{Pas} – AEC combined with the innovations orthogonalisation technique (Pascual-Marqui et al., 2017)). FC matrices obtained were compared to fMRI connectivity matrices (used as a ground truth) in order to determine which connectivity network is the most similar and correlated to fMRI networks. Study details and results will be reported in chapter 4 – study 2.

2.5.2. Clinical application

An emerging evidence in network neuroscience proved that neurological disorders are related to alterations in the structural and functional brain connectivity (Fornito and Bullmore, 2015; Fornito et al., 2015; Stam, 2014). Many studies were performed to compare between brain networks of healthy subjects and those of patients with brain disorders in order to identify alterations in networks associated with transition from normal to pathological state (Fornito et al., 2016; Monti et al., 2010b; Tijms et al., 2013).

Network neuroscience has revealed valuable information about the functional networks involved in epilepsy (Jmail et al., 2016; Nissen et al., 2017), Alzheimer (Engels et al., 2017; Stam et al., 2006), schizophrenia (Alexander-Bloch et al., 2010; Bassett et al., 2008; Damaraju et al., 2014), depression (Lu et al., 2013; Zhang et al., 2011) and Parkinson disease (Baggio et al., 2015; Hata et al., 2016). The identification of the altered brain regions related to neurological diseases allowed better understanding of the neural mechanisms underlying brain disorders, and consequently better patients monitoring.

One of these neurological pathologies is the disorders of consciousness (DOC). Severe brain injury can rob us of consciousness, whenever temporarily or forever. This can be caused by trauma to the head or by non-traumatic causes, such as hemorrhage or ischemia (Bagnato et al., 2010). Patients surviving brain injury typically go through a sequence of progressive stages towards recovery (Giacino et al., 2014). These patients are mainly characterized by dissociation between awareness and arousal (Bernat, 2009; Laureys, 2005).

Patients in coma show no signs of arousal or awareness. They typically only exhibit reflex activities and do not respond to external stimuli, even strong and obnoxious ones (Laureys et al., 2015). Patients who recovered from coma, but entered a vegetative state, have wake and sleep cycles but show no signs of awareness of the external world (remain unresponsive to any external stimulation). This state is known as the unresponsive wakefulness syndrome (UWS) (Laureys et al., 2010; Monti et al., 2010a). If the vegetative state persists for more than one month, the percentage of recovery becomes very low (only around 20% of UWS patients will regain responsiveness within two years (Estraneo et al., 2013)). When patients show minimal, non-reflexive, yet reproducible behavioral signs of consciousness, they are considered to be in the minimally conscious state (MCS) (Giacino et al., 2002). This group is subcategorized into

MCS- and MCS+ based on the level of complexity of the observed behavioral responses. MCS+ patients show the ability to understand language and follow simple commands (Bruno et al., 2011; Bruno et al., 2012). Once patients restore reliable communication and/or functional object use, they are considered to emerge from MCS (EMCS) (Giacino et al., 2014; Laureys et al., 2004). States of consciousness according to the level of awareness and arousal are presented in Fig6.

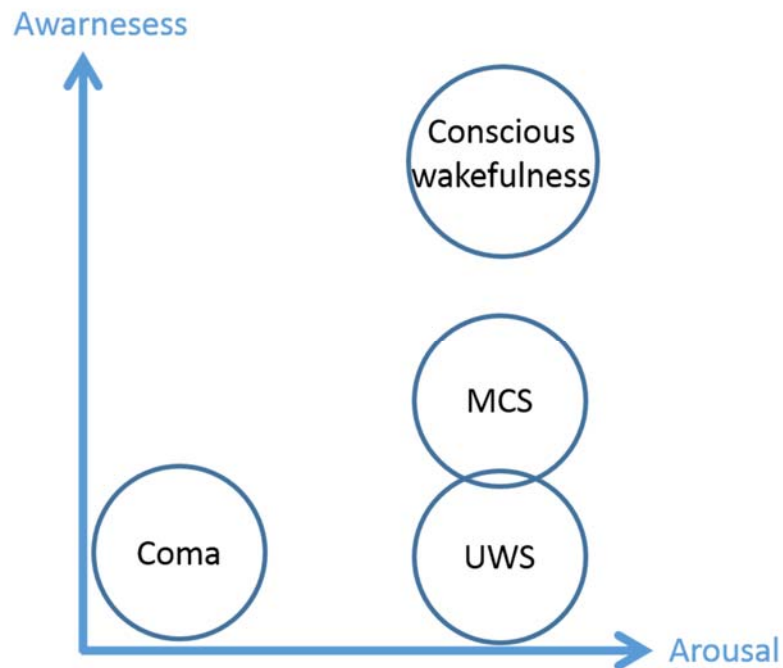


Figure 6: States of consciousness according to the level of awareness and arousal.

Establishing a proper clinical diagnosis in disorders of consciousness is not straightforward (Gantner et al., 2013). Behavioral clinical assessment methods like the Glasgow Coma Scale (Jones, 1979), the Coma Recovery Scale (CRS) (Giacino et al., 1991), or the Coma Recovery Scale Revised (CRS-R) (Giacino et al., 2004) are based on the observation of motor and oro-motor behaviors at the bedside and measure patients behavioral responsiveness.

However, absence of responsiveness does not necessarily correspond to absence of awareness (Giacino et al., 2014; Sanders et al., 2012). Some patients might have consciousness but not accessible through CRS-R (Gosseries et al., 2014; Schiff and Fins, 2016). Using only the CRS-R has led to high rates of misdiagnosis of the true level of consciousness in these patients (more than 40% of UWS patients have reportedly been misdiagnosed) (Schnakers et al., 2009). A range of motor-independent neuroimaging technologies have been developed to avoid

diagnostic error intrinsic to behavioral assessment and help the clinical differentiation between different groups (Bruno et al., 2010; Di Perri et al., 2016; Sanders et al., 2012).

Emerging evidence associates DoC with alterations in functional and/or structural brain networks, mainly those sustaining arousal and awareness (Amico et al., 2017; Annen et al., 2016; Annen et al., 2018; Bodien et al., 2017; Boly et al., 2012; Fernández-Espejo et al., 2012; Koch et al., 2016; Owen et al., 2009). Previous EEG network-based studies, in the context of DOC, have been performed at the scalp level (Chennu et al., 2014; Chennu et al., 2017; Estraneo et al., 2016) with satisfactory accuracies in classifying UWS and MCS patients (Chennu et al., 2017; Engemann et al., 2018; Sitt et al., 2014).

Since conscious processing involves synchronization of locally generated oscillations between remote groups of neurons (Melloni et al., 2007), high-density EEG functional connectivity at the source level is a promising approach to track such synchronizations. **Our objectives was to i) explore the changes in the network topology (integration and segregation) as a function of clinical consciousness levels and ii) track dynamic functional networks alterations in the case of DoC patients.** To do so, we combined EEG source connectivity with graph theory, applied to resting-state high-density-EEG (256 channels) data recorded from DoC patients, whose diagnosis has been established based on the Coma Recovery Scale-Revised (CRS-R). Two studies have been conducted in this context (static and dynamic). Studies details and results will be reported in chapter 4 – study 3 and study 4.

CHAPTER 3. MATERIALS AND METHODS

In this chapter we present the materials and methods used in this thesis. First, we present the three databases used to achieve the objectives of this thesis: i) track the dynamic brain network modularity changes during the recognition of meaningful and meaningless visual images ii) study the effect of removing zero-lag connections on networks reconstruction and the effect of EEG montages and iii) track functional networks alterations in the case of DoC patients and identify brain regions involved between groups in a static and dynamic way. Second, we describe the methods used to solve the inverse problem and to obtain the functional connectivity matrices. Third, we present the concept of dynamic connectivity and the modularity analysis.

3.1. Database

3.1.1. Study 1: BrainGraph database (picture naming)

Dense-EEG signals (256 channels, EGI, Electrical Geodesic Inc.) were recorded from twenty right-handed healthy participants (ten women and ten men; mean age 23 y). Experiments were performed in accordance with the relevant guidelines and regulations of the National Ethics Committee for the Protection of Persons (CPP), (BrainGraph study, agreement number 2014-A01461-46, promoter: Rennes University Hospital), which approved all the experimental protocol and procedures. All participants in the study provided written informed consents.

80 meaningful and 40 meaningless pictures (presented in Fig8), taken from the Alario and Ferrand database (Alario and Ferrand, 1999), were displayed on a screen as black drawings on a white background using E-Prime 2.0 software (Psychology Software Tools, Pittsburgh, PA). Subjects were asked to name the meaningful images. They were informed about the presence of meaningless pictures in the experiment and were instructed to say nothing when viewing them. The same number of stimuli was used in the further analysis by selecting 40 meaningful images (the same for all subjects).



Figure 7: The meaningful (left) and meaningless (right) images used in the study.

A typical trial started with a fixation cross that lasted 1 s, then a random image was shown during 2.5 s and followed by a blank screen for 1 or 2 s (randomly selected) (see Fig9). Order of presentation was randomized across participants. The time between the picture onset and the beginning of vocalization recorded by the system was considered as naming latencies. The analysis was performed from the stimulus onset up to 500 ms following the stimulus in order to avoid muscle artifacts (due to articulation since the fastest response over trials and subjects was 535 ms). Errors in naming were discarded for the analysis.

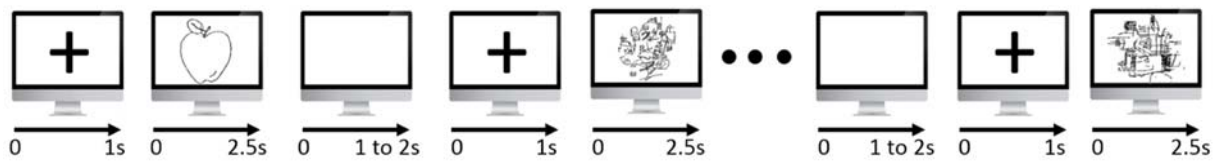


Figure 8: Picture naming experimental setup. The cognitive task consisted in naming visual stimuli of two categories: meaningful and meaningless pictures.

Dense EEG system (EGI, Electrical Geodesic Inc., 256 electrodes) was used to record brain activity. EEG signals were sampled at 1 KHz and then band-pass filtered between 0.3 and 45 Hz. For the preprocessing, EEGLAB (Delorme and Makeig, 2004) was used to remove the eye blinking effect (using ICA-based algorithm). For some subjects, few electrodes with poor signal quality were identified and interpolated using signals recorded by surrounding electrodes. The data of two females and 1 male participants were eliminated as EEG signals were very noisy due to electrodes impedance issues.

3.1.2. Study 2: BrainGraph database (resting state)

Dense-EEG signals (256 channels, EGI, Electrical Geodesic Inc.) were recorded from twenty right-handed healthy participants (ten women and ten men; mean age 23 y). Experiments were performed in accordance with the relevant guidelines and regulations of the National Ethics Committee for the Protection of Persons (CPP), (BrainGraph study, agreement number 2014-A01461-46, promoter: Rennes University Hospital), which approved all the experimental protocol and procedures. All participants in the study provided written informed consents and were asked to relax for 10 minutes with their eyes closed during the acquisition without falling asleep.

EEG signals were sampled at 1000 Hz, band-pass filtered within 0.1 - 45 Hz, and segmented into non-overlapping 40 s long epochs. Electrodes with poor signal quality (amplitude > 100

μV or $< -100 \mu\text{V}$) have been identified and interpolated using signals recorded by surrounding electrodes (spherical spline interpolating method, with a maximal distance between neighbors of 5 cm). Segments that have more than 20 electrodes interpolated have been excluded from the analysis. Three clean epochs per subject were then used for source estimation. One subject was excluded from the study due to noisy data.

3.1.3. Study 3 and 4: DoC database

Sixty-one patients (24 females, mean age 40 ± 14.5) and twenty-one healthy subjects (i.e. controls; 8 females, mean age 41 years ± 15.4) were included in this study (out of 115 patients' recordings, only 61 were kept since the other recordings were excessively contaminated by artefacts (e.g., muscle artefacts)). Etiology was traumatic in 28 patients and non-traumatic in 33. Time since injury was three years on average and ranged from nine days to 19 years. The Ethics Committee of the University Hospital of Liège approved this study. All healthy subjects and patients' legal surrogates gave informed written consent for participation to the study.

The CRS-R was repeated at least 5 times to minimize clinical misdiagnosis (Wannez et al., 2017). Patient's diagnosis was based on the best behaviors/highest item obtained over the repeated CRS-R assessments during the week of hospitalization (CRS-R response profile is presented in Fig9): patients were diagnosed as EMCS (n=6), MCS+ (n=29), MCS- (n=17) and UWS (n=9). The following demographic information (listed in Table 1) was also collected for each patient: age, gender, time since injury, traumatic or non-traumatic etiologies and best clinical diagnosis based on the CRS-R assessments.

JFK COMA RECOVERY SCALE-REVISED Record Form								
Patient:	Date:							
AUDITORY FUNCTION SCALE								
4-Consistent Movement to Command*								
3-Reproducible Movement to Command*								
2-Localization to Sound								
1-Auditory Startle								
0-None								
VISUAL FUNCTION SCALE								
5-Object Recognition*								
4-Object Localization: Reaching*								
3-Visual Pursuit*								
2-Fixation*								
1-Visual Startle								
0-None								
MOTOR FUNCTION SCALE								
6-Functional Object Use†								
5-Automatic Motor Response*								
4-Object Manipulation*								
3-Localization to Noxious Stimulation*								
2-Flexion Withdrawal								
1-Abnormal Posturing								
0-None/Flaccid								
OROMOTOR/VERBAL FUNCTION SCALE								
3-Intelligible Verbalization*								
2-Vocalization/Oral Movement								
1-Oral Reflexive Movement								
0-None								
COMMUNICATION SCALE								
3-Oriented†								
2-Functional: Accurate†								
1-Non-Functional: Intentional*								
0-None								
AROUSAL SCALE								
3-Attention*								
2-Eye Opening w/o Stimulation								
1-Eye Opening with Stimulation								
0-Unarousable								
TOTAL SCORE								

Abbreviation: w/o, without.

*Denotes MCS.

†Denotes emergence from MCS.

Figure 9: CRS-R response profile (Giacino et al., 2004).

Name	Age	Gender	Days since injury	Etiology	Best diagnosis
P1	27	F	1570	NT	MCS+
P2	27	M	1542	T	MCS+
P3	35	M	6950	NT	UWS
P4	60	M	9	NT	MCS-
P5	24	M	319	T	MCS-
P6	30	F	2406	NT	MCS-
P7	30	F	563	T	MCS-
P8	30	M	583	T	MCS+
P9	50	M	-	T	MCS+
P10	30	F	-	T	MCS+
P11	46	M	528	T	MCS+
P12	48	F	-	NT	MCS-
P13	37	M	1869	NT	MCS-
P14	59	F	-	NT	MCS-
P15	5	F	-	T	MCS+
P16	24	M	2681	NT	MCS+
P17	30	M	33	NT	MCS+
P18	43	M	3139	T	MCS-
P19	45	F	491	NT	UWS
P20	57	M	390	NT	MCS+
P21	25	F	308	NT	MCS+
P22	23	M	421	T	MCS+
P23	28	M	66	NT	MCS-
P24	53	M	1235	NT	MCS-
P25	24	M	-	T	MCS+
P26	36	F	-	NT	UWS
P27	22	M	2972	T	MCS-
P28	23	M	2035	T	MCS+
P29	73	M	28	NT	MCS-
P30	30	M	3337	T	MCS+
P31	47	F	-	NT	MCS-
P32	65	M	674	T	MCS+
P33	55	M	-	NT	MCS+
P34	19	M	426	T	MCS+
P35	39	F	1437	T	MCS-
P36	34	F	375	T	EMCS
P37	61	F	858	NT	MCS+
P38	14	M	185	NT	EMCS
P39	26	F	112	NT	UWS
P40	35	M	4154	NT	MCS+
P41	60	M	406	NT	EMCS
P42	62	M	672	NT	UWS
P43	67	F	1464	NT	MCS+
P44	23	M	456	NT	UWS
P45	42	F	220	NT	MCS-
P46	72	M	3062	NT	MCS+
P47	21	M	257	T	UWS
P48	30	M	402	T	MCS-
P49	28	M	2423	T	EMCS
P50	59	F	709	T	MCS+
P51	51	F	347	NT	UWS
P52	25	M	1283	T	MCS+
P53	42	M	1186	T	EMCS
P54	24	F	333	NT	MCS-
P55	43	F	40	T	UWS
P56	55	F	669	T	MCS+
P57	54	M	387	NT	MCS+
P58	38	M	541	T	MCS+
P59	43	F	98	NT	MCS+
P60	22	M	423	T	MCS+
P61	33	F	308	NT	EMCS

Table 1: Patients demographic information: age, gender, days since injury, traumatic (T) or non-traumatic (NT) etiology and clinical best diagnosis.

Resting state brain activity was recorded using a high-density EEG system (EGI, Electrical Geodesic Inc., 256 electrodes applied with a saline solution) with a sampling rate of either 250 Hz or 500 Hz (which were down-sampled to 250 Hz for consistency). During data collection, patients were awake in a silent and dark room and had their eyes open for 20 to 30 min. An examiner was present during the whole acquisition to ensure that the patients remained awake. Tactile or auditory stimuli were administered if patients were closing their eyes.

EEG data from 178 channels on the scalp were retained for analysis; neck, forehead and cheeks channels were discarded, since they are the most prone to muscular artifacts, as described in previous studies (Hassan et al., 2016; Kabbara et al., 2017). EEG signals were filtered between 0.3 and 45 Hz and then re-referenced using the average reference (Tadel et al., 2011). Data were segmented into non-overlapping 40 s long epochs.

All EEG epochs were visually inspected before Independent Components Analysis (ICA) was performed to remove eye blinking artifacts using EEGLAB (Delorme and Makeig, 2004). Electrodes with poor signal quality were interpolated in Brainstorm (Tadel et al., 2011), using signals recorded by surrounding electrodes (spherical spline interpolating method, with a maximal distance between neighbors of 5 cm). Segments that have more than 20 interpolated electrodes have been excluded from the analysis. Five clean epochs per subject were then used for source estimation.

3.2. EEG source connectivity

The EEG source connectivity method involves two main steps: i) solving the ill posed inverse problem and ii) choosing a functional connectivity measure among all the available ones (Fig10).

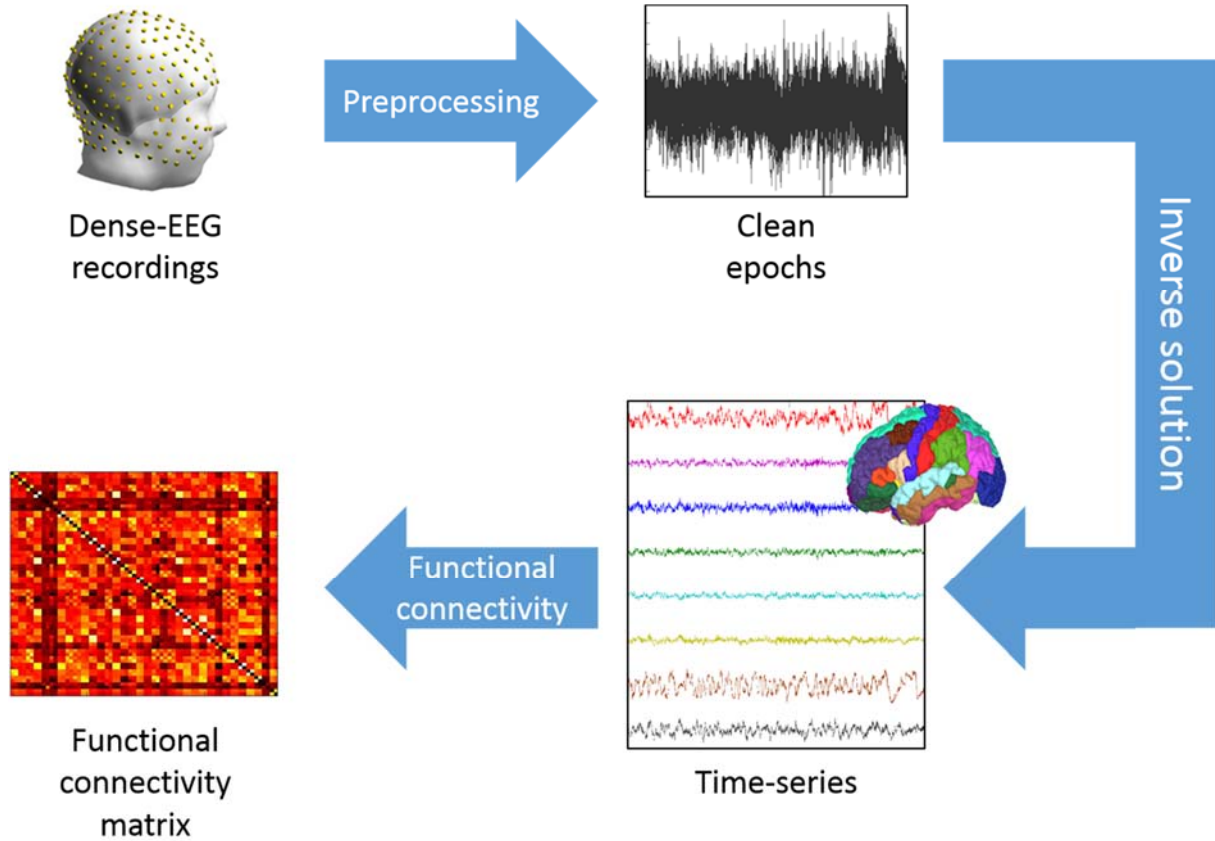


Figure 10: EEG source connectivity pipeline. EEG recorded at the scalp level are preprocessed before solving the inverse problem to obtain the regional time series. Finally, functional connectivity matrices are computed.

3.2.1. Inverse problem

The inverse problem consists in finding an estimate $\hat{S}(t)$ of the brain dipolar time-varying source parameters: position, orientation and magnitude given the EEG signals. According to the linear discrete equivalent current dipole theory, EEG signals $X(t)$, measured from M electrodes, are considered as linear combinations of N dipolar time-varying sources $S(t)$:

$$X(t) = G.S(t) + N(t)$$

Where G is the lead fields matrix of the dipolar sources and $N(t)$ is the additive noise. Structural MRI and EEG signals were co-registered through identification of the same anatomical landmarks (left and right tragus and nasion) using brainstorm (Tadel et al., 2011). Individual structural MRI was recorded and used for study 1, while, MRI template “Colin27” (Holmes et al., 1998) was used for all other studies. To compute the lead field matrix, using a multiple layer head model (volume conductor) and the electrodes positions are needed.

The head model explains how the electric currents or the magnetic fields generated at the source level reach the sensors (scalp level) after traversing the different tissues of the head (brain, skull and skin). The most used techniques to compute realistic head models are the Boundary Element Model (BEM) (Fuchs et al., 1998; Oostenveld and Oostendorp, 2002) and the Finite Element Model (FEM) (Zhang et al., 2006). These methods compute the individual specific head model by taking into account detailed features of the head anatomy. In our study, openMEEG toolbox (Gramfort et al., 2010) was used to compute a BEM head model.

While the inverse problem is ill-posed (number of dipolar sources is much higher than the number of electrodes), the solution to this problem is not unique. Thus, mathematical and physical constraints (amplitude, position and orientation) should be added to obtain a unique solution (Becker et al., 2015). Usually, the current dipoles are homogeneously distributed over the cortex, and normal to the cortical surface. To determine the source positions, high resolution mesh surface (usually 15000 vertices) is used.

Once the physical constraints are defined, time courses of a set of predefined brain regions (known as regions of interests -ROIs-) are estimated. Several anatomical and/or functional brain atlases can be used such as Desikan-Killiany composed of 68 ROIs (Desikan et al., 2006) or the Destrieux composed of 148 ROIs (Destrieux et al., 2010) for instance. Desikan-Killiany atlas (ROIS labels are listed in Table 2) was used for study 1. For the second and third study, a new anatomical framework was used, consisting of 221 ROIs identified by means of Desikan-Killiany using freesurfer (Fischl, 2012).

Acronyms	Name	Acronyms	Name
LING L	lingual L	sFG L	superiorfrontal L
LING R	lingual R	sFG R	superiorfrontal R
periCAL L	pericalcarine L	rMFG L	rostralmiddlefrontal L
periCAL R	pericalcarine R	rMFG R	rostralmiddlefrontal R
CUN L	cuneus L	cMFG L	caudalmiddlefrontal L
CUN R	cuneus R	cMFG R	caudalmiddlefrontal R
LOG L	lateraloccipital L	pOPER L	parsopercularis L
LOG R	lateraloccipital R	pOPER R	parsopercularis R
ENT L	entorhinal L	pTRI L	parstriangularis L
ENT R	entorhinal R	pTRI R	parstriangularis R
paraH L	parahippocampal L	pORB L	parsorbitalis L
paraH R	parahippocampal R	pORB R	parsorbitalis R
TP L	temporalpole L	LOF L	lateralorbitofrontal L
TP R	temporalpole R	LOF R	lateralorbitofrontal R
FUS R	fusiform R	MOF L	medialorbitofrontal L
FUS L	fusiform L	MOF R	medialorbitofrontal R
STG L	superiortemporal L	FP L	frontalpole L
STG R	superiortemporal R	FP R	frontalpole R
ITG L	inferiortemporal L	preC L	precentral L
ITG R	inferiortemporal R	preC R	precentral R
MTG L	middletemporal L	paraC L	paracentral L
MTG R	middletemporal R	paraC R	paracentral R
TT L	transversetemporal L	postC L	postcentral L
TT R	transversetemporal R	postC R	postcentral R
BSTS L	bankssts L	rACC L	rostralanteriorcingulate L
BSTS R	bankssts R	rACC R	rostralanteriorcingulate R
SMAR L	supramarginal L	cACC L	cAUDalanteriorcingulate L
SMAR R	supramarginal R	cACC R	cAUDalanteriorcingulate R
SPL L	superiorparietal L	PCC L	posteriorcingulate L
SPL R	superiorparietal R	PCC R	posteriorcingulate R
IPL L	inferiorparietal L	iCC L	isthmuscingulate L
IPL R	inferiorparietal R	iCC R	isthmuscingulate R
PCUN L	precuneus L	INS L	insula L
PCUN R	precuneus R	INS R	insula R

Table 2 : Summary of the 68 ROIs derived from the Desikan-Killiany atlas.

To solve the mathematical constraint, several methods can be used (see (Becker et al., 2015) for review). In this thesis, the weighted minimum norm estimate (wMNE), which aims to identify sources with the smallest energy, was used to reconstruct the cortical sources by introducing a weighting matrix:

$$\hat{\mathbf{S}}_{\text{wMNE}} = (\mathbf{G}^T \mathbf{W}_x \mathbf{G} + \lambda \mathbf{I})^{-1} \mathbf{G}^T \mathbf{W}_x \mathbf{X}$$

where the diagonal matrix \mathbf{W}_x is built from the lead field matrix \mathbf{G} with non-zero terms inversely proportional to the norm of the lead field vectors. The choice of the regularization parameter λ is important: many approaches have been proposed to estimate it although there is no agreement on any optimal solution. Here, λ is computed relatively to the signal to noise ratio ($\lambda=0.1$ in our analysis). Finally, reconstructed regional time series were filtered in six different frequency bands: Delta (0.5 Hz - 4 Hz), Theta (4 Hz - 8 Hz), Alpha (8 Hz - 13 Hz), Beta (13 Hz - 30 Hz), Gamma (30 Hz - 45 Hz) and broadband (0.5 Hz - 45 Hz) before performing the connectivity analysis.

3.2.2. Functional connectivity (FC)

Functional connectivity (FC) measures represent the statistical dependencies between brain regions. Several methods have been proposed to characterize the brain functional connectivity. Some of the most used measures are: Phase Locking Value (PLV), Phase Lag Index (PLI), weighted Phase Lag Index (wPLI), Amplitude Envelope Correlation (AEC), Coherence (Coh), Imaginary part of the coherence (ImCoh), Partial Coherence (PC), Mutual information (MI), etc.

These connectivity measures are divided into two families: i) FC measures that keep zero lag connections such as PLV, AEC, Coh, etc. and ii) FC measures that remove zero lag connections such as PLI, wPLI, Imcoh, etc. In this thesis, we tested three FC measures: PLV, PLI and AEC in order to study the effect of removing zero lag connections on the reconstructed networks. PLV was used for the last two studies.

- Phase Locking Value (*PLV*)

The phase locking value between two signals x and y is defined as (Lachaux et al., 1999):

$$PLV(t) = \left| \frac{1}{\delta} \int_{t-\delta/2}^{t+\delta/2} e^{j(\varphi_y(t)-\varphi_x(t))} dt \right|$$

where $\varphi_y(t)$ and $\varphi_x(t)$ are the phases of the signals x and y at time t extracted using the Hilbert transform. δ denotes the size of the window in which PLV is calculated. Here, we used a sliding window technique for each epoch to compute the FC matrices in a dynamic way (De Pasquale et al., 2016). The smallest window length recommended by (Lachaux et al., 2000) was used,

equal to $\frac{\text{number of cycles}}{\text{central frequency}}$ where the number of cycles at the given frequency band is equal to

six. PLV method is normalized so values range from 0 (independent signals) to 1 (fully synchronized signals).

- Phase Lag Index (*PLI*)

The PLI was introduced as an alternative measure of PLV and less sensitive to the influence field spread and amplitude effects. It is defined as follows (Stam et al., 2007):

$$PLI = \left\langle \left| \text{sign}[\varphi_y(t) - \varphi_x(t)] \right| \right\rangle$$

Where $\varphi_y(t)$ and $\varphi_x(t)$ are the phases of the signals x and y at time t and $\langle \rangle$ denotes the average over the time. PLI method is normalized so values range from 0 (independent signals) to 1 (fully synchronized signals).

- Amplitude Envelope Correlation (*AEC*)

The envelopes of the regional time series were estimated using Hilbert transform then Pearson correlation between amplitude envelopes can be computed (Brookes et al., 2004).

FC values estimated between all pairs of ROIs using one of the mentioned connectivity measurements leads to connectivity matrix of dimension $N \times N$, where N denotes the number of ROIs. For the dynamic analyses, we used PLV with the sliding window approach. The regional time series were segmented into non-overlapping time windows of length δ . Then, at each time window, a functional matrix was computed. Finally, a dynamic connectivity tensor (dimension: $N \times N \times L$, L = number of windows) was obtained.

3.3. Orthogonalisation approach

As mentioned previously, some of the connectivity methods seeking to be robust to source leakage remove zero lag-connections directly (Nolte et al., 2004; Stam et al., 2007). In other hand, some researchers attempt to correct for leakage before performing connectivity methods using the orthogonalisation approach (Brookes et al., 2012; Colclough et al., 2015; Hipp et al., 2012; Pascual-Marqui et al., 2017). Two orthogonalisation techniques were tested in this thesis: the “symmetric orthogonalisation” technique developed by (Colclough et al., 2015) and the “innovations orthogonalisation” method proposed by (Pascual-Marqui et al., 2017).

The “symmetric orthogonalisation” approach was used to correct for signal leakage by removing any correlations with zero temporal lag between all ROIs. The corrected time-series are constructed in two stages, as illustrated in Fig11. First, the closest set of orthonormal time-courses was found. Second, the normality constraint was taken into consideration and the solution was refined by iteratively adjusting the lengths and orientations of the corrected vectors until converging to a solution as close as possible to the uncorrected time-courses (Colclough et al., 2015).

The “innovations orthogonalisation” removes the spurious zero-lag interactions, by estimating the required orthogonalisation on the residuals of a multivariate autoregressive processes which requires the choice of an appropriate model order for the multivariate autoregressive process. The model order is estimated using Akaike's information criterion (AIC) (Akaike, 1974).

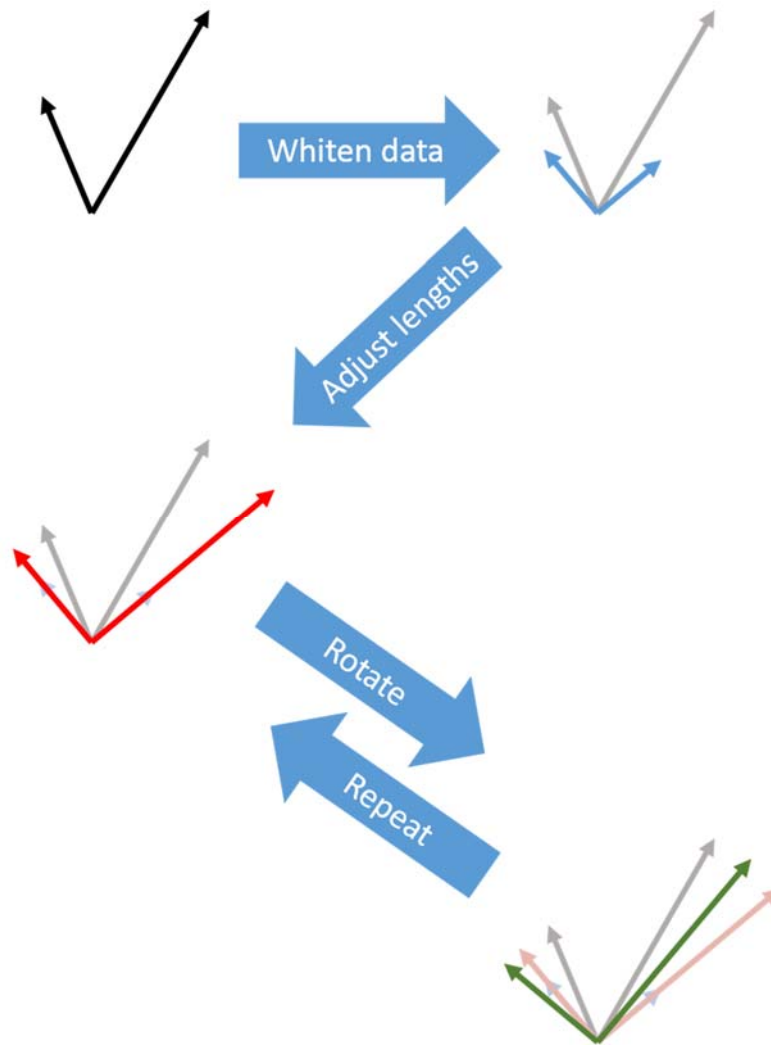


Figure 11: Symmetric orthogonalisation approach. The correlations between ROIs introduced during source reconstruction can be removed by mutually orthogonalising the ROI time-series, illustrated here for two vectors in two dimensions. An optimal set of corrected time-series is reconstructed by iterating towards the closest set of orthogonal vectors to the starting time-series. The process is initialized with the closest orthonormal matrix to the uncorrected vectors, then adjusts in turn the vector magnitudes and orientations to minimize the Euclidean distance between the corrected and uncorrected time-series, adapted from (Colclough et al., 2015).

3.4. Modularity

The modularity consists of partitioning a network into a number of clusters or modules (also called communities) where nodes are more connected internally with each other than with other external parts of the network. The strongly connected nodes in a module share common functions when weakly connected nodes in different modules have their functions segregated from each other.

Modularity maximization method was proposed to partition the network into non overlapping modules by maximizing the modularity index Q (Blondel et al., 2008) defined as:

$$Q = \frac{1}{2m} \sum_{ij} [A_{ij} - \gamma P_{ij}] \delta(\sigma_i, \sigma_j)$$

where A_{ij} represents the weight of the edge between nodes i and j assigned to communities σ_i and σ_j respectively. γ is a structural resolution parameter. $P_{ij} = \frac{K_i K_j}{2m}$ is the expected weight of the edge connecting node i and node j under a specified null model where $K_i = \sum_j A_{ij}$ is the sum of the weights of the edges attached to node i . The δ -function $\delta(u, v)$ is 1 if $u = v$ and 0 otherwise and $m = \frac{1}{2} \sum_{ij} A_{ij}$.

A partition achieves a greater value closer to unity of the modularity index Q if the communities are more internally dense than would be expected by chance (Good et al., 2010). Q measures the difference between the observed connectivity within modules and its expected value for a random graph with the same degree sequence (in the case of binary graph).

To track the modularity of the brain dynamically, the functional connectivity matrices were split into time-varying modules using a multislice community detection algorithm (Mucha et al., 2010). It consists of introducing a coupling parameter that links nodes across slices (each node is only connected to itself in the adjacent layers) before performing the modularity maximization procedure (Fig12) (Bassett et al., 2011; Bassett et al., 2013; Bassett et al., 2015).

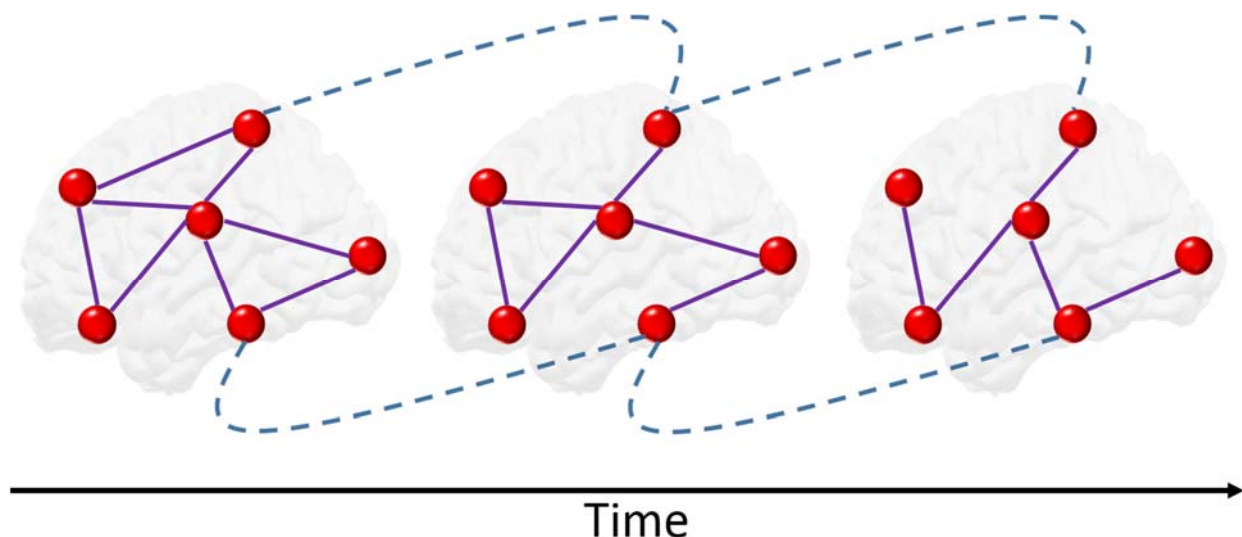


Figure 12: Multislice modularity approach. A coupling parameter that links nodes across time windows is introduced before performing the modularity maximization procedure to dynamically track modules changes during time.

The multislice modularity is defined as:

$$Q_{ml} = \frac{1}{2\mu} \sum_{ijlr} \left\{ \left(A_{ijl} - \gamma_l \frac{k_i k_{jl}}{2m_l} \right) \delta_{lr} + \delta_{ij} C_{jlr} \right\} \delta(M_{il}, M_{jr})$$

where nodes i and j are assigned to communities M_{il} and M_{jl} in layer l respectively. A_{ijl} represents the weight of the edge between these two nodes and γ_l is the structural resolution parameter of layer l . C_{jlr} is the connection strength between node j in layer r and node j in layer l . The structural resolution parameter γ and the inter-layer coupling parameter C are usually set to 1. k_{il} is the strength of node i in layer l , the δ -function $\delta(x, y)$ is 1 if $x = y$ and 0 otherwise, $m = \frac{1}{2} \sum_{ij} A_{ij}$ and $\mu = \frac{1}{2} \sum_{jr} k_{jr}$. This yields for every brain region at every time window a community assignment reflecting the module allegiance.

However, slightly different outputs can result after running the same algorithm on the same connectivity matrix due to a degeneracy problem in the modularity algorithms (Good et al., 2010). Hence, the multilayer network modularity was computed 100 times and a 221 by 221 association matrix was generated (Bassett et al., 2013; Fornito et al., 2016; Lancichinetti and Fortunato, 2012). The association matrix elements indicate the number of times each node was assigned to the same module with the other nodes across these 100 partitions. The association matrix was then compared to a null-model generated from 100 random permutation from the originals partitions, and only significant values ($p < 0.05$) were kept (Bassett et al., 2011). Finally, the Louvain algorithm (Blondel et al., 2008) was applied on the association matrix to cluster the network, resulting in a partition that is the most representative of network modularity. In study 1 and 3, a final consensus matrix was calculated over time for each subject. However, in study 4, the dynamic aspect was conserved and the dynamic matrices obtained for each subject were used in the analysis.

3.5. Modular states algorithm

The categorical version of the modular states algorithm developed by (Kabbara et al., 2019) was used in this study in order to find the main modular structures over time. It consists of decomposing each temporal brain network into a modular structure using modularity methods, then assessing the similarity between the resultant temporal modular structures. This yields to

a $T \times T$ similarity matrix where T is the number of time windows. Then, the algorithm clusters the similarity matrix into “categorical” modular states (MS) using the consensus modularity method which combines similar temporal modular structures in the same community (Fig13).

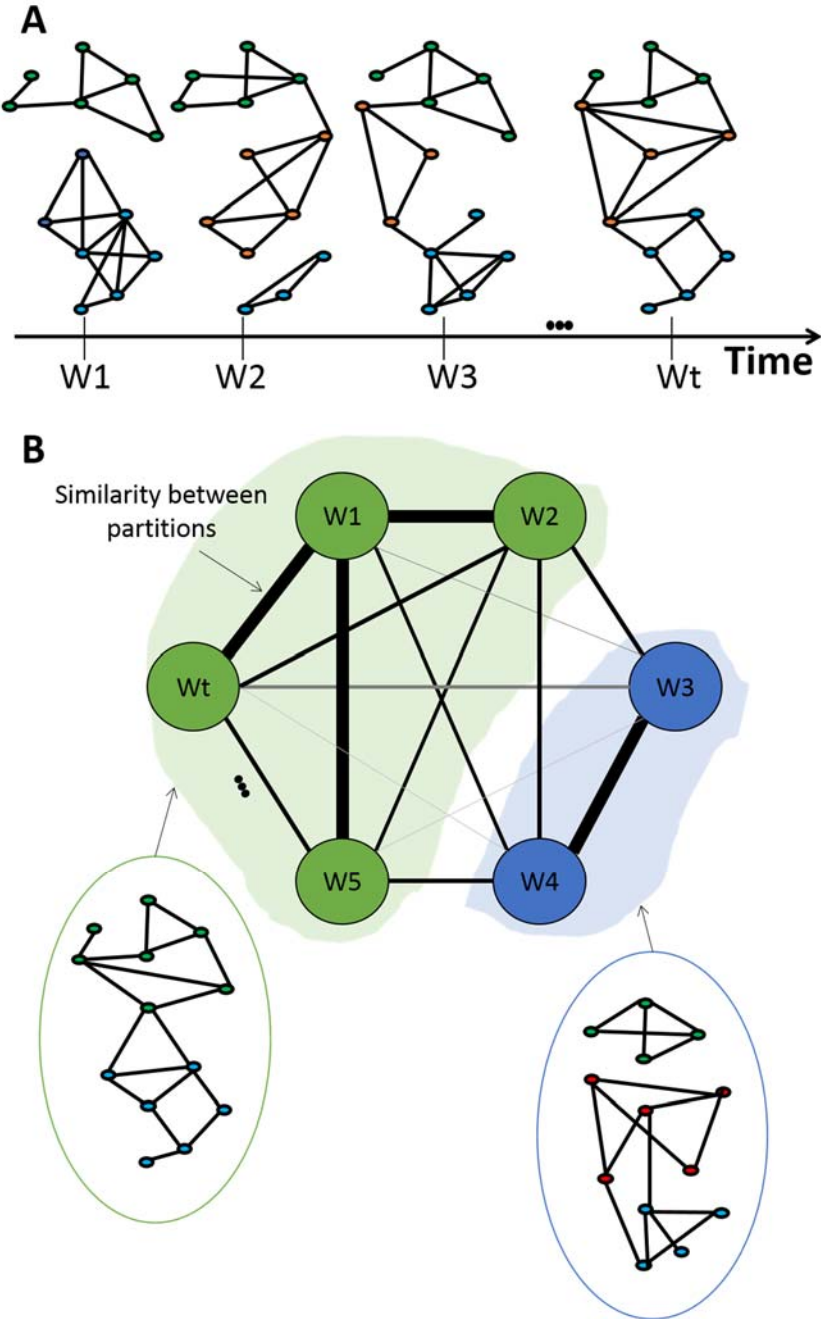


Figure 13: Modular states algorithm pipeline. (A) Computing the modules for the dynamic networks using multislice modularity method then (B) computing the similarity between the dynamic modular structures and clustering the similarity matrix into “categorical modules (adapted from by (Kabbara et al., 2019)).

CHAPTER 4. RESULTS

In this chapter, a brief summary of each study is presented, followed by the full-text of the corresponding published or submitted article.

Study 1: Dynamic reshaping of functional brain networks during visual object recognition

J. Rizkallah, P. Benquet, A. Kabbara, O. Dufor, F. Wendling, M. Hassan

Published in: Journal of neural engineering (2018)

Objectives: recent studies showed that the brain's modular organization allows for better and efficient cognitive performance which occur in a sub-second time scale, such as the visual object recognition. Two questions were raised in this study: i) does the dynamic brain network modularity change during meaningful and meaningless pictures recognition? And (ii) is there a correlation between network modularity and the participants' reaction time?

Methods: Dense-electroencephalography (EEG, 256 channels) data were collected from 20 healthy participants performing a cognitive task consisting of naming meaningful (tools, animals...) and meaningless (scrambled) images. EEG source connectivity method was used to estimate the functional brain networks in both categories. Finally, multislice modularity algorithm was used to track the dynamic reconfiguration of functional networks during the recognition of both meaningful and meaningless images.

Results: A difference in the modules' characteristics of both conditions in term of integration and occurrence was found. They were greater for meaningless than for meaningful images. Results revealed also that the occurrence within the right frontal regions and the left occipito-temporal can help to predict the ability of the brain to rapidly recognize and name visual stimuli. We speculate that these observations are applicable not only to other fast cognitive functions but also to detect fast disconnections that can occur in some brain disorders.

Key words: brain networks, dense EEG, object recognition

PAPER

Dynamic reshaping of functional brain networks during visual object recognition

To cite this article: J Rizkallah *et al* 2018 *J. Neural Eng.* **15** 056022

View the [article online](#) for updates and enhancements.

Related content

- [Reduced integration and improved segregation of functional brain networks in Alzheimer's disease](#)
A Kabbara, H Eid, W El Falou *et al.*
- [K-shell decomposition reveals hierarchical cortical organization of the human brain](#)
Nir Lahav, Baruch Ksherim, Eti Ben-Simon *et al.*
- [Comparison of connectivity analyses for resting state EEG data](#)
Elzbieta Olejarczyk, Laura Marzetti, Vittorio Pizzella *et al.*



IOP | ebooks™

Bringing you innovative digital publishing with leading voices to create your essential collection of books in STEM research.

Start exploring the collection - download the first chapter of every title for free.

Dynamic reshaping of functional brain networks during visual object recognition

J Rizkallah^{1,2}, P Benquet¹, A Kabbara^{1,2}, O Dufor³, F Wendling^{1,4}
and M Hassan^{1,4,5} 

¹ Univ Rennes, LTSI, F-35000 Rennes, France

² AZM center-EDST, Lebanese University, Tripoli, Lebanon

³ IMT Atlantique Bretagne Pays de la Loire, UMR CNRS Lab-STICC, Brest, France

E-mail: mahmoud.hassan@univ-rennes1.fr (M Hassan)

Received 9 February 2018, revised 17 July 2018

Accepted for publication 2 August 2018

Published 20 August 2018




Abstract

Objective. Emerging evidence shows that the modular organization of the human brain allows for better and efficient cognitive performance. Many of these cognitive functions are very fast and occur in a sub-second time scale such as the visual object recognition. *Approach.* Here, we investigate brain network modularity while controlling stimuli meaningfulness and measuring a participant's reaction time. We particularly raised two questions: i) does the dynamic brain network modularity change during the recognition of meaningful and meaningless visual images? And (ii) is there a correlation between network modularity and the reaction time of the participants?

To tackle these issues, we collected dense-electroencephalography (EEG, 256 channels) data from 20 healthy human subjects performing a cognitive task consisting of naming meaningful (tools, animals...) and meaningless (scrambled) images. Functional brain networks in both categories were estimated at the sub-second time scale using the EEG source connectivity method. By using multislice modularity algorithms, we tracked the reconfiguration of functional networks during the recognition of both meaningful and meaningless images. *Main results.* Results showed a difference in the module's characteristics of both conditions in term of integration (interactions between modules) and occurrence (probability on average of any two brain regions to fall in the same module during the task). Integration and occurrence were greater for meaningless than for meaningful images. Our findings revealed also that the occurrence within the right frontal regions and the left occipito-temporal can help to predict the ability of the brain to rapidly recognize and name visual stimuli. *Significance.* We speculate that these observations are applicable not only to other fast cognitive functions but also to detect fast disconnections that can occur in some brain disorders.

Keywords: brain networks, dense EEG, object recognition

 Supplementary material for this article is available [online](#)

(Some figures may appear in colour only in the online journal)

Introduction

Information is continuously processed and integrated in the human brain. To ensure efficient cognitive function, complex brain networks are characterized by two key features. On the one hand, recent studies show that their modularity facilitates

information processing as compared to non-modular organization (Sporns and Betzel 2016). Typically, in a large study of 77 cognitive tasks, Bertolero *et al* showed that the presence of network modules (defined as a set of brain regions strongly connected to each other and weakly connected to the rest of the network) is correlated with different cognitive functions such as memory, visual processing and motor programming (Bertolero *et al* 2015).

⁴ These authors contributed equally to this work.

⁵ Authors to whom any correspondence should be addressed.

On the other hand, emerging evidence shows that the dynamic behavior of brain networks is fundamental to understand cognition (Bassett *et al* 2015). Typically, during a learning task, Bassett *et al* showed that the flexibility (defined as how often a given node changes its modular affiliation over time) of the networks facilitates the prediction of individual future performances in next learning sessions (Bassett *et al* 2011). Both flexibility and integration (defined as the interactions between modules) in the frontal lobe during a 2-back working memory task were shown to be correlated with the performance accuracy (Braun *et al* 2015).

All the above-mentioned studies were performed using fMRI, the spatial resolution of which allows for appropriate identification of brain areas involved in considered cognitive processing. However, most of cognitive processes occur on a very short duration and are likely to involve modular dynamic changes occurring at sub-second time scale. Unfortunately, such changes cannot be tracked with fMRI due to intrinsic time resolution (on the order of 1 s). Therefore, our knowledge about the dynamic modifications of the modular organization of brain networks at a sub-second time-scale during cognitive activity remains elusive.

To tackle this issue, i.e. to assess how functional brain network modules dynamically reconfigure to ensure information processing and integration, we chose the well-defined visual object recognition and naming task (DiCarlo *et al* 2012) which involves fast cognitive processes (a few hundred of ms from stimulus onset to reaction). In order to guarantee sufficiently fast tracking of functional brain networks, we collected dense-electroencephalography (EEG, 256 channels) data from 20 healthy human subjects performing a cognitive task consist of naming meaningful (tools, animals...) and meaningless (scrambled) visual stimuli. Functional brain networks in both categories were estimated using ‘dense-EEG source connectivity’ method (Hassan and Wendling 2018). By applying multislice modularity algorithms to neocortical networks, we tracked the reconfiguration of brain modules at sub-second time scale during the recognition of these two object categories. Results showed that two relevant parameters, namely the integration and occurrence (defined as the probability on average of any two brain regions to fall in the same module during the task) parameters, exhibited stronger values for meaningless as compared with meaningful images. Our findings also revealed that the occurrence within the right frontal regions and the left occipito-temporal can help to predict the ability of the brain to rapidly recognize and name meaningful visual stimuli.

Materials and methods

Participants

Twenty healthy volunteers (ten women and ten men; mean age 23 y) with no neurological diseases participated in this study (the data of two females and 1 male participants were eliminated as EEG signals were very noisy due to electrodes impedance issues). 80 meaningful and 40 meaningless

pictures (figure S1 (stacks.iop.org/JNE/15/056022/mmedia)), taken from the Alario and Ferrand database (Alario and Ferrand 1999), were displayed on a screen as black drawings on a white background and the participants were asked to name the presented images. The same number of stimuli was used in the further analysis by selecting 40 meaningful images (the same for all subjects). E-Prime 2.0 software (Psychology Software Tools, Pittsburgh, PA) was used to display the pictures.

A typical trial started with a fixation cross that lasted 1 s, then the image was shown during 2.5 s and followed by a blank screen for 1 or 2 s (randomly selected) (figure 1(A), see also table S1 for more details about the images used in the study). The time between the picture onset and the beginning of vocalization recorded by the system was considered as naming latencies. The voice onset times were then analyzed using Praat software (Boersma and Weenink 2018). The fastest response over trials and subjects was 535 ms. Therefore, the analysis was performed from the stimulus onset up to 500 ms following the stimulus in order to avoid muscle artifacts (due to articulation). Errors in naming were discarded for the following analysis. Subjects were informed about meaningless objects presence in the experiment and were instructed to say nothing when viewing them. All participants provided a written informed consent to participate in this study which was approved by the National Ethics Committee for the Protection of Persons (CPP), Braingraph study, agreement number (2014-A01461-46), and promoter: Rennes University Hospital.

Data recording and preprocessing

A dense EEG system (EGI, Electrical Geodesic Inc., 256 electrodes) was used to record brain activity. EEG signals were sampled at 1 KHz and then band-pass filtered between 0.3 and 45 Hz. For the preprocessing, EEGLAB (Delorme and Makeig 2004) was used to reject and exclude the epochs contaminated by eye blinking (using ICA-based algorithm) and any other noise source. For some subjects, few electrodes with poor signal quality were identified. For these electrodes, the EEG signal was interpolated using signals recorded by surrounding electrodes.

In addition to dense EEGs, individual structural MRI was also available for each participant. A realistic head model was built by segmenting the anatomical MRI using Freesurfer (Fischl 2012). The individual MRI anatomy and EEGs were co-registered through identification of the same anatomical landmarks (left and right tragus and nasion). The lead field matrix was then computed for a cortical mesh of 15000 vertices using Brainstorm (Tadel *et al* 2011) and OpenMEEG (Gramfort *et al* 2010). An atlas-based approach was used to project EEG signals onto a subject-specific anatomical framework consisting of 68 cortical regions (summarized in table S2 and visualized in figure 1(B)) identified by means of the Desikan-Killiany, (Desikan *et al* 2006). Time series belonging to the same ROI were averaged after flipping the sign of sources with opposite directions.

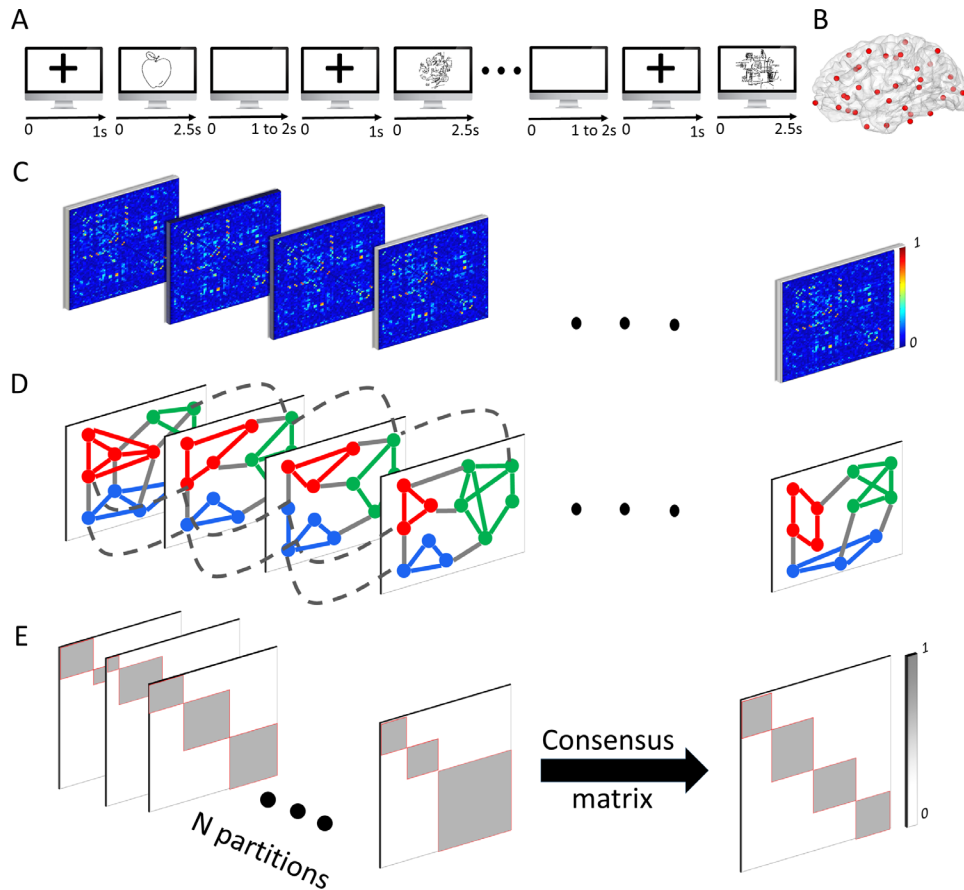


Figure 1. Experimental setup. (A) The cognitive task consisted in naming visual stimuli of two categories of: meaningful and meaningless pictures. (B) 68 cortical regions defined from the Desikan-Killiany atlas (Desikan *et al* 2006) were used. (C) Functional connectivity was computed between these 68 regional time series for a period of 500 ms using the dense EEG source connectivity method in the gamma frequency band (30–45 Hz). (D) A dynamic module detection algorithm (Bassett *et al* 2011, 2013, 2015) was used to identify network modules in each time window and to follow their evolution over time. Briefly, this algorithm constructs a modular allegiance matrix over the 100 runs at each window in which each element is 1 if two nodes are in the same module and is equal to zero otherwise. (E) All matrices are then summed for each condition to obtain the global modular allegiance matrix, whose elements indicate the fraction of time windows in which nodes have been assigned to the same module. Then a community detection algorithm is applied to obtain a ‘consensus partition’ as described in Braun *et al* (2015), which represents the common modular structure across all time windows.

Construction of the functional networks

Functional networks were constructed using the dense-EEG source connectivity method (Hassan *et al* 2014, 2015a). This method includes two main steps: (i) reconstruction of the temporal dynamics of the cortical regions from the scalp EEG signals and (ii) measurement of the functional connectivity between reconstructed regional time series. The weighted minimum norm estimate (wMNE) was used to reconstruct the cortical sources. A phase locking value (PLV) (Lachaux *et al* 1999) algorithm was then used to estimate the functional connectivity. Two versions of PLV were proposed by Lachaux *et al* (1999). The first method consists of looking at the ‘inter-trial’ phase synchrony, which provides pair-wise connectivity values at each time point. This version works only in the case of task-related paradigms and in the presence of a high number of trials. The second version consists of choosing a sliding window, adapted to the analyzed frequency band. In the case of gamma band: 30–45 Hz, the duration of the smallest time window that contains a sufficient number of cycles ($N = 5$) for PLV computation is ~ 0.133 s. As shown by Lachaux *et al*

(1999), both versions provide very similar results. In this study, we used the first version.

This choice of wMNE/PLV was supported by two comparative analyses performed in Hassan *et al* (2014, 2017) that reported the superiority of wMNE/PLV over other combinations of five inverse algorithms and five connectivity measures. Briefly, in Hassan *et al* (2017), the network identified by each of the inverse/connectivity combination used to identify cortical brain networks from scalp EEG was compared to a simulated network (ground truth). The combination that showed the highest similarity between scalp-EEG-based network and reference network (using a network similarity algorithm) was considered as the optimal combination. This was the case for the wMNE/PLV. The dense-EEG source connectivity method benefits from the intrinsically-excellent time resolution of the EEG. This lead to time-varying functional networks which spatio-temporal dynamics directly characterize the cognitive processes involved in considered task. Regarding technical details, readers can refer to Kabbara *et al* (2017, 2018) for detailed methodological description of the dense EEG source

connectivity method as computed in this paper. The inverse solutions were computed using Brainstorm (Tadel *et al* 2011).

The wMNE/PLV combination was computed in the gamma band (30–45 Hz). For each subject, this procedure yielded a set of weighted adjacency matrices describing the functional connectivity in each time window (figure 1(C)).

Finally, not all elements of the connectivity matrix reflect significant functional relationships and that a threshold should be applied to retain only the ‘true’ functional connections. Here, we adopted the approach proposed in Bassett *et al* (2011). Briefly, for each connectivity matrix A_{ij} , a p -value matrix P_{ij} was computed, based on the t -statistic. The computed p -values were corrected for multiple comparisons using the false discovery rate (FDR) approach of $p < 0.05$. All A_{ij} whose p -values P_{ij} passed the statistical FDR threshold were retained (their values remained unchanged). Otherwise, the values were set to zero (Bassett *et al* 2011) to build a thresholded weighted connectivity matrix.

Multislice network modularity

The resultant matrices were split into time-varying modules using a multislice community detection algorithm described in Mucha *et al* (2010). This algorithm consists of introducing a coupling parameter that links nodes across slices (time windows) before performing the modularity maximization procedure (figure 1(D)). This algorithm was recently applied on functional brain networks (Bassett *et al* 2011, 2013, 2015). The multislice modularity is defined as:

$$Q_{ml} = \frac{1}{2\mu} \sum_{ijlr} \left\{ \left(A_{ijl} - \gamma_l \frac{k_{il}k_{jl}}{2m_l} \right) \delta_{lr} + \delta_{ij} C_{jlr} \right\} \delta(M_{il}, M_{jr})$$

where nodes i and j are assigned to communities M_{il} and M_{jl} in layer l , respectively. A_{ijl} represents the weight of the edge between these two nodes and γ_l is the structural resolution parameter of layer l . C_{jlr} is the connection strength between node j in layer r and node j in layer l . The structural resolution parameter γ and the inter-layer coupling parameter C are usually set to 1. k_{il} is the strength of node i in layer l , the δ -function $\delta(x, y)$ is 1 if $x = y$ and 0 otherwise, $m = \frac{1}{2} \sum_{ij} A_{ij}$ and $\mu = \frac{1}{2} \sum_{jr} k_{jr}$. This produces for every brain region at every time window a modular assignment reflecting the module allegiance.

The multilayer network modularity was computed 100 times as Q may vary from run to run, due to heuristics in the algorithm: each run can produce slightly different partitions of nodes into modules (Good *et al* 2010). To deal with this problem, we computed a consensus matrix, also called ‘co-classification matrix’ (Bassett *et al* 2013, Fornito *et al* 2016) whose elements indicate the ratio of each node to be in the same module with the other nodes among these 100 partitions (figure 1(E)). Only elements in the consensus matrix higher than an appropriate random null model were taken into account, as described in Bassett *et al* (2011). Finally, by applying the Louvain algorithm (Blondel *et al* 2008) on the consensus matrix, we obtained a partition that is most representative of the network segregation. Brain regions repeatedly

classified in the same module (over the runs) will have a high weight in the consensus matrix and will more likely be assigned to the same module after applying the modularity maximization algorithm. To investigate the consistency of the modules over time, we computed a final consensus matrix (same procedure as described above) by calculating the ratio of each node to be with the other nodes in the same module, among the time windows.

Integration and occurrence metrics

To quantitatively analyze the contribution of each module during the task, first we used the integration metric as described in Bassett *et al* (2011) and Braun *et al* (2015). Integration values reflect how modules are interacting with each other. It is computed as the average number of links each node in a given module has with the nodes in the other modules.

We calculated also a new metric called occurrence (%). In our case, the occurrence defined as the probability on average of any two nodes to fall in the same module over time, from 0 to 500 ms. This metric reflects the importance of the strong (or weak) temporal interactions between any two brain regions during the cognitive task.

Software

The connectivity measures, network measures and network visualization were performed using BCT (Rubinov and Sporns 2010), EEGNET (Hassan *et al* 2015b) and BrainNet viewer (Xia *et al* 2013), respectively. The Network Community Toolbox (<http://commdetect.weebly.com/>) was used to compute the consensus matrices as well as the values provided by the integration and flexibility metrics.

Statistical test

A Wilcoxon rank sum test was used to assess the statistical difference between the functional brain networks respectively associated to meaningful and meaningless objects. The difference between the two conditions was considered as significant when the p -value was less than 0.05. The Bonferroni method was used to correct for multiple comparisons.

Results

Meaningful versus meaningless networks

For each participant, the network modularity was computed over time for both categories (meaningful and meaningless). A global consensus matrix was computed over all participants for each category, as described in the methods section. As depicted in figure 2(A), the qualitative visual inspection of the obtained matrices, indicated that both conditions have a different modular configuration in term of network integration (connections outside the square red lines) and occurrence (weights of the matrix values).

The resulting modules were projected on a 3D cortical surface, as illustrated in figure 2(B). Modules having

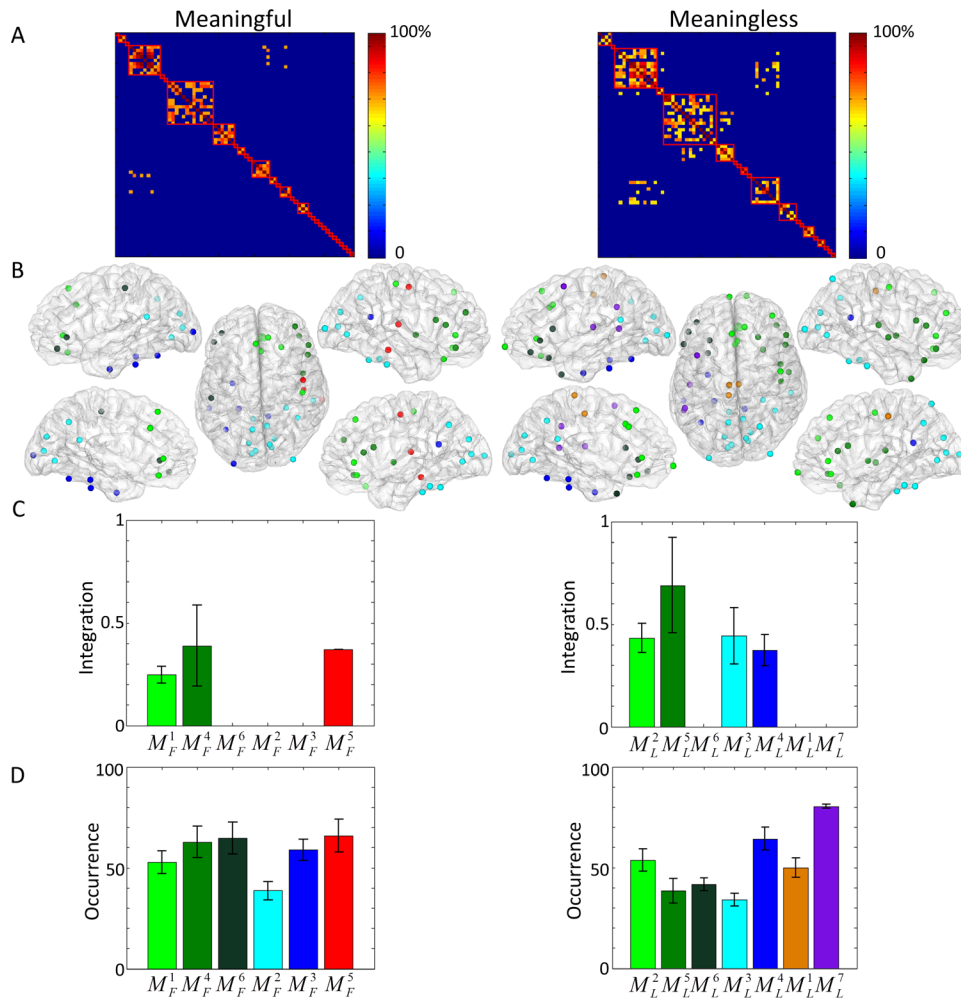


Figure 2. (A) The modular allegiance matrices for meaningful (left) and meaningless (right) conditions. (B) A mapping of the different modules identified for both conditions (6 and 7 modules for the meaningful and meaningless categories). (C) The values of integration for each module in both conditions. (D) The values of occurrence for each module in both conditions. Note that modules having similar regions in both conditions are visualized by the same color. (M_F and M_L stand for meaningful and meaningless, respectively.)

spatially-neighbor regions in both conditions are visualized by the same color and the region's names for each module are reported in table 1. To assess an average quantitative difference between the two categories, integration (figure 2(C)) and occurrence (figure 2(D)) values were computed from the final consensus matrix for each module. For both meaningful and meaningless objects, M_F^4 and M_L^5 modules located in the frontal and the temporo-frontal lobes respectively have the highest integration values. The temporo-central module M_F^5 was interacting with other modules only for meaningful objects (figure 2(C) left) while the occipital and occipito-temporal modules (M_L^3 and M_L^4) were integrated only for meaningless objects (figure 2(C) right). Concerning the occurrence values, which represent the probability of any two brain regions to fall in the same module during the task, results showed fewer differences in both conditions (figure 2(D)). Globally, the M_F^1 , M_F^4 and M_F^6 modules (located mainly in the frontal cortex) showed higher occurrence values for meaningful than meaningless frontal modules (M_L^2 , M_L^5 and M_L^6).

We then computed the statistical difference between the two conditions in term of integration and occurrence at the level

of each brain region. Significant differences were obtained at three brain regions: the left isthmus cingulate (iCC.L), the right lingual (LING.R) and the right fusiform (FUS.R) as illustrated in figure 3(A) ($p < 0.01$, *uncorrected for multiple comparisons*). Significant differences in the occurrence values were also obtained at four edges connecting the right caudal anterior cingulate (cACC.R) with the right pars opercularis (pOPER.R), the right cuneus (CUN.R) with the right pars opercularis (pOPER.R), the left lateral occipital (LOG.L) with the right pars opercularis (pOPER.R) and the right parahippocampal (paraH.R) with the right pars obitalis (pORB.R), as illustrated in figure 3(B) ($p < 0.01$, *uncorrected for multiple comparisons*). Interestingly, these occipito-frontal and temporo-frontal connections were mainly located in the right hemisphere.

Correlation between dynamic modularity and reaction time

Here, we explored the correlation that may exist between the network modularity and the participant's reaction time, available only for 12 participants and defined as the time interval between the stimulus onset and the instant when participants

Table 1. Modules obtained for both categories (meaningful and meaningless) in the consensus matrices.

Meaningful	Meaningless
M_F^1 caudalanteriorcingulate.R (cACC.R), lateralorbitofrontal.R (LOF.R), medialorbitofrontal.L/R (MOF.L/R), postcentral.R (postC.R), rostralanteriorcingulate.L/R (rACC.L/R), superiorfrontal.L/R (sFG.L/R)	M_L^2 caudalanteriorcingulate.L/R (cACC.L/R), frontalpole.L (FP.L), frontalpole.R (FP.R), medialorbitofrontal.L/R (MOF.L/R), precentral.R (preC.R), rostralanteriorcingulate.L/R (rACC.L/R), rostralmiddlefrontal (rMFG.R), superiorfrontal.L/R (sFG.L/R),
M_F^2 cuneus.L/R (CUN.L/R), fusiform.R (FUS.R), inferiortemporal.R (ITG.R), isthmuscingulate.L (iCC.L), lateraloccipital.R (LOG.R), lingual.L/R (LING.L/R), parahippocampal.R (paraH.R), pericalcarine.L/R (periCAL.L/R), precuneus.L/R (PCUN.L/R)	M_L^3 cuneus.L/R (CUN.L/R), fusiform.R (FUS.R), inferiortemporal.R (ITG.R), isthmuscingulate.L (iCC.L), lateraloccipital.L/R (LOG.L/R), lingual.L/R (LING.L/R), parahippocampal.R (paraH.R), pericalcarine.L/R (periCAL.L/R), precuneus.L/R (PCUN.L/R), superiorparietal.R (SPL.R)
M_F^3 entorhinal.L (ENT.L), fusiform.L (FUS.L), inferiortemporal.L (ITG.L), isthmuscingulate.R (iCC.R), lateraloccipital.L (LOG.L), parahippocampal.L (paraH.L)	M_L^4 entorhinal.L (ENT.L), fusiform.L (FUS.L), inferiortemporal.L (ITG.L), isthmuscingulate.R (iCC.R), parahippocampal.L (paraH.L)
M_F^4 Insula.R (INS.R), parsopercularis.R (pOPER.R), parsorbitalis.R (pORB.R), parstriangularis.R (pTRI.R), rostralmiddlefrontal.R (rMFG.R)	M_L^5 Insula.R (INS.R), lateralorbitofrontal.R (LOF.R), parsopercularis.R (pOPER.R), parsorbitalis.R (pORB.R), parstriangularis.R (pTRI.R), superiorotemporal.R (STG.R), temporalpole.R (TP.R), transversetemporal.R (TT.R)
M_F^5 middletemporal.R (MTG.R), precentral.R (preC.R), transversetemporal.R (TT.R)	M_L^6 paracentral.L (paraC.L), posteriorcingulate.L/R (PCC.L/R)
M_F^6 parsorbitalis.L (pORB.L), parstriangularis.L (pTRI.L), postcentral.L (postC.L)	M_L^7 lateralorbitofrontal.L (LOF.L), parsopercularis.L (pOPER.L), parsorbitalis.L (pORB.L), parstriangularis.L (pTRI.L), temporalpole.L (TPL)
	M_L^8 bankssts.L (BSTS.L), caudalmiddlefrontal.L (cMFG.L), supramarginal.L (SMAR.L), transversetemporal.L (TT.L)

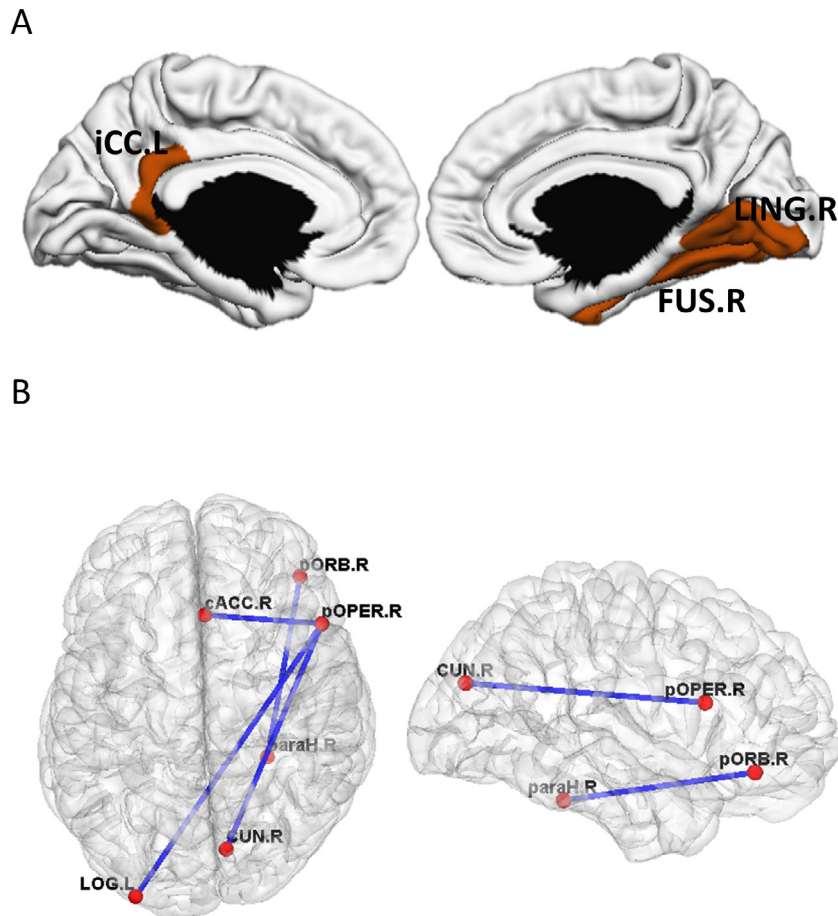


Figure 3. (A) Brain regions showing significant differences (meaningless > meaningful) in term of integration ($p < 0.01$, uncorrected for multiple comparisons). (B) Brain connections showing significant difference (meaningless > meaningful) in term of occurrence ($p < 0.01$, uncorrected for multiple comparisons). See table S2 for the full name of the reported regions.

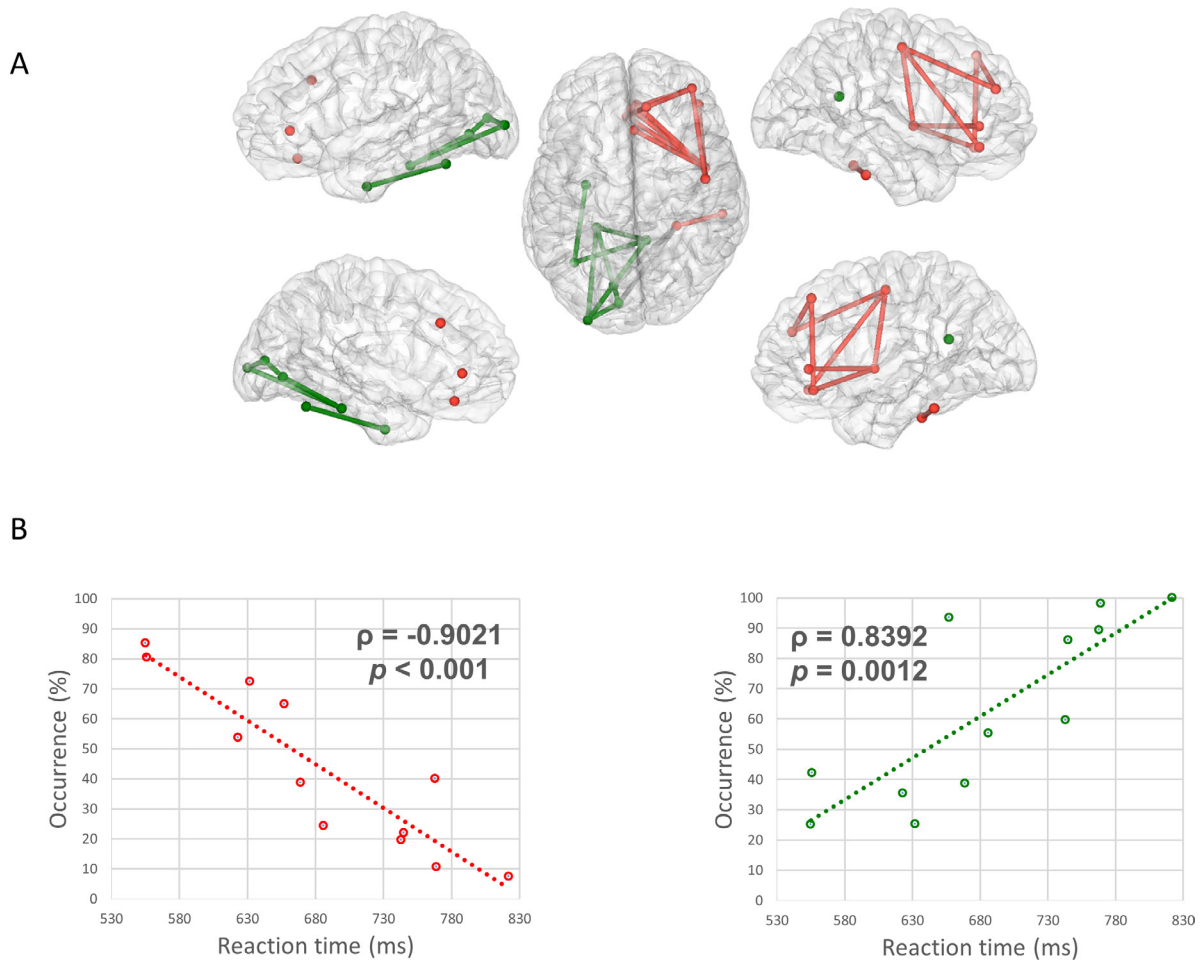


Figure 4. (A) Brain regions of 12 participants that showed significant correlation between their occurrence values and the participant's reaction time. (B) Correlation between the average occurrence over these connections and the minimal reaction time for each participant. (Note that this part was realized only on the meaningful pictures as for meaningless pictures participants were asked to say nothing and for only 12 participants as the reaction time was only available for them.)

start to name the displayed picture. We computed the values of the integration and the occurrence metrics for each region and edge, respectively. This part was realized only on the meaningful pictures as for meaningless pictures participants were asked to say nothing. Results (not shown here) revealed no significant correlation between the module's integration and the reaction times. However, the occurrence computed for each link showed positive and negative correlations at a set of connections. Figure 4(A) shows the connections where significant correlations ($p < 0.01$, *uncorrected for multiple comparisons*) between the occurrence and the reaction time were observed. The positive correlations (green lines) were mainly located at the occipito-temporal regions while the negative correlations (red lines) were mainly located at the frontal cortex. By averaging the values of those edges (their occurrence), figure 4(B) shows the strong correlations in both negative ($\rho = -0.9$, $p < 0.001$) and positive ($\rho = -0.83$, $p = 0.001$) cases.

Discussion

Emerging evidence shows that the human brain network is essentially organized into modules allowing the required adaptability to external drivers without necessarily modifying

underlying structures (Braun *et al* 2015). In a previous preliminary work (performed in a 'static' way), we showed that the network modularity could be a powerful tool to explore the overall reconfiguration of brain networks during visual object identification (Rizkallah *et al* 2016, Mheich *et al* 2017). Yet, this modular architecture is dynamic and may rapidly reshape according to external stimuli. Here, we showed that the functional connectivity during object recognition is dynamically organized into adapting modules and that this adapting modular architecture could be related to the 'meaning' of the visual stimuli. By quantifying these dynamic modules, we showed that network modularity (in term of occurrence) can predict the speed of object recognition and naming. Results are further discussed hereafter.

Brain network modularity and cognitive functions

The modular architecture of the human brain networks was reported using various neuroimaging techniques and at different scales (Sporns and Betzel 2016). It was firstly revealed on large scale structure network by Hagmann *et al* (2008). Regarding the functional role of brain network modules, numerous studies revealed that the brain is organized into a set

of modules of functionally interconnected regions (Meunier *et al* 2009b, Power *et al* 2011). The modular architecture of the human brain was shown to be related to individual cognitive state (Andric and Hasson 2015), development (Meunier *et al* 2009a) and brain diseases (Fornito *et al* 2015). In addition, it was revealed that network modular architecture provides more flexible learning and promotes functional specialization (Bassett *et al* 2015, Sporns and Betzel 2016).

Here, we investigated the possible functional role of brain network modularity during recognition (and naming) of meaningful and meaningless images. We showed that the two conditions have different modular organization mainly in the module's node integration and module's edge occurrence.

Our findings showed higher integration and occurrence values for meaningless compared to meaningful images. Higher integration for meaningless images was observed at right lingual and right fusiform regions. Interestingly, these regions are known for their essential role in visual processing (Cai *et al* 2015). For instance, in a PET study aimed at identifying brain structures involved in animal picture identification by comparison to meaningless shapes, results showed a primary activation of the lingual gyrus and the fusiform gyrus (Perani *et al* 1999). Our results also suggest that the left isthmus also shows significantly different integration between the two conditions (meaningless > meaningful). A possible explanation relates to the role of this region in the regulation of the focus of attention (Leech and Sharp 2014).

The increase in module integration for meaningless objects can be interpreted as an enhancement of communication between nodes, due to multiple attempts to match the detected image characteristics present in the visual stimuli with object representations already encoded in the memory involving the ventral visual pathway. Indeed, the complex shape information of scrambled images cannot be instantly linked to a recognized object in the brain database. Thus, searching for coherent signal (corresponding image) through visual pathway would increase module communication from the low/intermediate (image reconstruction) to high level of visual processing (image identification).

In terms of occurrence, the occipito-frontal connections were found to be higher for meaningless than meaningful objects. As the occurrence is defined as the probability of two brain regions to stay in the same module during the task, thus it also provides a measure of the duration of communication between these two regions. A possible interpretation of higher occurrence values is that the coherent communication in networks involved in object identification (visual pathway) and decision making in case of unclear choice (prefrontal cortex) is not immediate for meaningless images. Indeed, the difficulty to identify and the unsuccessful multiple trials to match the image might increase the number of times the brain regions inter-communicate, and thus the occurrence values. Interestingly, denser scalp-EEG networks for meaningless images compared to meaningful images were also reported in Gruber and Müller (2005). The lateralization of the connections during object recognition was also reported previously and several clinical studies linked the right hemisphere with object recognition. For instance, studies showed that patients

with right-hemisphere disease (RHD) performed significantly worse than subjects with left-hemisphere disease (LHD) when asked to discriminate between faces, to discriminate between emotional faces, and to name emotional scenes (DeKosky *et al* 1980).

Methodological issues

First, we computed the functional networks at the EEG gamma band (30–45 Hz). This choice was supported by previous studies in the field of object recognition and naming. These studies reported that gamma is the most involved frequency band in the information processing during this cognitive task (Liljeström *et al* 2015, Hassan *et al* 2015a, Rodriguez *et al* 1999). Nevertheless, other frequency bands (and some frequency-frequency couplings), can be indeed involved in other aspects of this task such as the memory process. This issue is however beyond the scope of this study.

Second, the muscle artifact in the gamma band is a serious methodological issue. Here, we have reduced the effect of the muscle artifacts by (i) asking the participants to not moving as much as possible (ii) limiting our network-based dynamic analysis between the onset (presentation of the visual stimuli) to the moment before the fastest responses, in order to avoid the muscle artifacts due to articulation (naming) and (iii) selecting the low gamma band (<45 Hz) which is less contaminated by muscle artifacts comparing to high gamma (>50 Hz).

Third, although significant results were obtained for region-wise analysis (integration) or edges-wise analysis (occurrence), these results did not resist the correction for the multiple comparisons. Thus, results should be interpreted with caution. Nevertheless, the results showed very strong correlations (>0.8) values between the network metrics (mainly the occurrence) and the reaction time.

Fourth, a variety of thresholding methods are available, but none is free of bias. For example, one could apply a threshold that ensures only the top 10% of connections across a sample of individuals are retained. In this case, it is recommended to repeat analyses across a range of threshold (values and approaches) to ensure that any results obtained are robust to this methodological parameter. Here we adopted the automatic threshold method used in Bassett *et al* (2011), where authors dealt also with the dynamics of functional brain networks. The main advantage of this method is that it is based on statistical tests and not an arbitrary choice of the threshold value.

Fifth, it is important to keep in mind that measuring the functional connectivity is generally corrupted by the volume conduction problem, a known problem regarding functional couplings at the scalp level (Schoffelen and Gross 2009, Brookes *et al* 2014). Therefore, connectivity analysis at source level was shown to reduce the effect of volume conduction as connectivity methods are applied to 'local' time-series (analogous to local field potentials) generated by cortical neuronal assemblies modelled as current dipole sources. Nevertheless, these so-called 'mixing effects' can also occur in the source space but can be reduced by an appropriate choice of connectivity measures. Indeed, false functional couplings can

be generated by some connectivity methods when applied to mixed signals such as estimated brain sources. To address this issue, a number of methods were developed based on the rejection of zero-lag correlation. In particular, ‘unmixing’ methods, called ‘leakage correction’ (including the orthogonalization approach), have been reported which force the reconstructed signals to have zero cross-correlation at lag zero (Colclough et al 2015). Although handling this problem -theoretically- helps interpretation, a very recent study showed that the current correction methods also produce erroneous human connectomes under very broad conditions (Pascual-Marqui et al 2017). In addition, several experimental studies reported the presence of zero-lag corrections in the human brain. We believe that there is no ideal solution yet for this issue and that further methodological efforts are needed to completely solve the spatial leakage problem.

Behavioral significance of network modularity

Several functional network modularity-based metrics have previously been linked to many behavioral modifications in brain network dynamics in response to cognitive difficulties by predicting individual differences in learning (Bassett et al 2011), working memory (Braun et al 2015) and other cognitive tasks (Cole et al 2013, Mattar et al 2016). Here we showed that the network occurrence, essentially for prefrontal brain regions, was negatively correlated with the reaction time (defined as the time from the stimulus onset to the instant when participant starts the naming process). On the other side, a positive correlation between the occurrence values of occipito-temporal connections was observed with the reaction time.

The occurrence values, that reflect the duration of communication between brain regions, increased in the occipito-temporal ventral visual pathway (including lingual cortex, lateral occipital cortex, entorhinal cortex, fusiform gyrus and parahippocampal cortex) which is known to be involved in the categorization and identification of the visual stimuli (Clarke and Tyler 2015), along with the reaction time. This result suggests that the longer it takes to identify the object, the longer is the occurrence in the occipito-temporal pathway and the longer is the reaction time.

Conversely, an immediate recognition and identification of a visual stimuli is associated with a decrease of occurrence values between brain regions involved in task-conflict (anterior cingulate (Shenhav et al 2014)) and decisions associated to image identification such as the frontal cortex (namely the superior frontal cortex, rostral middle frontal cortex, medial orbitofrontal cortex and precentral cortex) (Gilbert and Li 2013). This result suggests a decreased processing time of cognitive information as soon as the image is identified; the participant is ready to name the proper object and consequently a shorter reaction time. It is noteworthy that these results and interpretations should be taken with some cautions as the number of subjects is relatively small ($N = 12$).

Finally, this prediction of the visual object recognition time can be easily extended not only to other cognitive tasks using

other modalities (auditory, motor) but also to understand the possible modifications of network dynamics in patients with brain disorders, an issue that was recently discussed using other network modularity metrics (Mattar et al 2016, Zhang et al 2016).

Acknowledgment

This work was supported by the Rennes University Hospital (COREC Project named BrainGraph, 2015–17). The work has received a French government support granted to the Comin-Labs excellence laboratory and managed by the National Research Agency in the ‘Investing for the Future’ program under reference ANR-10-LABX-07-01. This work was also supported by the European Research Council under the European Union’s Seventh Framework Programme (FP7/2007–2013)/ERC grant agreement no 290901.

ORCID iDs

M Hassan  <https://orcid.org/0000-0003-0307-5086>

References

- Alario F X and Ferrand L 1999 A set of 400 pictures standardized for French: norms for name agreement, image agreement, familiarity, visual complexity, image variability, and age of acquisition *Behav. Res. Methods* **31** 531–52
- Andric M and Hasson U 2015 Global features of functional brain networks change with contextual disorder *NeuroImage* **117** 103–13
- Bassett D S, Porter M A, Wymbs N F, Grafton S T, Carlson J M and Mucha P J 2013 Robust detection of dynamic community structure in networks *Chaos* **23** 013142
- Bassett D S, Wymbs N F, Porter M A, Mucha P J, Carlson J M and Grafton S T 2011 Dynamic reconfiguration of human brain networks during learning *Proc. Natl Acad. Sci.* **108** 7641–6
- Bassett D S, Yang M, Wymbs N F and Grafton S T 2015 Learning-induced autonomy of sensorimotor systems *Nat. Neurosci.* **18** 744–51
- Bertolero M A, Yeo B T and D’Esposito M 2015 The modular and integrative functional architecture of the human brain *Proc. Natl Acad. Sci.* **112** E6798–807
- Blondel V D, Guillaume J-L, Lambiotte R and Lefebvre E 2008 Fast unfolding of communities in large networks *J. Stat. Mech.* **P10008**
- Boersma P and Weenink D 2018 Praat: doing phonetics by computer. Version 6.0.37 (<http://www.praat.org/>, retrieved 14 March 2018)
- Braun U, Schäfer A, Walter H, Erk S, Romanczuk-Seiferth N, Haddad L, Schweiger J I, Grimm O, Heinz A and Tost H 2015 Dynamic reconfiguration of frontal brain networks during executive cognition in humans *Proc. Natl Acad. Sci.* **112** 11678–83
- Brookes M J, Woolrich M W and Price D 2014 An introduction to MEG connectivity measurements *Magnetoencephalography* (Berlin: Springer) pp 321–58
- Cai S, Chong T, Zhang Y, Li J, von Deneen K M, Ren J, Dong M, Huang L and Alzheimer’s Disease Neuroimaging Initiative 2015 Altered functional connectivity of fusiform gyrus in subjects with amnesic mild cognitive impairment: a resting-state fMRI study *Front. Hum. Neurosci.* **9** 471

- Clarke A and Tyler L K 2015 Understanding what we see: how we derive meaning from vision *Trends Cogn. Sci.* **19** 677–87
- Colclough G, Brookes M, Smith S and Woolrich M 2015 A symmetric multivariate leakage correction for MEG connectomes *NeuroImage* **117** 439–48
- Cole M W, Reynolds J R, Power J D, Repovs G, Anticevic A and Braver T S 2013 Multi-task connectivity reveals flexible hubs for adaptive task control *Nat. Neurosci.* **16** 1348–55
- DeKosky S T, Heilman K M, Bowers D and Valenstein E 1980 Recognition and discrimination of emotional faces and pictures *Brain Lang.* **9** 206–14
- Delorme A and Makeig S 2004 EEGLAB: an open source toolbox for analysis of single-trial EEG dynamics including independent component analysis *J. Neurosci. Methods* **134** 9–21
- Desikan R S, Ségonne F, Fischl B, Quinn B T, Dickerson B C, Blacker D, Buckner R L, Dale A M, Maguire R P and Hyman B T 2006 An automated labeling system for subdividing the human cerebral cortex on MRI scans into gyral based regions of interest *NeuroImage* **31** 968–80
- DiCarlo J J, Zoccolan D and Rust N C 2012 How does the brain solve visual object recognition? *Neuron* **73** 415–34
- Fischl B 2012 FreeSurfer *NeuroImage* **62** 774–81
- Fornito A, Zalesky A and Breakspear M 2015 The connectomics of brain disorders *Nat. Rev. Neurosci.* **16** 159–72
- Fornito A, Zalesky A and Bullmore E 2016 *Fundamentals of Brain Network Analysis* (New York: Academic)
- Gilbert C D and Li W 2013 Top-down influences on visual processing *Nat. Rev. Neurosci.* **14** 350–63
- Good B H, de Montjoye Y-A and Clauset A 2010 Performance of modularity maximization in practical contexts *Phys. Rev. E* **81** 046106
- Gramfort A, Papadopoulos T, Olivi E and Clerc M 2010 OpenMEEG: opensource software for quasistatic bioelectromagnetics *Biomed. Eng. OnLine* **9** 45
- Gruber T and Müller M M 2005 Oscillatory brain activity dissociates between associative stimulus content in a repetition priming task in the human EEG *Cerebral Cortex* **15** 109–16
- Hagmann P, Cammoun L, Gigandet X, Meuli R, Honey C J, Wedeen V J and Sporns O 2008 Mapping the structural core of human cerebral cortex *PLoS Biol.* **6** e159
- Hassan M, Benquet P, Biraben A, Berrou C, Dufor O and Wendling F 2015a Dynamic reorganization of functional brain networks during picture naming *Cortex* **73** 276–88
- Hassan M, Dufor O, Merlet I, Berrou C and Wendling F 2014 EEG source connectivity analysis: from dense array recordings to brain networks *PLoS One* **9** e105041
- Hassan M, Merlet I, Mheich A, Kabbara A, Biraben A, Nica A and Wendling F 2017 Identification of interictal epileptic networks from dense-EEG *Brain Topogr.* **30** 60–76
- Hassan M, Shamas M, Khalil M, El Falou W and Wendling F 2015b EEGNET: an open source tool for analyzing and visualizing M/EEG connectome *PLoS One* **10** e0138297
- Hassan M and Wendling F 2018 Electroencephalography source connectivity: aiming for high resolution of brain networks in time and space *IEEE Signal Process. Mag.* **35** 81–96
- Kabbara A, Eid H, El Falou W, Khalil M, Wendling F and Hassan M 2018 Reduced integration and improved segregation of functional brain networks in Alzheimer's disease *J. Neural Eng.* **15** 026023
- Kabbara A, Falou W E, Khalil M, Wendling F and Hassan M 2017 The dynamic functional core network of the human brain at rest *Sci. Rep.* **7** 2936
- Lachaux J-P, Rodriguez E, Martinerie J and Varela F J 1999 Measuring phase synchrony in brain signals *Hum. Brain Mapp.* **8** 194–208
- Leech R and Sharp D J 2014 The role of the posterior cingulate cortex in cognition and disease *Brain* **137** 12–32
- Liljeström M, Kujala J, Stevenson C and Salmelin R 2015 Dynamic reconfiguration of the language network preceding onset of speech in picture naming *Hum. Brain Mapp.* **36** 1202–16
- Mattar M G, Betzel R F and Bassett D S 2016 The flexible brain *Brain* **139** 2110–2
- Meunier D, Achard S, Morcom A and Bullmore E 2009a Age-related changes in modular organization of human brain functional networks *NeuroImage* **44** 715–23
- Meunier D, Lambiotte R, Fornito A, Ersche K D and Bullmore E T 2009b Hierarchical modularity in human brain functional networks *Front. Neuroinf.* **3** 37
- Mheich A, Hassan M, Khalil M, Gripon V, Dufor O and Wendling F 2017 SimiNet: a novel method for quantifying brain network similarity *IEEE Trans. Pattern Anal. Mach. Intell.* pp 2238–49
- Mucha P J, Richardson T, Macon K, Porter M A and Onnela J-P 2010 Community structure in time-dependent, multiscale, and multiplex networks *Science* **328** 876–8
- Pascual-Marqui R D, Biscay R J, Bosch-Bayard J, Faber P, Kinoshita T, Kochi K, Milz P, Nishida K and Yoshimura M 2017 Innovations orthogonalization: a solution to the major pitfalls of EEG/MEG 'leakage correction' (arXiv:1708.05931)
- Perani D, Schnur T, Tettamanti M, Cappa S F and Fazio F 1999 Word and picture matching: a PET study of semantic category effects *Neuropsychologia* **37** 293–306
- Power J D, Cohen A L, Nelson S M, Wig G S, Barnes K A, Church J A, Vogel A C, Laumann T O, Miezin F M and Schlaggar B L 2011 Functional network organization of the human brain *Neuron* **72** 665–78
- Rizkallah J, Benquet P, Wendling F, Khalil M, Mheich A, Dufor O and Hassan M 2016 Brain network modules of meaningful and meaningless objects *3rd Middle East Conf. on Biomedical Engineering (MECBME)* (IEEE) pp 34–7
- Rodriguez E, George N, Lachaux J-P, Martinerie J, Renault B and Varela F J 1999 Perception's shadow: long-distance synchronization of human brain activity *Nature* **397** 430–3
- Rubinov M and Sporns O 2010 Complex network measures of brain connectivity: uses and interpretations *NeuroImage* **52** 1059–69
- Schoffelen J M and Gross J 2009 Source connectivity analysis with MEG and EEG *Hum. Brain Mapp.* **30** 1857–65
- Shenhav A, Straccia M A, Cohen J D and Botvinick M M 2014 Anterior cingulate engagement in a foraging context reflects choice difficulty, not foraging value *Nat. Neurosci.* **17** 1249–54
- Sporns O and Betzel R F 2016 Modular brain networks *Annu. Rev. Psychol.* **67** 613–40
- Tadel F, Baillet S, Mosher J C, Pantazis D and Leahy R M 2011 Brainstorm: a user-friendly application for MEG/EEG analysis *Comput. Intell. Neurosci.* **2011** 8
- Xia M, Wang J and He Y 2013 BrainNet viewer: a network visualization tool for human brain connectomics *PLoS One* **8** e68910
- Zhang J, Cheng W, Liu Z, Zhang K, Lei X, Yao Y, Becker B, Liu Y, Kendrick K M and Lu G 2016 Neural, electrophysiological and anatomical basis of brain-network variability and its characteristic changes in mental disorders *Brain* **139** 2307–21

Study 1 Supplementary Materials: Dynamic reshaping of functional brain networks during visual object recognition

Dynamic reshaping of functional brain networks during visual object recognition

Rizkallah J.^{1,2}, Benquet P.¹, Kabbara A.^{1,2}, Dufor O.⁴, Wendling F.^{1*}, Hassan M.^{1*}

¹ Univ Rennes, LTSI, F-35000 Rennes, France

² AZM center-EDST, Lebanese University, Tripoli, Lebanon

³ IMT Atlantique Bretagne Pays de la Loire, UMR CNRS Lab-STICC, Brest, France

* These authors contributed equally to this work.

Corresponding author:

Mahmoud Hassan

mahmoud.hassan@univ-rennes1.fr



Figure S1: The meaningful (left) and meaningless/scrambled (right) images used in the study (Alario and Ferrand, 1999).

	N-A	Im-A		Fam		Im-C		Im-V		A-o-A		Freq
	%	M	SD	M	SD	M	SD	M	SD	M	SD	
M	96,86	3,65	0,86	2,67	0,81	3,2	0,64	2,90	0,92	2,21	0,81	55,7
Min	86	1,23	0,34	1,07	0,18	1	0	2,03	0,32	1,12	0,33	0
Max	100	4,87	1,31	4,97	1,32	5	1,04	4,5	1,32	3,65	1,16	892,0

Table S1: mean (**M**), min and max scores for the list of our items from the 400 pictures database standardize for French of Alario & Ferrand 1999. **N-A**: Naming Agreement, **Im-A**: Image agreement, **Fam**: Familiarity, **Im-C**: Image Complexity, **Im-V**: Image variability, **A-o-A**: Age of Acquisition, **Freq**: **Frequency**. Details about what is measured can be found in (Alario and Ferrand, 1999) and <http://www.lexique.org>

	Acronyms	Name		Acronyms	Name
Occipital	LING L	lingual L	Frontal	sFG L	superiorfrontal L
	LING R	lingual R		sFG R	superiorfrontal R
	periCAL L	pericalcarine L		rMFG L	rostralmiddlefrontal L
	periCAL R	pericalcarine R		rMFG R	rostralmiddlefrontal R
	CUN L	cuneus L		cMFG L	caudalmiddlefrontal L
	CUN R	cuneus R		cMFG R	caudalmiddlefrontal R
	LOG L	lateraloccipital L		pOPER L	parsopercularis L
	LOG R	lateraloccipital R		pOPER R	parsopercularis R
Temporal	ENT L	entorhinal L	pTRI L	parstriangularis L	
	ENT R	entorhinal R	pTRI R	parstriangularis R	
	paraH L	parahippocampal L	pORB L	parsorbitalis L	
	paraH R	parahippocampal R	pORB R	parsorbitalis R	
	TP L	temporalpole L	LOF L	lateralorbitofrontal L	
	TP R	temporalpole R	LOF R	lateralorbitofrontal R	
	FUS R	fusiform R	MOF L	medialorbitofrontal L	
	FUS L	fusiform L	MOF R	medialorbitofrontal R	
	STG L	superiortemporal L	FP L	frontalpole L	
	STG R	superiortemporal R	FP R	frontalpole R	
	ITG L	inferiortemporal L	Central	preC L	precentral L
	ITG R	inferiortemporal R		preC R	precentral R
	MTG L	middletemporal L		paraC L	paracentral L
	MTG R	middletemporal R		paraC R	paracentral R
	TT L	transversetemporal L		postC L	postcentral L
	TT R	transversetemporal R		postC R	postcentral R
BSTS L	bankssts L	rACC L		rostralanteriorcingulate L	
BSTS R	bankssts R	rACC R		rostralanteriorcingulate R	
Parietal	SMAR L	supramarginal L	Cingulate	cACC L	cAUDalanteriorcingulate L
	SMAR R	supramarginal R		cACC R	cAUDalanteriorcingulate R
	SPL L	superiorparietal L		PCC L	posteriorcingulate L
	SPL R	superiorparietal R		PCC R	posteriorcingulate R
	IPL L	inferiorparietal L		iCC L	isthmuscingulate L
	IPL R	inferiorparietal R		iCC R	isthmuscingulate R
	PCUN L	precuneus L	INS L	insula L	
	PCUN R	precuneus R	INS R	insula R	

Table S2. A summary of the 68 ROIs used in our study as derived from the Desikan-Killiany atlas (Desikan et al., 2006).

References

Alario, F.X., Ferrand, L., 1999. A set of 400 pictures standardized for French: Norms for name agreement, image agreement, familiarity, visual complexity, image variability, and age of acquisition. *Behavior Research Methods*. 31, 531-552.

Desikan, R.S., et al., 2006. An automated labeling system for subdividing the human cerebral cortex on MRI scans into gyral based regions of interest. *Neuroimage*. 31, 968-980.

Study 2: The effect of removing zero-lag functional connections on EEG-source space networks at rest

J. Rizkallah, H. Amoud, M. Fraschini, F. Wendling, M. Hassan

Under revision in: Brain Topography

Objectives: Magneto/Electro-encephalography (M/EEG) source connectivity is an emerging approach to estimate brain networks with high time/space resolution. However, this method is still immature and several pitfalls can affect its accuracy in reconstructing brain networks at the source level, such as the source leakage problem.

Methods: Here, our aim was to evaluate the functional connectivity (FC) methods' effect on M/EEG-source space networks at rest. Two main families of FC methods were tested: i) FC methods that do not remove zero-lag connectivity including Phase Locking Value (PLV) and Amplitude Envelope Correlation (AEC) and ii) FC methods that remove zero-lag connections such as Phase Lag Index (PLI) and orthogonalisation approaches combined with PLV (PLV_{Col} and PLV_{Pas}) and AEC (AEC_{Col} and AEC_{Pas}). Methods were evaluated on resting state dense-EEG signals recorded from 27 healthy participants and MEG data collected from 44 participants (from the Human Connectome Project). Networks obtained by each FC method were compared with fMRI networks (from the Human Connectome Project, N=487).

Results: Results showed that PLV and AEC networks were significantly correlated with fMRI, while other methods were not. These observations are consistent for all EEG frequency bands and for different FC matrices threshold. Our main message is to be careful when selecting FC methods, mainly those that remove zero-lag connections, as they can affect the network characteristics. More comparative studies (based on simulation and real data) are needed to make EEG source connectivity a mature technique that can address questions in cognitive and clinical neuroscience.

Key words: electroencephalography, magnetoencephalography, functional brain networks, connectivity measures, electrodes density

The effect of removing zero-lag functional connections on EEG-source space networks at rest

Jennifer Rizkallah^{1,2}, Hassan Amoud², Matteo Frascini³, Fabrice Wendling¹ and Mahmoud Hassan¹

¹ Univ Rennes, LTSI, F-35000 Rennes, France

² Azm Center for Research in Biotechnology and its Application, EDST, Lebanese University, Lebanon

³ Department of Electrical and Electronic Engineering, University of Cagliari, Piazza D'armi, Cagliari, I-09123, Italy

* Corresponding author: jennifer.rizkallah.jr@gmail.com

Abstract

Electro/magneto-encephalography (EEG/MEG) source connectivity is an emerging approach to estimate brain networks with high time/space resolution. Here, we aim to evaluate the functional connectivity (FC) methods effect on M/EEG-source space networks at rest. Two main FC families are tested: i) FC methods that do not remove zero-lag connectivity including Phase Locking Value (*PLV*) and Amplitude Envelope Correlation (*AEC*) and ii) FC methods that remove zero-lag connections such as Phase Lag Index (*PLI*) and two orthogonalisation approaches combined with *PLV* (*PLV_{Col}*, *PLV_{Pas}*) and *AEC* (*AEC_{Col}*, *AEC_{Pas}*). Methods are evaluated on resting state high density EEG signals recorded from 27 healthy participants and MEG data collected from 44 participants (from the Human Connectome Project). Networks obtained by each FC method are compared with fMRI networks (from the Human Connectome Project, N=487). Results show low correlations for all FC methods, however *PLV* and *AEC* networks are significantly correlated with fMRI networks, while other methods are not. These observations are consistent for all EEG frequency bands and for different FC matrices threshold. Our main message is to be careful when selecting FC methods, mainly those that remove zero-lag connections as they can affect the network characteristics. More comparative studies (based on simulation and real data) are needed to make M/EEG source connectivity a mature technique that can address questions in cognitive and clinical neuroscience.

Keywords:

electroencephalography, magnetoencephalography, functional brain networks, connectivity measures

Introduction

Electro/magneto-encephalography (EEG/MEG) source-space connectivity is a unique non-invasive technique, which enables the tracking of large-scale brain network dynamics on a sub-second time-scale (Schoffelen and Gross 2009, Hassan and Wendling 2018, O'Neill, Tewarie et al. 2018). Benefiting from the excellent time resolution of the M/EEG (sub-millisecond), the method consists of identifying brain networks in the cortical space through sensor-level signals. However, several methodological choices should be carefully accounted for to avoid pitfalls.

In this regard, the spatial leakage (presence of spurious connections) was considered as one of the main challenges that affects the accuracy of the M/EEG source-space networks. This leakage effect was shown to lead to false positive observations: artificial interactions caused directly by signal mixing regardless of whether true connections are present and spurious interactions, also known as ghost interactions, arising indirectly from the spread of signals from true interacting sources to nearby false loci (Palva, Wang et al. 2018, Wang, Lobier et al. 2018). Source signals are spread by mixing to produce artificial synchronization and the true interactions are mirrored in several spurious interactions (Palva and Palva 2012). To deal with this problem, most existing approaches are based on the hypothesis that leakage generates inflated connectivity between estimated sources, which manifests as zero-phase-lag correlations. Thus, these methods dealt with the leakage problem by removing the zero lag connections (Nolte, Bai et al. 2004, Stam, Nolte et al. 2007) or adopting orthogonalisation-based approach (Brookes, Woolrich et al. 2012, Hipp, Hawellek et al. 2012, Pascual-Marqui, Biscay et al. 2017).

Several studies have been conducted to explore the reliability of M/EEG resting-state functional connectivity (FC) methods (De Vico Fallani, Richiardi et al. 2014, Bastos and Schoffelen 2016) (Liuzzi, Gascoyne et al. 2017) (Maldjian, Davenport et al. 2014) (Colclough, Woolrich et al. 2016). Globally, the MEG-based studies showed good consistency between FC methods to produce the population's connectivity pattern and intra/inter subjects variability. Concerning the EEG-based analyses, methods were first compared at the sensor-space (Hardmeier, Hatz et al. 2014) or comparing functional and effective metrics at the source-space (Mahjoory, Nikulin et al. 2017).

Here we compare two families of functional connectivity (FC) methods: i) the FC methods that do not remove the zero-lag-phase connectivity including the Phase Locking Value (*PLV*) and the Amplitude Envelope Correlation (*AEC*) and ii) the FC methods that remove the zero-lag connections such as the Phase Lag Index (*PLI*) and two orthogonalisation approaches developed by (Colclough, Brookes et al. 2015) and (Pascual-

Marqui, Biscay et al. 2017) were combined with *PLV* (PLV_{Col} , PLV_{Pas}) and *AEC* (AEC_{Col} , AEC_{Pas}). Networks obtained by each method were compared with the networks obtained using fMRI (HCP database, N=487) chosen as a reference.

Materials and Methods

Participants

High density EEG recordings (256 channels, EGI, Electrical Geodesic Inc.) were collected from thirty healthy participants (16 women and 14 men; mean age, 38 y). Experiments were performed in accordance with the relevant guidelines and regulations of the National Ethics Committee for the Protection of Persons (CPP), (BrainGraph study, agreement number 2014-A01461-46, promoter: Rennes University Hospital), which approved all the experimental protocol and procedures. All participants in the study provided written informed consents. Participants were asked to relax for 10 minutes with their eyes closed during the acquisition without falling asleep.

Data acquisition and preprocessing

EEG signals were sampled at 1000 Hz, band-pass filtered within 0.1–45 Hz, and segmented into non-overlapping 40 s long epochs (Chu, Kramer et al. 2012, Fraschini, Demuru et al. 2016). Electrodes with poor signal quality (amplitude $> 100 \mu\text{V}$ or $< -100 \mu\text{V}$) have been identified and interpolated using signals recorded by surrounding electrodes. Segments that have more than 20 electrodes interpolated have been excluded from the analysis. Three clean epochs per subject were then used for source estimation. Three subject was excluded from the study due to noisy data.

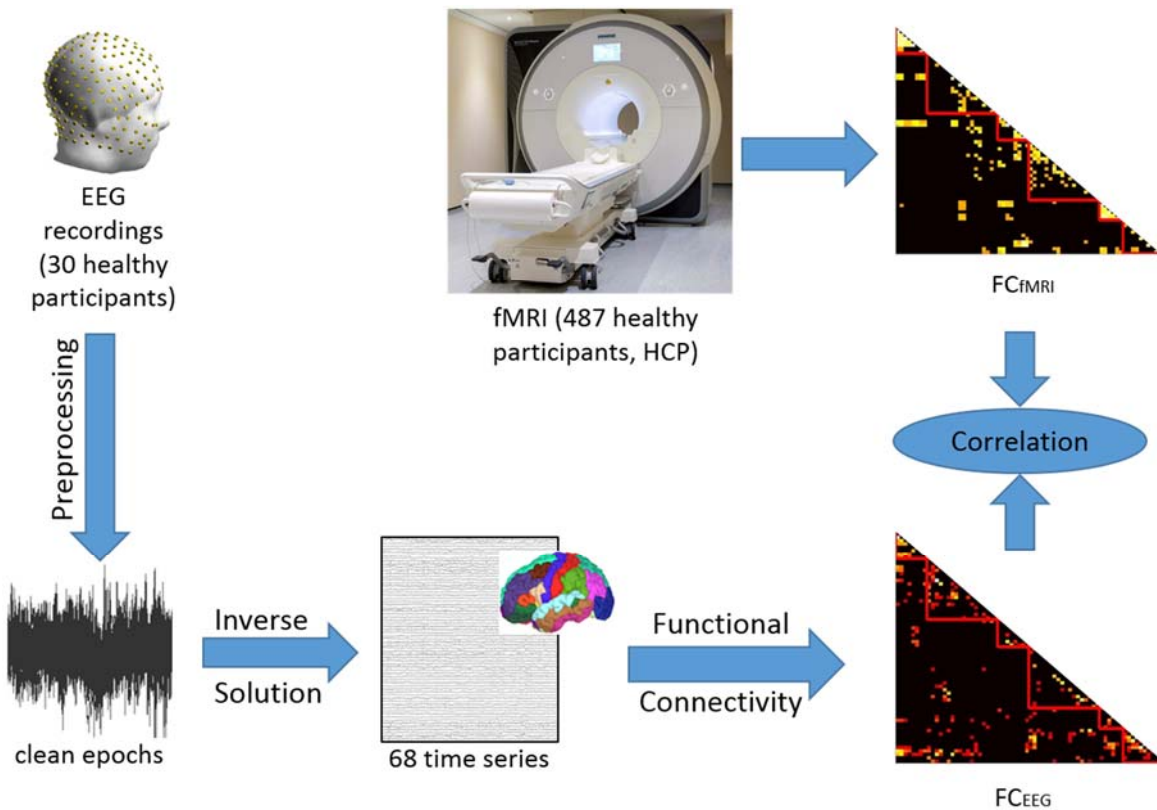


Fig.1 Study pipeline. EEG recordings were preprocessed and clean EEG epochs were used to solve the inverse problem using wMNE. Statistical couplings were then computed between the reconstructed sources using different methods (*PLV*, *AEC*, *PLI*, *PLV_{Col}*, *AEC_{Col}*, *PLV_{Pas}* and *AEC_{Pas}*). Then, the identified matrices were compared with the fMRI functional connectivity matrix obtained from HCP. Abbreviations: EEG: electroencephalogram; wMNE: weighted Minimum Norm Estimate; PLV: phase locking value; AEC: amplitude envelope correlation; PLI: phase lag index; fMRI: functional magnetic resonance imaging; HCP: human connectome project

Estimation of regional time series

First, the MRI template “Colin27” (Holmes, Hoge et al. 1998) and EEG channel locations were co-registered using Brainstorm (Tadel, Baillet et al. 2011). The lead field matrix was then computed for a cortical mesh of 15000 vertices using OpenMEEG (Gramfort, Olivi et al. 2010). The noise covariance matrix was calculated using a long segment of EEG data at rest, as recommended in (Tadel, Baillet et al. 2011). An atlas-based approach was used to project EEG signals onto an anatomical framework consisting of 68 cortical regions identified by means of the Desikan-Killiany atlas (Desikan, Ségonne et al. 2006). To reconstruct the regional time series, we used the weighted Minimum Norm Estimate (wMNE), widely used in the context of EEG source localization (Hauk 2004, Gramfort, Kowalski et al. 2012, Hassan, Benquet et al. 2015, Kabbara, Falou et al. 2017, Rizkallah, Benquet et al. 2018) and showed higher performance than other algorithms in several comparative studies (Hassan, Dufor et al. 2014, Hassan, Merlet et al. 2016). Each regional time-series correspond to the average of number of vertices after flipping the sign of sources with opposite directions. The regional time series were then band-passed filtered using zero-phase forward and reverse digital IIR filtering in

the different EEG frequency bands: Delta [0.5-4 Hz], Theta [4-8 Hz], alpha [8-13 Hz], beta [13-30 Hz] and gamma [30-45 Hz]. Results are presented in beta band, in which previous studies have reported its importance in driving large-scale spontaneous neuronal interactions (Brookes, Woolrich et al. 2011, de Pasquale, Della Penna et al. 2012), results for other frequency bands are presented in the supplementary materials. Finally, functional networks were computed using EEG source connectivity method (Schoffelen and Gross 2009, Sakkalis 2011, Hassan, Dufor et al. 2014, Hassan, Benquet et al. 2015, Rizkallah, Benquet et al. 2018) by measuring the functional connectivity between the reconstructed regional time series (Fig.1).

Connectivity measures

The functional connectivity analysis was performed by computing pair-wise statistical interdependence between regional time series using:

1) Phase locking value (PLV)

The phase locking value between two signals x and y is defined as (Lachaux, Rodriguez et al. 1999):

$$PLV(t) = \left| \frac{1}{\delta} \int_{t-\delta/2}^{t+\delta/2} e^{j(\varphi_y(t) - \varphi_x(t))} d\tau \right|$$

where $\varphi_y(t)$ and $\varphi_x(t)$ are the phases of the signals x and y at time t extracted using the Hilbert transform. δ denotes the size of the window in which PLV is calculated. Here, we used a sliding window technique for each epoch to compute the FC matrices. The smallest window length recommended by (Lachaux, Rodriguez et al.

2000) was used, equal to $\frac{\text{number of cycles}}{\text{central frequency}}$ where the number of cycles at the given frequency band is

equal to six. Finally, FC were averaged over the 40s epoch.

2) Phase lag index (PLI)

The PLI was introduced as an alternative measure of PLV and less sensitive to the influence field spread and amplitude effects. It is defined as follows (Stam, Nolte et al. 2007):

$$PLI = \left\langle \left| \text{sign}[\varphi_y(t) - \varphi_x(t)] \right| \right\rangle$$

Where $\varphi_y(t)$ and $\varphi_x(t)$ are the phases of the signals x and y at time t and $\langle \rangle$ denotes the average over the time.

3) Amplitude envelope correlation (AEC)

The envelopes of the regional time series were estimated using Hilbert transform then Pearson correlation between amplitude envelopes was computed (Brookes, Gibson et al. 2004).

4) *Orthogonalisation approach*

Two different orthogonalisation approaches were used to remove all shared signal at zero lag between regional time series in the time domain: the symmetric orthogonalisation technique developed by (Colclough, Brookes et al. 2015) and the innovations orthogonalisation developed by (Pascual-Marqui, Biscay et al. 2017). Here, we applied these approaches after extracting and filtering the time series before computing *PLV* and *AEC*.

fMRI networks

Here, we used data from 487 participants at rest collected from the human connectome project (HCP) (Van Essen, Smith et al. 2013). In brief, functional connectivity between each of the 68 cortical regions using Desikan-Killiany atlas (Desikan, Ségonne et al. 2006) was assessed by means of analysis of the resting-state fMRI data of the HCP (Q3 release, voxel-size 2 mm isotropic, TR/TE 720/33.1 ms, 1200 volumes, 14:33 minutes). Images were realigned, co-registered with the T1 image, filtered (0.03 - 0.12 Hz), corrected for global effects of motion (realignment parameters), global signal mean, ventricle and white matter signal by means of linear regression and ‘motion-scrubbed’ for potential movement artifacts. Regional time-series were computed by averaging the time-series of the voxels in each of the cortical regions, and functional connectivity between all region pairs was derived by means of correlation analysis. A group-averaged weighted functional connectivity (FC) matrix was formed by averaging the individual matrices, see (van den Heuvel, Scholtens et al. 2016) for more detailed information.

MEG networks

Here, we used preprocessed resting state MEG data from 44 participants (26 women and 18 men; mean age between 28 and 32 years old) collected at the human connectome project (HCP) (Van Essen, Smith et al. 2013). We chose only the participants for whom both MEG and fMRI recordings are available. Same steps as for EEG were performed to estimate the MEG regional time series and estimate the functional networks.

Statistical comparisons

To statistically assess the difference between the connectivity methods, we thresholded the matrices (EEG and fMRI) by keeping the highest 10% connections (Garrison, Scheinost et al. 2015, Kabbara, Falou et al. 2017), results for other threshold values are presented in the supplementary materials. Spearman correlation values with the averaged fMRI were computed for each EEG FC method. In order to test differences between correlations of FC methods that keep zero lag connections and FC methods that remove zero lag connections, we used a

percentile bootstrap approach for non-overlapping correlations (Wilcox 2016), using 500 repetitions. The code is available at <https://github.com/GRousselet/blog/tree/master/comp2dcorr>. Spearman correlation values between EEG connectivity matrices and the averaged fMRI connectivity matrix were calculated for each participant. Mann-Whitney U Test was used to assess the statistical difference between FC methods ($p < 0.01/7$).

Results

Effect of connectivity measures

The EEG FC matrices (averaged over subjects) obtained by each of the FC methods (in beta band) are illustrated in Fig.2. These matrices were reordered according to brain lobes. The red module represents the occipital lobe, the green one represents the temporal brain regions, the blue section represents the parietal lobe, the purple module represents the frontal regions, the orange section represents the central lobe and the last module in grey represents the cingulate regions (details are presented in supplementary materials Table1). The fMRI FC matrix averaged over all participants is also illustrated in Fig.2. The visual investigation of these results revealed that matrices obtained from *PLV* and *AEC* connectivity methods were more consistent with the fMRI matrix compared to the other methods after removing zero lag connections. The latter FC methods connections between brain regions were sparser.

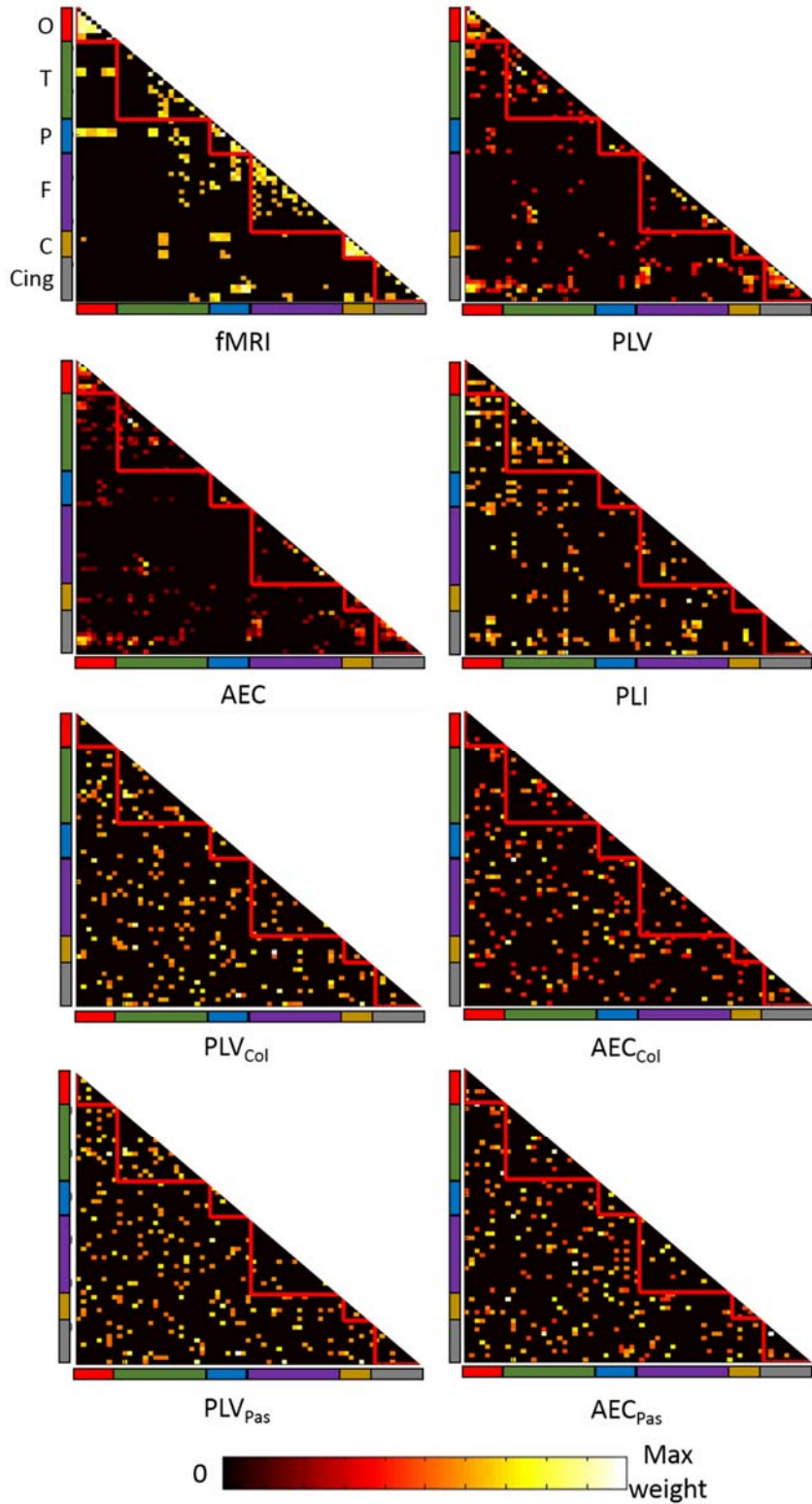


Fig.2 Functional connectivity matrices obtained in beta band from averaged fMRI and EEG networks. Matrices were ordered according to brain lobes (red: Occipital lobe - O, green: Temporal lobe - T, blue: Parietal lobe - P, purple: Frontal lobe - F, orange: Central lobe - C and grey: Cingulate - Cing). PLV: Phase Locking Value, AEC: Amplitude Envelope Correlation, PLI: Phase Lag Index, PLV_{Col} : Phase locking Value after applying symmetric orthogonalisation technique (Colclough, Brookes et al. 2015), AEC_{Col} : Amplitude Envelope Correlation after applying symmetric orthogonalisation technique (Colclough, Brookes et al. 2015), PLV_{Pas} : Phase locking Value after applying the innovations orthogonalisation (Pascual-Marqui, Biscay et al. 2017) and AEC_{Pas} : Amplitude Envelope Correlation after applying the innovations orthogonalisation (Pascual-Marqui, Biscay et al. 2017).

We then explored the Spearman correlations between the EEG networks (averaged over subjects) obtained from the seven FC methods and the fMRI network at the level of each network connection (edge's weight) (results are presented in Fig.3). EEG results showed low correlations for all the FC methods, however *PLV* and *AEC* networks were significantly correlated with fMRI networks ($\rho = 0.11$, $p = 10^{-7}$ and $\rho = 0.06$, $p = 0.007$, respectively). However, the networks obtained after using methods with leakage correction (*PLI*, *PLV_{Col}*, *AEC_{Col}*, *PLV_{Pas}* and *AEC_{Pas}*) were not significantly correlated with fMRI networks ($\rho = 0.02$, $p = 0.25$; $\rho = -0.01$, $p = 0.59$; $\rho = 0.04$, $p = 0.05$; $\rho = -0.006$, $p = 0.7$ and $\rho = 0.05$, $p = 0.03$ respectively). Percentile bootstrap results, presented in Table 1, showed that *PLV* network was significantly more correlated with fMRI network compared to all the other methods and *AEC* networks were significantly more correlated than *PLV_{Col}* and *PLV_{Pas}*.

FC method 1	FC method 2	Difference	Confidence interval	P value
<i>PLV</i> ($\rho = 0.11$)	<i>AEC</i> ($\rho = 0.06$)	0.05	[0.015 0.092]	0
	<i>PLI</i> ($\rho = 0.02$)	0.09	[0.035 0.139]	0
	<i>PLV_{Col}</i> ($\rho = -0.01$)	0.12	[0.064 0.179]	0
	<i>AEC_{Col}</i> ($\rho = 0.04$)	0.07	[0.007 0.125]	0.024
	<i>PLV_{Pas}</i> ($\rho = -0.006$)	0.116	[0.062 0.17]	0
	<i>AEC_{Pas}</i> ($\rho = 0.05$)	0.06	[0.004 0.119]	0.048
<i>AEC</i> ($\rho = 0.06$)	<i>PLV_{Col}</i> ($\rho = -0.01$)	0.07	[0.007 0.125]	0.028
	<i>PLV_{Pas}</i> ($\rho = -0.006$)	0.066	[0.004 0.122]	0.044

Table 1. EEG percentile bootstrap results. ρ difference between FC method 1 and FC method 2, 95% percentile bootstrap confidence interval and the p value obtained are reported.

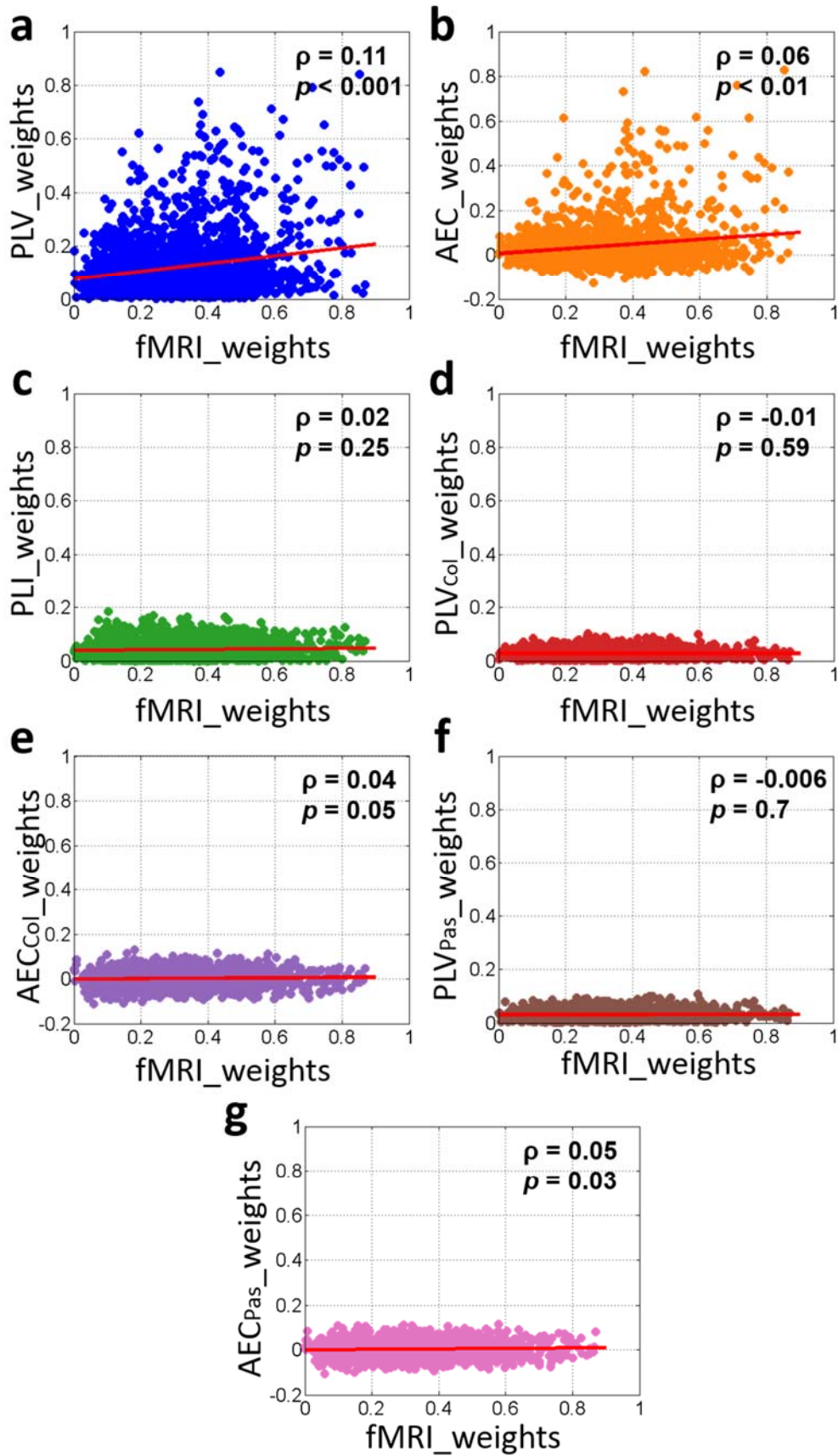


Fig.3 Spearman correlation between different averaged EEG connectivity methods and average fMRI edges weights

To quantitatively assess the difference between EEG FC methods, Spearman correlation coefficients between FC matrices for each participant and the averaged fMRI connectivity matrix were calculated and presented in Fig.4. Results showed significantly higher correlation with fMRI using the *PLV* and *AEC* as compared to the other three methods. *PLV* correlation values were significantly higher than *PLI* ($p = 3 \times 10^{-10}$), *PLV_{Col}* ($p = 4.7 \times 10^{-10}$), *AEC_{Col}* ($p = 2.5 \times 10^{-7}$), *PLV_{Pas}* ($p = 4.2 \times 10^{-10}$) and *AEC_{Pas}* ($p = 4.2 \times 10^{-8}$). *AEC* correlation values were also higher than *PLI* ($p = 1.6 \times 10^{-6}$), *PLV_{Col}* ($p = 7.4 \times 10^{-6}$), *AEC_{Col}* ($p = 0.001$), *PLV_{Pas}* ($p = 1.8 \times 10^{-5}$) and *AEC_{Pas}* ($p = 0.001$). These results were consistent in the delta, theta, alpha and gamma frequency bands (see figures S1 to S4 in supplementary materials) and after using different thresholds (5%, 20%, 30%, 50% and 80%), see figures S5 to S9 in supplementary materials.

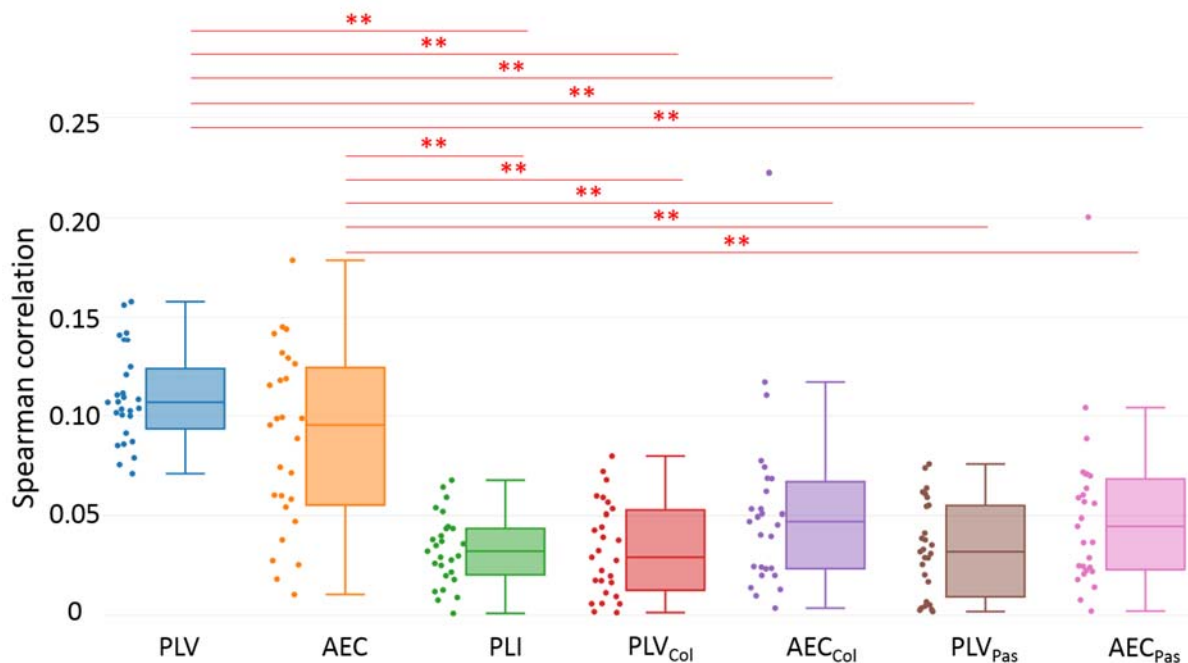


Fig.4 Spearman correlation values between averaged fMRI network and EEG networks in beta band. Individual participant correlations are shown in the scatter plot next to the box plot. ** represents significant differences obtained between methods using Bonferroni correction ($p < 0.01/7$).

MEG results

In this section, we evaluate the effect of FC methods on MEG data by computing the correlation values between MEG and fMRI networks from the same 44 subjects collected from HCP. The MEG FC matrices (averaged over subjects) obtained by each of the FC methods (in beta band) are illustrated in Fig.5. Same as EEG, MEG matrices were reordered according to brain lobes. The fMRI FC matrix averaged over the 44 participants is also illustrated in Fig.4. The visual investigation of these results revealed that matrices obtained from *PLV* and *AEC* connectivity methods were more similar with the fMRI matrix compared to the other methods showing sparser connections.

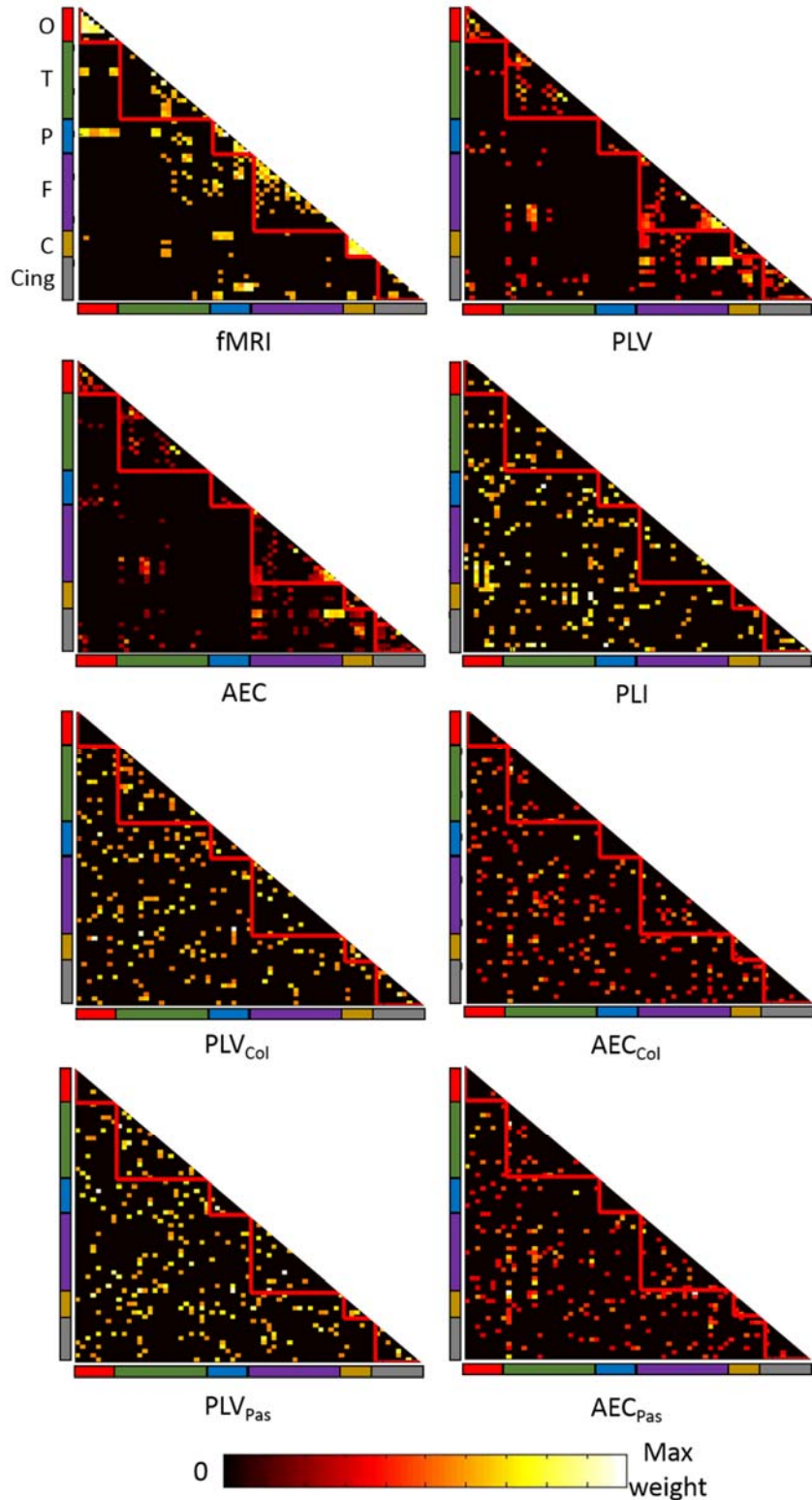


Fig.5 Functional connectivity matrices obtained in beta band from averaged fMRI and MEG networks over 44 participants from the HCP. Matrices were ordered according to brain lobes (red: Occipital lobe - O, green: Temporal lobe - T, blue: Parietal lobe - P, purple: Frontal lobe - F, orange: Central lobe - C and grey: Cingulate - Cing). PLV: Phase Locking Value, AEC: Amplitude Envelope Correlation, PLI: Phase Lag Index, PLV_{Col} : Phase locking Value after applying symmetric orthogonalisation technique (Colclough, Brookes et al. 2015), AEC_{Col} : Amplitude Envelope Correlation after applying symmetric orthogonalisation technique (Colclough, Brookes et al. 2015), PLV_{Pas} : Phase locking Value after applying the innovations orthogonalisation (Pascual-Marqui, Biscay et al. 2017) and AEC_{Pas} : Amplitude Envelope Correlation after applying the innovations orthogonalisation (Pascual-Marqui, Biscay et al. 2017).

We then explored the Spearman correlations between the MEG networks (averaged over subjects) obtained from the seven FC methods and the fMRI network at the level of each network connection (edge's weight), Fig.6. Results showed that only *PLV* networks were significantly (but with very low correlation value) correlated with fMRI networks ($\rho = 0.07, p = 0.001$). However, all the networks (*AEC*, *PLI*, *PLV_{Col}*, *AEC_{Col}*, *PLV_{Pas}* and *AEC_{Pas}*) were not significantly correlated with fMRI networks ($\rho = 0.003, p = 0.86$; $\rho = 0.01, p = 0.56$; $\rho = -0.01, p = 0.37$; $\rho = 0.01, p = 0.58$; $\rho = -0.001, p = 0.95$ and $\rho = 0.002, p = 0.9$ respectively). Percentile bootstrap results, presented in Table 2, showed that only the *PLV* network was more correlated with fMRI network compared to all the other methods except *PLI*.

FC method 1	FC method 2	Difference	Confidence interval	P value
<i>PLV</i> ($\rho = 0.07$)	<i>AEC</i> ($\rho = 0.003$)	0.067	[0.027 0.101]	0
	<i>PLV_{Col}</i> ($\rho = -0.01$)	0.08	[0.022 0.143]	0.012
	<i>AEC_{Col}</i> ($\rho = 0.01$)	0.06	[0.005 0.109]	0.028
	<i>PLV_{Pas}</i> ($\rho = -0.001$)	0.071	[0.007 0.123]	0.024
	<i>AEC_{Pas}</i> ($\rho = 0.002$)	0.068	[0.011 0.118]	0.004

Table 2. MEG percentile bootstrap results. ρ difference between FC method 1 and FC method 2, 95% percentile bootstrap confidence interval and the p value obtained are reported.

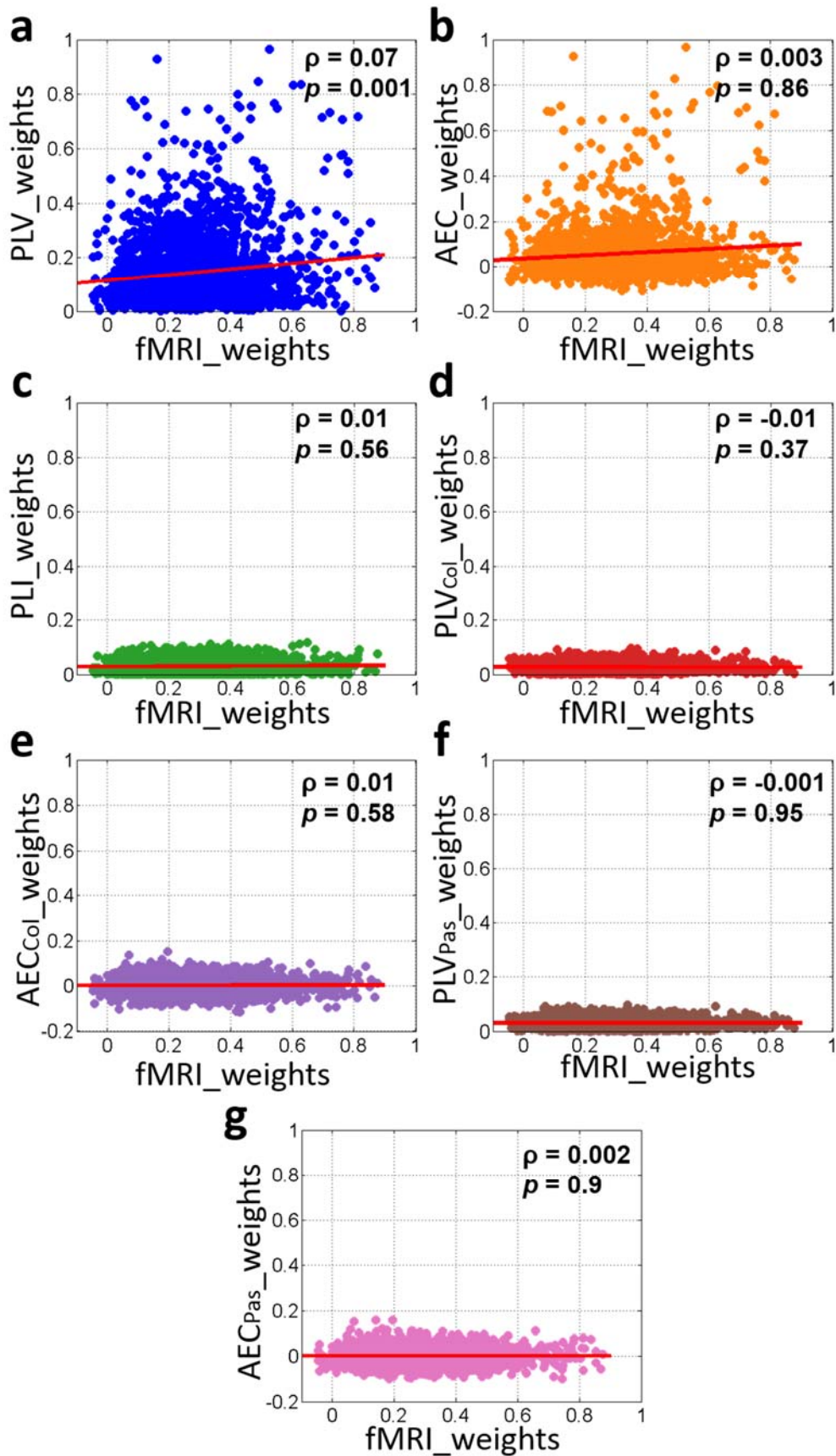


Fig.6 Spearman correlation between different averaged MEG connectivity methods and average fMRI edges weights

Finally, to quantitatively assess the difference between FC methods, Spearman correlation coefficients between FC matrices for each participant and its corresponding fMRI connectivity matrix were calculated and presented in Fig.7. *PLV* correlation values were significantly higher than *PLI* ($p = 1.6 \times 10^{-8}$), *PLV_{Col}* ($p = 7.7 \times 10^{-11}$) and *PLV_{Pas}* ($p = 3.5 \times 10^{-11}$). *AEC* correlation values were higher than *PLI* ($p = 7.5 \times 10^{-9}$), *PLV_{Col}* ($p = 8.2 \times 10^{-11}$), *PLV_{Pas}* ($p = 8.2 \times 10^{-11}$) and *AEC_{Pas}* ($p = 0.0003$). Moreover, correlation values of networks obtained after applying *AEC* method combined with symmetric orthogonalisation techniques (*AEC_{Col}*) were significantly higher than correlation values of networks obtained after applying *PLV* method combined with orthogonalisation techniques (*PLV_{Col}* ($p = 4.7 \times 10^{-6}$) and *PLV_{Pas}* ($p = 6.9 \times 10^{-6}$) respectively). Also, correlation values of networks obtained after applying *AEC* method combined with symmetric orthogonalisation techniques (*AEC_{Pas}*) were significantly higher than correlation values of networks obtained after applying *PLV* method combined with orthogonalisation techniques (*PLV_{Col}* ($p = 6.9 \times 10^{-6}$) and *PLV_{Pas}* ($p = 3.3 \times 10^{-5}$) respectively). No statistical difference was found between other methods.

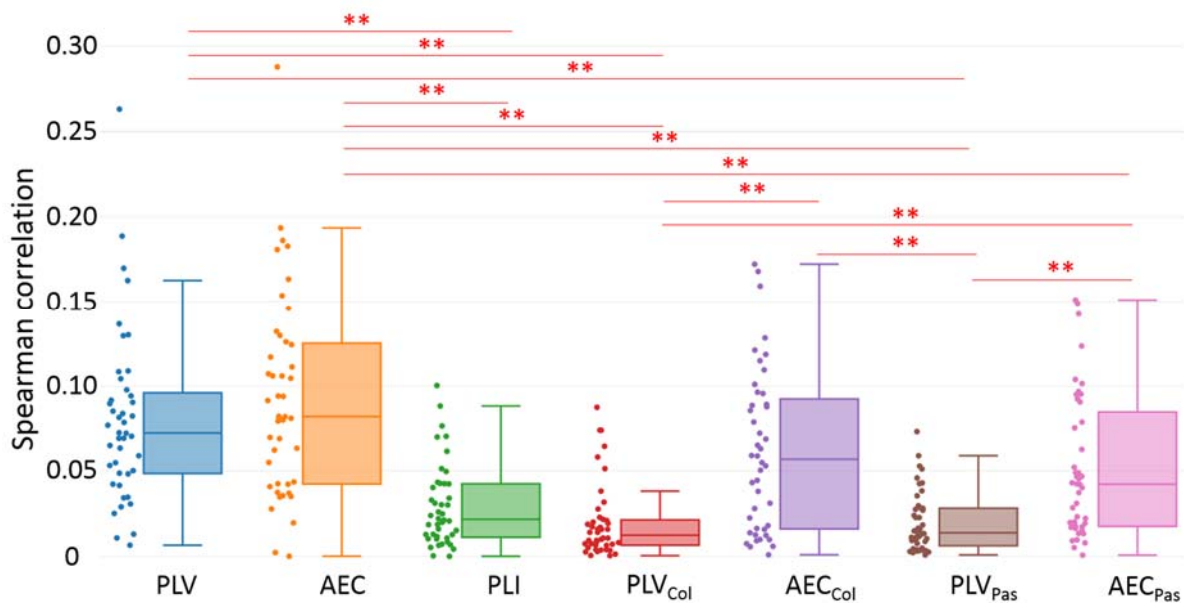


Fig.7 Spearman correlation values between the corresponding fMRI network and MEG network in beta band for each participant. Individual participant correlations are shown in the scatter plot next to the box plot. ** represents significant differences obtained between methods using Bonferroni correction ($p < 0.01/7$).

Discussion

Connectivity measures

While a large number of FC methods are available, their reliability and consistency are still under exploration. Also, the effect of leakage correction on M/EEG source-space networks by removing zero lag connections is not sufficiently studied. This paper (and some other recent papers (Colclough, Woolrich et al. 2016)) is a step toward this exploration in which we decided to compare the M/EEG FC matrices to those obtained using fMRI (HCP databases). Our results showed mainly low correlations for all the FC methods. Slightly higher correlation values between EEG and fMRI resting state networks were found in other study (Liu, Ganzetti et al. 2018). Despite the low correlations, our results showed that EEG FC matrices estimated using methods that keep the zero-lag correlations (*PLV* and *AEC*) were significantly correlated with the averaged fMRI functional connectivity matrix as compared to the other methods.

The non-significance between *PLI*, *PLV_{Col}*, *AEC_{Col}*, *PLV_{Pas}* and *AEC_{Pas}* with fMRI network can be explained by the fact that not all zero-lag connections are spurious. Several previous study described the presence and potential mechanisms for zero-lag connectivity (Roelfsema, Engel et al. 1997, Gollo, Mirasso et al. 2014). Recent study showed that removing zero lag connections may indeed reveal false and significantly different estimated connectivity from the true connectivity (Palva, Wang et al. 2018). Another study reported that *PLV* showed the best matching between simulations and empirical data and that zero-lag correlation are very crucial to assess the structural/functional relationships (Finger, Bonstrup et al. 2016).

Same study was conducted using MEG and fMRI recordings from the same subjects (44 participants). Similar results were obtained as EEG study, *PLV* averaged matrix was significantly more correlated with fMRI averaged matrix than all the other connectivity methods. However, no significant differences were found between *PLV*, *AEC*, *AEC_{Col}* and *AEC_{Pas}* at the individual level.

Methodological considerations

First, in this study the fMRI connectivity matrices were used as a 'reference' in order to evaluate the results of each of the FC connectivity measures applied to EEG regional time series. However, the EEG and fMRI data were not collected from the same participants. To that end, we used an averaged matrix over a large number of healthy participants (N=487). We were aware about this limitation and that the ideal situation was to have EEG and fMRI recordings for the same subjects. To that end, we conducted the same study on MEG data collected from HCP to obtain MEG and fMRI recordings for the same subjects. Of course, the fMRI matrices cannot be considered as an absolute 'ground truth' as preprocessing and analysis choices can produce different results

(Carp 2012). However, the spatial resolution of the fMRI networks (not affected by the leakage issue) and the consistency of these networks (we have tested another fMRI-based dataset over 10 healthy subjects and the two networks were highly correlated: correlation is equal to 0.8) can indeed justify its use as performance criteria for analyzing the EEG source-space networks.

Second, the connectivity matrices were thresholded by keeping only the highest 10% connectivity values. It was used to standardize the comparison between the two connectivity methods and fMRI matrices, as network measures are stable across proportional thresholds, as opposed to absolute thresholds (Garrison, Scheinost et al. 2015). We are aware about the effect of this threshold and we have tested other thresholds and the results are very consistent over different threshold values (see figures S5 to S9 in supplementary materials).

Third, it was shown that fMRI and M/EEG connectivity decreases with anatomical distance. This makes difficult the interpretation of our results without considering the effects of anatomical distance. In this regard, we added a correlation analysis between the fMRI, EEG and MEG matrices (for the different method) with the distance. The results (presented in supplementary materials, figure S12 and S13) showed that some of the methods were negatively correlated with the distance while other were not. This indicate the need for more investigation of the effect of the anatomical distance when dealing with the functional connectivity methods.

Conclusion

M/EEG source connectivity is a unique tool to identify high resolution functional brain networks in time and space. However, results are dependent on the choice of processing methods. In this paper, we analyzed the impact of the method used to measure the functional connectivity. Our results showed that among the different connectivity measures tested, *PLV* and *AEC* provided closer results to fMRI network compared to the three other methods that removes the zero-lag connections. We believe that more comparative studies (based on simulation and real data) should be done to make M/EEG source connectivity a mature technique to address questions in cognitive and clinical neuroscience.

Acknowledgements

This study was supported by the Future Emerging Technologies (H2020-FETOPEN-2014-2015-RIA under agreement No. 686764) as part of the European Union's Horizon 2020 research and training program 2014–2018. This work has received a French government support granted to the CominLabs excellence laboratory and managed by the National Research Agency in the “Investing for the Future” program under reference ANR-10-LABX-07-01. This work was also financed by the AZM and SAADE Association, Tripoli, Lebanon and by the

National Council for Scientific Research (CNRS) in Lebanon. Authors would like to thank Campus France, Programme Hubert Curien CEDRE (PROJET N° 42257YA), for supporting this study. HCP data was provided by the Human Connectome Project, WU-Minn Consortium (Principal Investigators: David Van Essen and Kamil Ugurbil; 1U54MH091657) funded by the 16 NIH Institutes and Centers that support the NIH Blueprint for Neuroscience Research; and by the McDonnell Center for Systems Neuroscience at Washington University. Authors would like to thank Olivier Dufor for collecting the EEG data and Martijn Van Den Heuvel for providing the fMRI connectivity matrices from the human connectome project.

Conflict of Interest: The authors declare that they have no conflict of interest.

References

- Bastos, A. M. and J.-M. Schoffelen (2016). "A tutorial review of functional connectivity analysis methods and their interpretational pitfalls." *Frontiers in systems neuroscience* **9**: 175.
- Brookes, M. J., A. M. Gibson, S. D. Hall, P. L. Furlong, G. R. Barnes, A. Hillebrand, K. D. Singh, I. E. Holliday, S. T. Francis and P. G. Morris (2004). "A general linear model for MEG beamformer imaging." *NeuroImage* **23**(3): 936-946.
- Brookes, M. J., M. Woolrich, H. Luckhoo, D. Price, J. R. Hale, M. C. Stephenson, G. R. Barnes, S. M. Smith and P. G. Morris (2011). "Investigating the electrophysiological basis of resting state networks using magnetoencephalography." *Proceedings of the National Academy of Sciences*: 201112685.
- Brookes, M. J., M. W. Woolrich and G. R. Barnes (2012). "Measuring functional connectivity in MEG: a multivariate approach insensitive to linear source leakage." *Neuroimage* **63**(2): 910-920.
- Carp, J. (2012). "On the plurality of (methodological) worlds: estimating the analytic flexibility of fMRI experiments." *Frontiers in neuroscience* **6**: 149.
- Chu, C. J., M. A. Kramer, J. Pathmanathan, M. T. Bianchi, M. B. Westover, L. Wison and S. S. Cash (2012). "Emergence of stable functional networks in long-term human electroencephalography." *Journal of Neuroscience* **32**(8): 2703-2713.
- Colclough, G. L., M. J. Brookes, S. M. Smith and M. W. Woolrich (2015). "A symmetric multivariate leakage correction for MEG connectomes." *NeuroImage* **117**: 439-448.
- Colclough, G. L., M. W. Woolrich, P. Tewarie, M. J. Brookes, A. J. Quinn and S. M. Smith (2016). "How reliable are MEG resting-state connectivity metrics?" *Neuroimage* **138**: 284-293.
- de Pasquale, F., S. Della Penna, A. Z. Snyder, L. Marzetti, V. Pizzella, G. L. Romani and M. Corbetta (2012). "A cortical core for dynamic integration of functional networks in the resting human brain." *Neuron* **74**(4): 753-764.
- De Vico Fallani, F., J. Richiardi, M. Chavez and S. Achard (2014). "Graph analysis of functional brain networks: practical issues in translational neuroscience." *Philosophical Transactions of the Royal Society B: Biological Sciences* **369**(1653): 20130521.
- Desikan, R. S., F. Ségonne, B. Fischl, B. T. Quinn, B. C. Dickerson, D. Blacker, R. L. Buckner, A. M. Dale, R. P. Maguire and B. T. Hyman (2006). "An automated labeling system for subdividing the human cerebral cortex on MRI scans into gyral based regions of interest." *Neuroimage* **31**(3): 968-980.
- Finger, H., M. Bonstrup, B. Cheng, A. Messe, C. Hilgetag, G. Thomalla, C. Gerloff and P. Konig (2016). "Modeling of Large-Scale Functional Brain Networks Based on Structural Connectivity from DTI: Comparison with EEG Derived Phase Coupling Networks and Evaluation of Alternative Methods along the Modeling Path." *PLoS Comput Biol* **12**(8): e1005025.
- Fraschini, M., M. Demuru, A. Crobe, F. Marrosu, C. J. Stam and A. Hillebrand (2016). "The effect of epoch length on estimated EEG functional connectivity and brain network organisation." *Journal of neural engineering* **13**(3): 036015.
- Garrison, K. A., D. Scheinost, E. S. Finn, X. Shen and R. T. Constable (2015). "The (in) stability of functional brain network measures across thresholds." *Neuroimage* **118**: 651-661.
- Gollo, L. L., C. Mirasso, O. Sporns and M. Breakspear (2014). "Mechanisms of zero-lag synchronization in cortical motifs." *PLoS computational biology* **10**(4): e1003548.
- Gramfort, A., M. Kowalski and M. Hämmäläinen (2012). "Mixed-norm estimates for the M/EEG inverse problem using accelerated gradient methods." *Physics in Medicine & Biology* **57**(7): 1937.

Gramfort, A., E. Olivi, M. Clerc and T. Papadopoulo (2010). "OpenMEEG: opensource software for quasistatic bioelectromagnetics." *Biomedical engineering online* **9**(1): 45.

Hardmeier, M., F. Hatz, H. Bousleiman, C. Schindler, C. J. Stam and P. Fuhr (2014). "Reproducibility of functional connectivity and graph measures based on the phase lag index (PLI) and weighted phase lag index (wPLI) derived from high resolution EEG." *PloS one* **9**(10): e108648.

Hassan, M., P. Benquet, A. Biraben, C. Berrou, O. Dufor and F. Wendling (2015). "Dynamic reorganization of functional brain networks during picture naming." *Cortex* **73**: 276-288.

Hassan, M., O. Dufor, I. Merlet, C. Berrou and F. Wendling (2014). "EEG source connectivity analysis: from dense array recordings to brain networks." *PloS one* **9**(8): e105041.

Hassan, M., I. Merlet, A. Mheich, A. Kabbara, A. Biraben, A. Nica and F. Wendling (2016). "Identification of interictal epileptic networks from dense-EEG." *Brain Topography*: 1-17.

Hassan, M. and F. Wendling (2018). "Electroencephalography Source Connectivity: Aiming for High Resolution of Brain Networks in Time and Space." *IEEE Signal Processing Magazine* **35**(3): 81-96.

Hauk, O. (2004). "Keep it simple: a case for using classical minimum norm estimation in the analysis of EEG and MEG data." *Neuroimage* **21**(4): 1612-1621.

Hipp, J. F., D. J. Hawellek, M. Corbetta, M. Siegel and A. K. Engel (2012). "Large-scale cortical correlation structure of spontaneous oscillatory activity." *Nature neuroscience* **15**(6): 884.

Holmes, C. J., R. Hoge, L. Collins, R. Woods, A. W. Toga and A. C. Evans (1998). "Enhancement of MR images using registration for signal averaging." *Journal of computer assisted tomography* **22**(2): 324-333.

Kabbara, A., W. E. Falou, M. Khalil, F. Wendling and M. Hassan (2017). "The dynamic functional core network of the human brain at rest." *Scientific Reports* **7**.

Lachaux, J.-P., E. Rodriguez, M. Le Van Quyen, A. Lutz, J. Martinerie and F. J. Varela (2000). "Studying single-trials of phase synchronous activity in the brain." *International Journal of Bifurcation and Chaos* **10**(10): 2429-2439.

Lachaux, J.-P., E. Rodriguez, J. Martinerie and F. J. Varela (1999). "Measuring phase synchrony in brain signals." *Human brain mapping* **8**(4): 194-208.

Liu, Q., M. Ganzetti, N. Wenderoth and D. Mantini (2018). "Detecting large-scale brain networks using EEG: impact of electrode density, head modeling and source localization." *Frontiers in neuroinformatics* **12**: 4.

Liuzzi, L., L. E. Gascoyne, P. K. Tewarie, E. L. Barratt, E. Boto and M. J. Brookes (2017). "Optimising experimental design for MEG resting state functional connectivity measurement." *Neuroimage* **155**: 565-576.

Mahjoory, K., V. V. Nikulin, L. Botrel, K. Linkenkaer-Hansen, M. M. Fato and S. Haufe (2017). "Consistency of EEG source localization and connectivity estimates." *Neuroimage* **152**: 590-601.

Maldjian, J. A., E. M. Davenport and C. T. Whitlow (2014). "Graph theoretical analysis of resting-state MEG data: Identifying interhemispheric connectivity and the default mode." *Neuroimage* **96**: 88-94.

Nolte, G., O. Bai, L. Wheaton, Z. Mari, S. Vorbach and M. Hallett (2004). "Identifying true brain interaction from EEG data using the imaginary part of coherency." *Clinical neurophysiology* **115**(10): 2292-2307.

O'Neill, G. C., P. Tewarie, D. Vidaurre, L. Liuzzi, M. W. Woolrich and M. J. Brookes (2018). "Dynamics of large-scale electrophysiological networks: a technical review." *Neuroimage* **180**: 559-576.

Palva, J. M., S. H. Wang, S. Palva, A. Zhigalov, S. Monto, M. J. Brookes, J.-M. Schoffelen and K. Jerbi (2018). "Ghost interactions in MEG/EEG source space: A note of caution on inter-areal coupling measures." *Neuroimage* **173**: 632-643.

Palva, S. and J. M. Palva (2012). "Discovering oscillatory interaction networks with M/EEG: challenges and breakthroughs." *Trends in cognitive sciences* **16**(4): 219-230.

Pascual-Marqui, R. D., R. J. Biscay, J. Bosch-Bayard, P. Faber, T. Kinoshita, K. Kochi, P. Milz, K. Nishida and M. Yoshimura (2017). "Innovations orthogonalization: a solution to the major pitfalls of EEG/MEG" leakage correction". *arXiv preprint arXiv:1708.05931*.

Rizkallah, J., P. Benquet, A. Kabbara, O. Dufor, F. Wendling and M. Hassan (2018). "Dynamic reshaping of functional brain networks during visual object recognition." *Journal of neural engineering* **15**(5): 056022.

Roelfsema, P. R., A. K. Engel, P. König and W. Singer (1997). "Visuomotor integration is associated with zero time-lag synchronization among cortical areas." *Nature* **385**(6612): 157.

Sakkalis, V. (2011). "Review of advanced techniques for the estimation of brain connectivity measured with EEG/MEG." *Computers in biology and medicine* **41**(12): 1110-1117.

Schoffelen, J. M. and J. Gross (2009). "Source connectivity analysis with MEG and EEG." *Human brain mapping* **30**(6): 1857-1865.

Stam, C. J., G. Nolte and A. Daffertshofer (2007). "Phase lag index: assessment of functional connectivity from multi channel EEG and MEG with diminished bias from common sources." *Human brain mapping* **28**(11): 1178-1193.

Tadel, F., S. Baillet, J. C. Mosher, D. Pantazis and R. M. Leahy (2011). "Brainstorm: a user-friendly application for MEG/EEG analysis." *Computational intelligence and neuroscience* **2011**: 8.

van den Heuvel, M. P., L. H. Scholtens, M. A. de Reus and R. S. Kahn (2016). "Associated microscale spine density and macroscale connectivity disruptions in schizophrenia." Biological psychiatry **80**(4): 293-301.

Van Essen, D. C., S. M. Smith, D. M. Barch, T. E. Behrens, E. Yacoub, K. Ugurbil and W.-M. H. Consortium (2013). "The WU-Minn human connectome project: an overview." Neuroimage **80**: 62-79.

Wang, S. H., M. Lobier, F. Siebenhüner, T. Puoliväli, S. Palva and J. M. Palva (2018). "Hyperedge bundling: A practical solution to spurious interactions in MEG/EEG source connectivity analyses." NeuroImage **173**: 610-622.

Wilcox, R. R. (2016). "Comparing dependent robust correlations." British Journal of Mathematical and Statistical Psychology **69**(3): 215-224.

Study 2 Supplementary Materials: The effect of removing zero-lag functional connections on EEG-source space networks at rest

The effect of removing zero-lag functional connections on EEG-source space networks at rest

Jennifer Rizkallah^{1,2}, Hassan Amoud², Matteo Fraschini³, Fabrice Wendling¹
and Mahmoud Hassan¹

¹ Univ Rennes, LTSI, F-35000 Rennes, France

² Azm Center for Research in Biotechnology and its Application, EDST, Lebanese University, Lebanon

³ Department of Electrical and Electronic Engineering, University of Cagliari, Piazza D'armi, Cagliari, I-09123, Italy

* Corresponding author: jennifer.rizkallah.jr@gmail.com

	Acronyms	Name		Acronyms	Name		
Occipital	LING L	lingual L	Frontal	sFG L	superiorfrontal L		
	LING R	lingual R		sFG R	superiorfrontal R		
	periCAL L	pericalcarine L		rMFG L	rostralmiddlefrontal L		
	periCAL R	pericalcarine R		rMFG R	rostralmiddlefrontal R		
	CUN L	cuneus L		cMFG L	caudalmiddlefrontal L		
	CUN R	cuneus R		cMFG R	caudalmiddlefrontal R		
	LOG L	lateraloccipital L		pOPER L	parsopercularis L		
	LOG R	lateraloccipital R		pOPER R	parsopercularis R		
Temporal	ENT L	entorhinal L		pTRI L	parstriangularis L		
	ENT R	entorhinal R		pTRI R	parstriangularis R		
	paraH L	parahippocampal L		pORB L	parsorbitalis L		
	paraH R	parahippocampal R		pORB R	parsorbitalis R		
	TP L	temporalpole L		LOF L	lateralorbitofrontal L		
	TP R	temporalpole R		LOF R	lateralorbitofrontal R		
	FUS R	fusiform R		MOF L	medialorbitofrontal L		
	FUS L	fusiform L		MOF R	medialorbitofrontal R		
	STG L	superiortemporal L		FP L	frontalpole L		
	STG R	superiortemporal R		FP R	frontalpole R		
	Parietal	ITG L		inferiortemporal L	Central	preC L	precentral L
		ITG R		inferiortemporal R		preC R	precentral R
		MTG L		middletemporal L		paraC L	paracentral L
		MTG R		middletemporal R		paraC R	paracentral R
		TT L		transversetemporal L		postC L	postcentral L
		TT R		transversetemporal R		postC R	postcentral R
BSTS L		bankssts L	rACC L	rostralanteriorcingulate L			
BSTS R		bankssts R	rACC R	rostralanteriorcingulate R			
SMAR L		supramarginal L	cACC L	cAUDalanteriorcingulate L			
SMAR R		supramarginal R	cACC R	cAUDalanteriorcingulate R			
Cingulate	SPL L	superiorparietal L	PCC L	posteriorcingulate L			
	SPL R	superiorparietal R	PCC R	posteriorcingulate R			
	IPL L	inferiorparietal L	iCC L	isthmuscingulate L			
	IPL R	inferiorparietal R	iCC R	isthmuscingulate R			
	PCUN L	precuneus L	INS L	insula L			
	PCUN R	precuneus R	INS R	insula R			

Table1. A summary of the 68 ROIs used in our study as derived from the Desikan-Killiany atlas (Desikan et al., 2006).

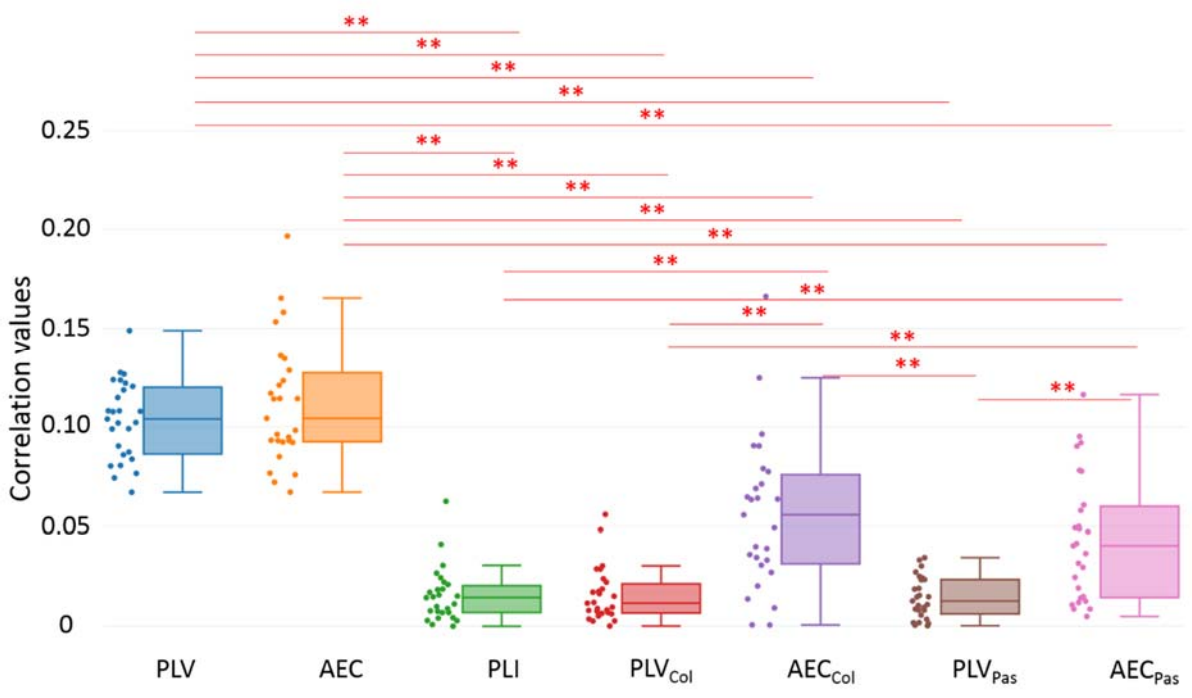


Fig S1: Correlation values between fMRI network and EEG networks in delta band. Individual participant correlations are shown in the scatter plot next to the box plot.

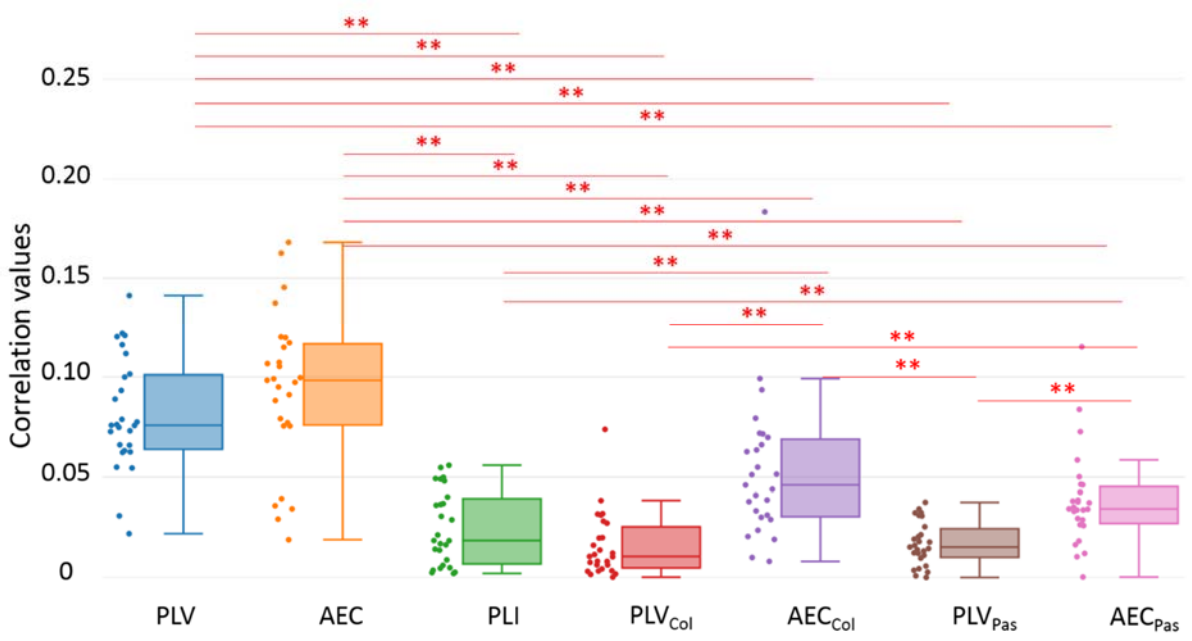


Fig S2: Correlation values between fMRI network and EEG networks in theta band. Individual participant correlations are shown in the scatter plot next to the box plot.

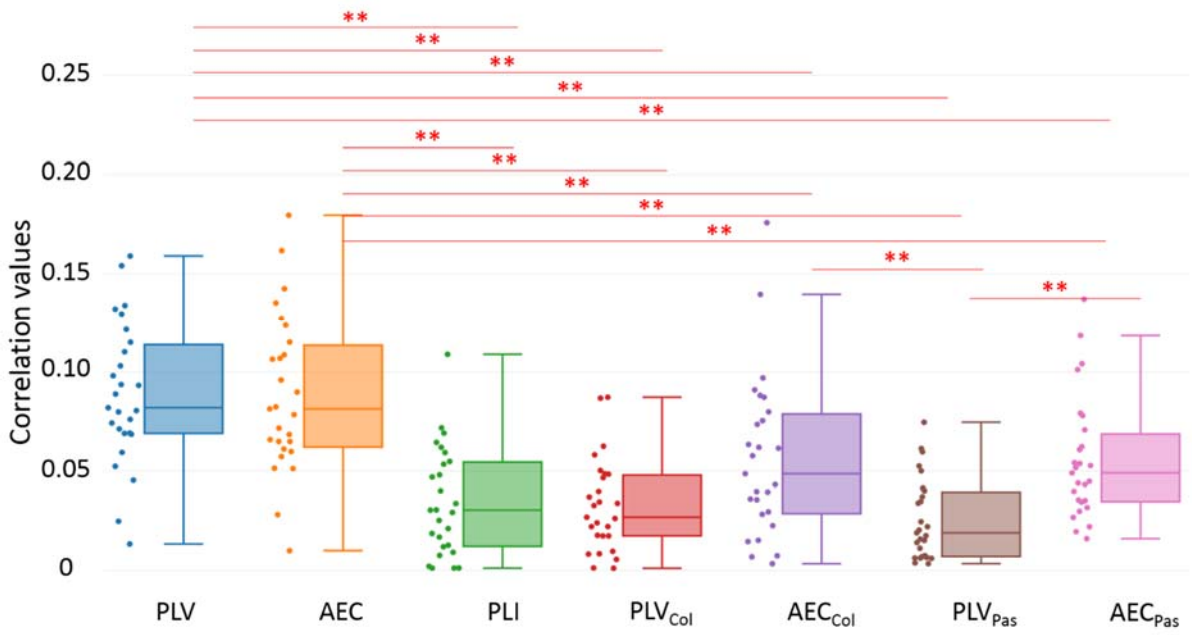


Fig S3: Correlation values between fMRI network and EEG networks in alpha band. Individual participant correlations are shown in the scatter plot next to the box plot.

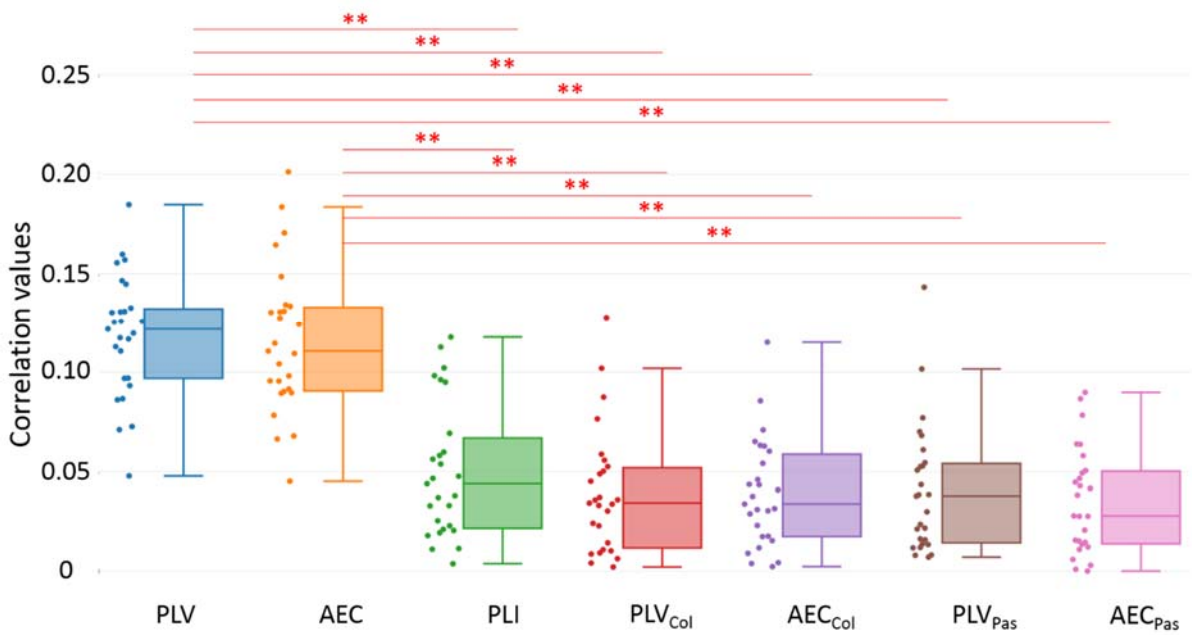


Fig S4: Correlation values between fMRI network and EEG networks in gamma band. Individual participant correlations are shown in the scatter plot next to the box plot.

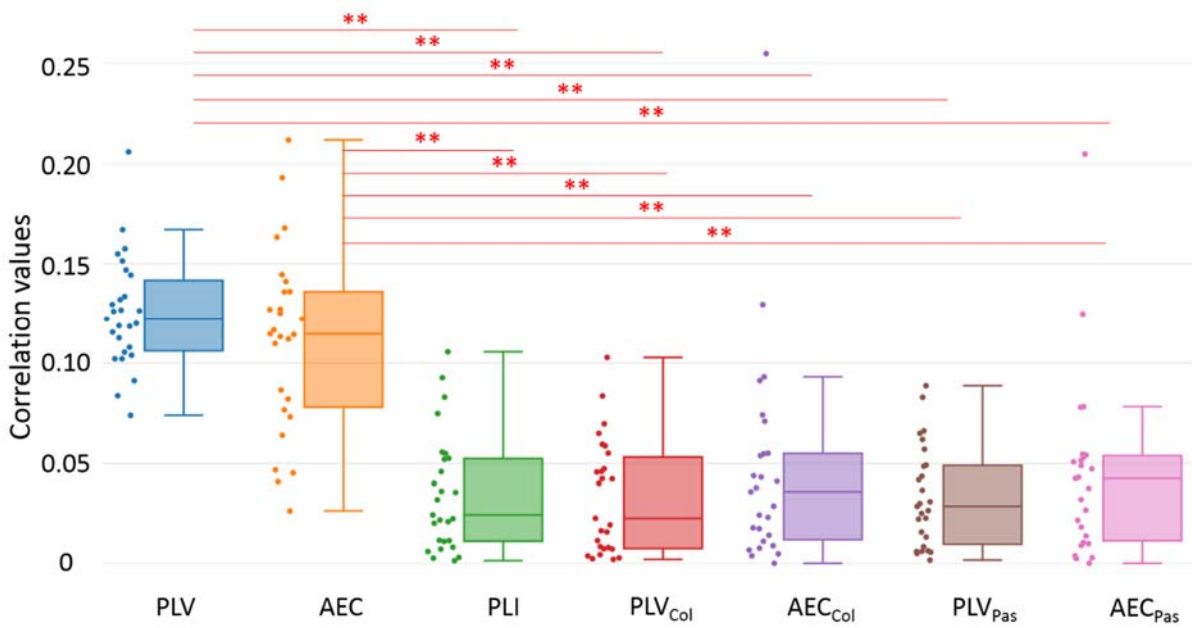


Fig S5: Correlation values between fMRI network and EEG networks in beta band using threshold equal to 5%. Individual participant correlations are shown in the scatter plot next to the box plot.

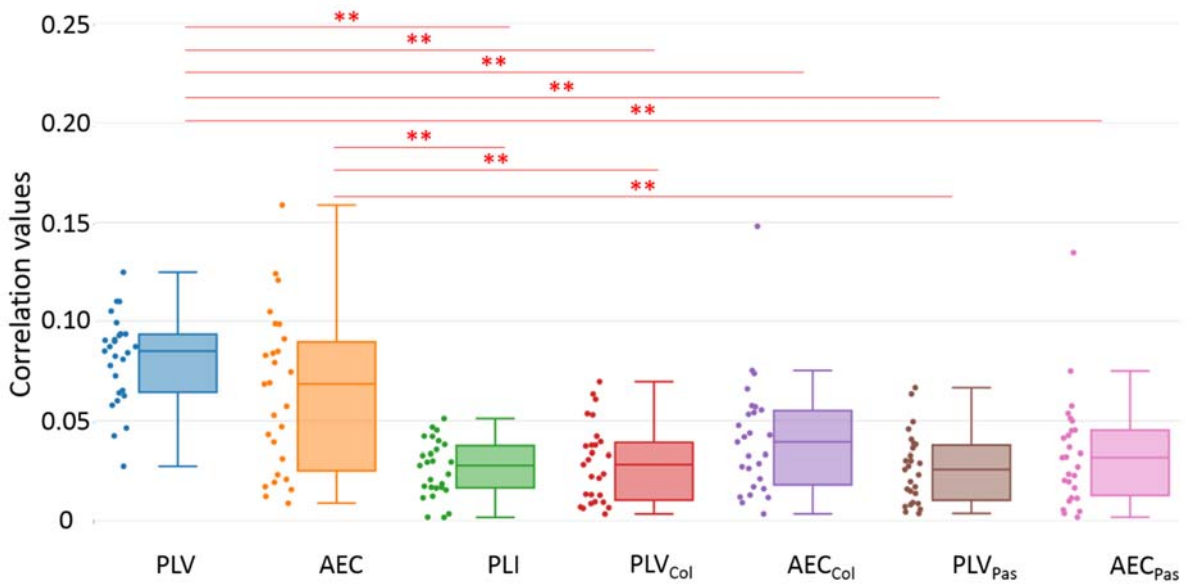


Fig S6: Correlation values between fMRI network and EEG networks in beta band using threshold equal to 20%. Individual participant correlations are shown in the scatter plot next to the box plot.

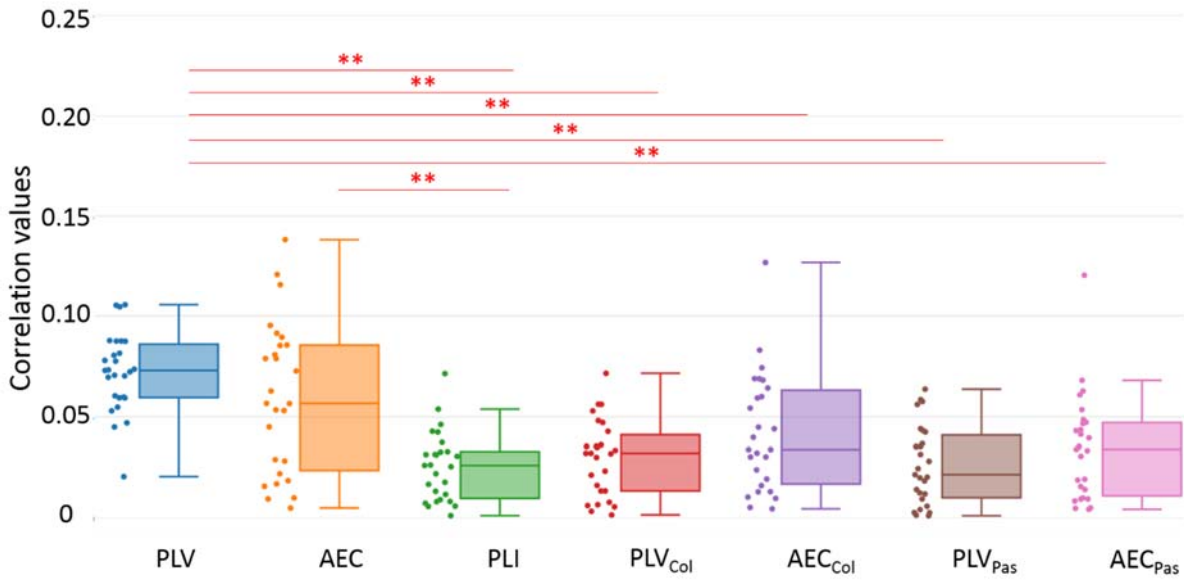


Fig S7: Correlation values between fMRI network and EEG networks in beta band using threshold equal to 30%. Individual participant correlations are shown in the scatter plot next to the box plot.

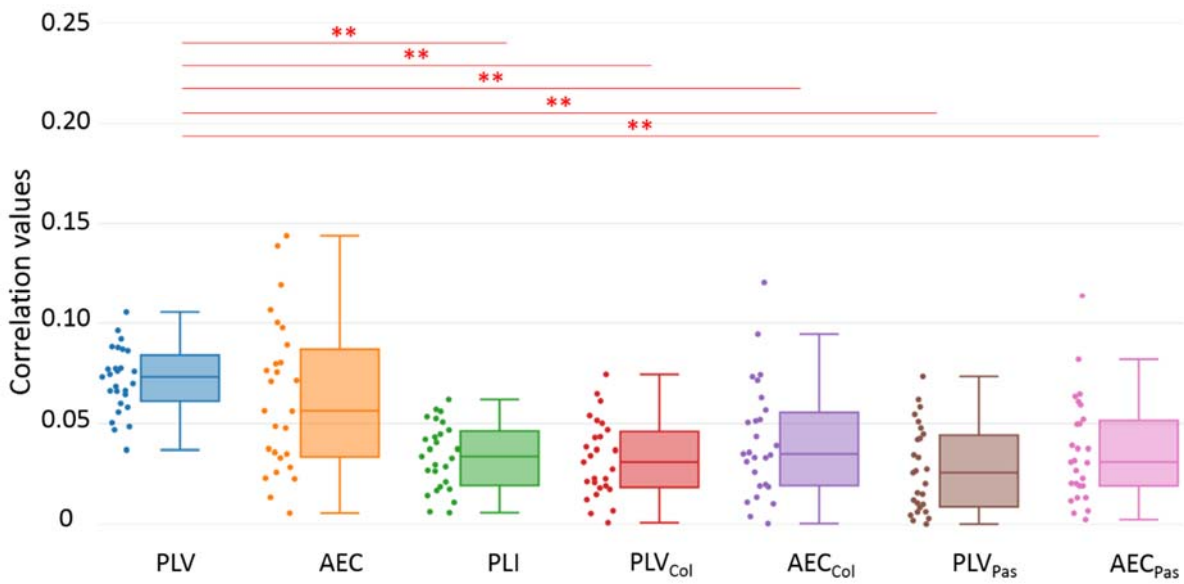


Fig S8: Correlation values between fMRI network and EEG networks in beta band using threshold equal to 50%. Individual participant correlations are shown in the scatter plot next to the box plot.

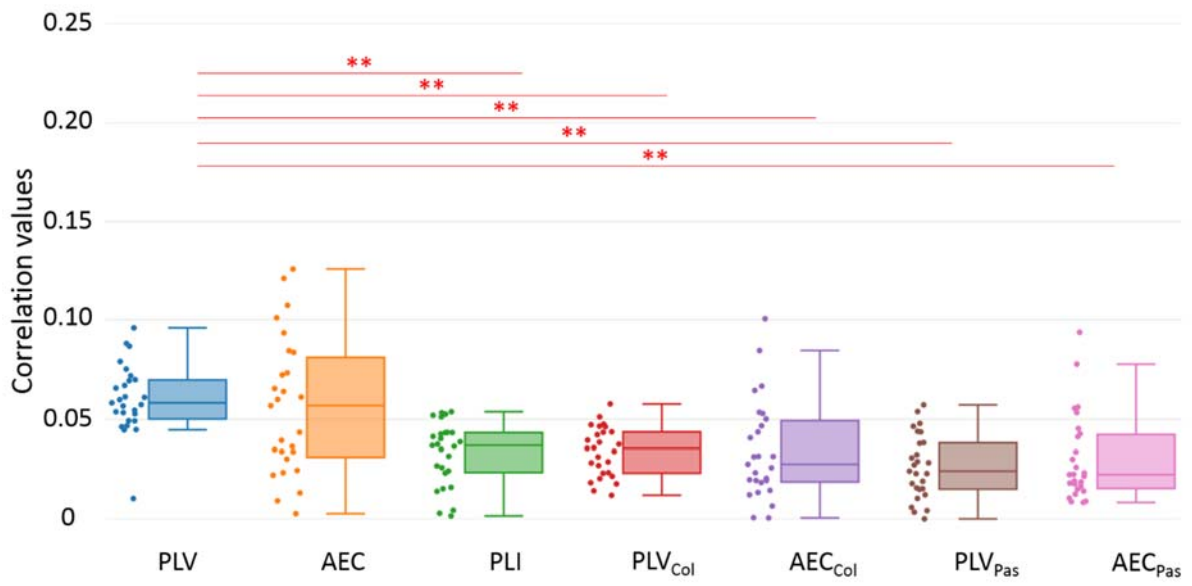


Fig S9: Correlation values between fMRI network and EEG networks in beta band using threshold equal to 80%. Individual participant correlations are shown in the scatter plot next to the box plot.

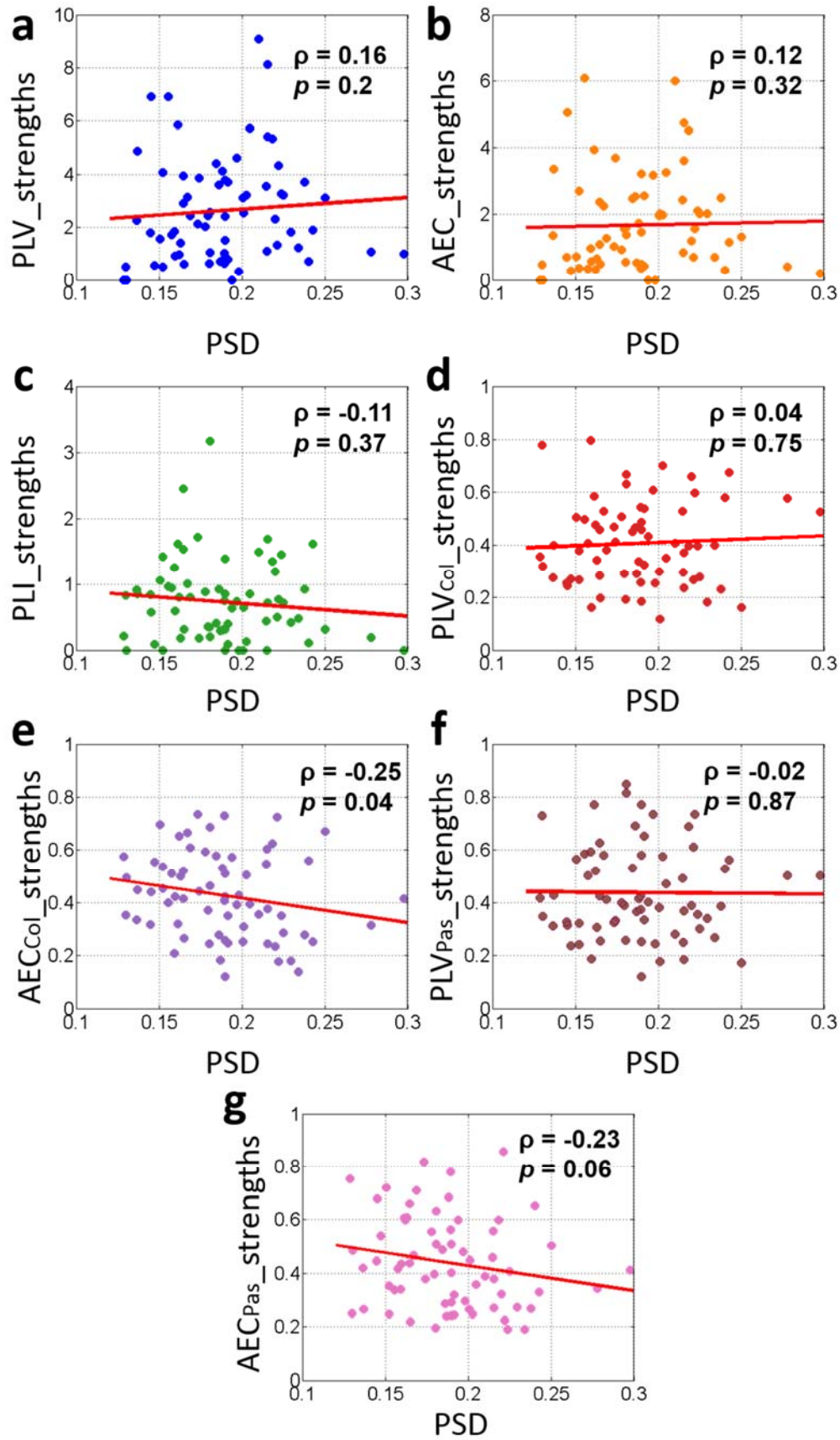


Fig S10: Spearman correlation between the beta relative power spectral density (PSD) and the EEG networks strengths.

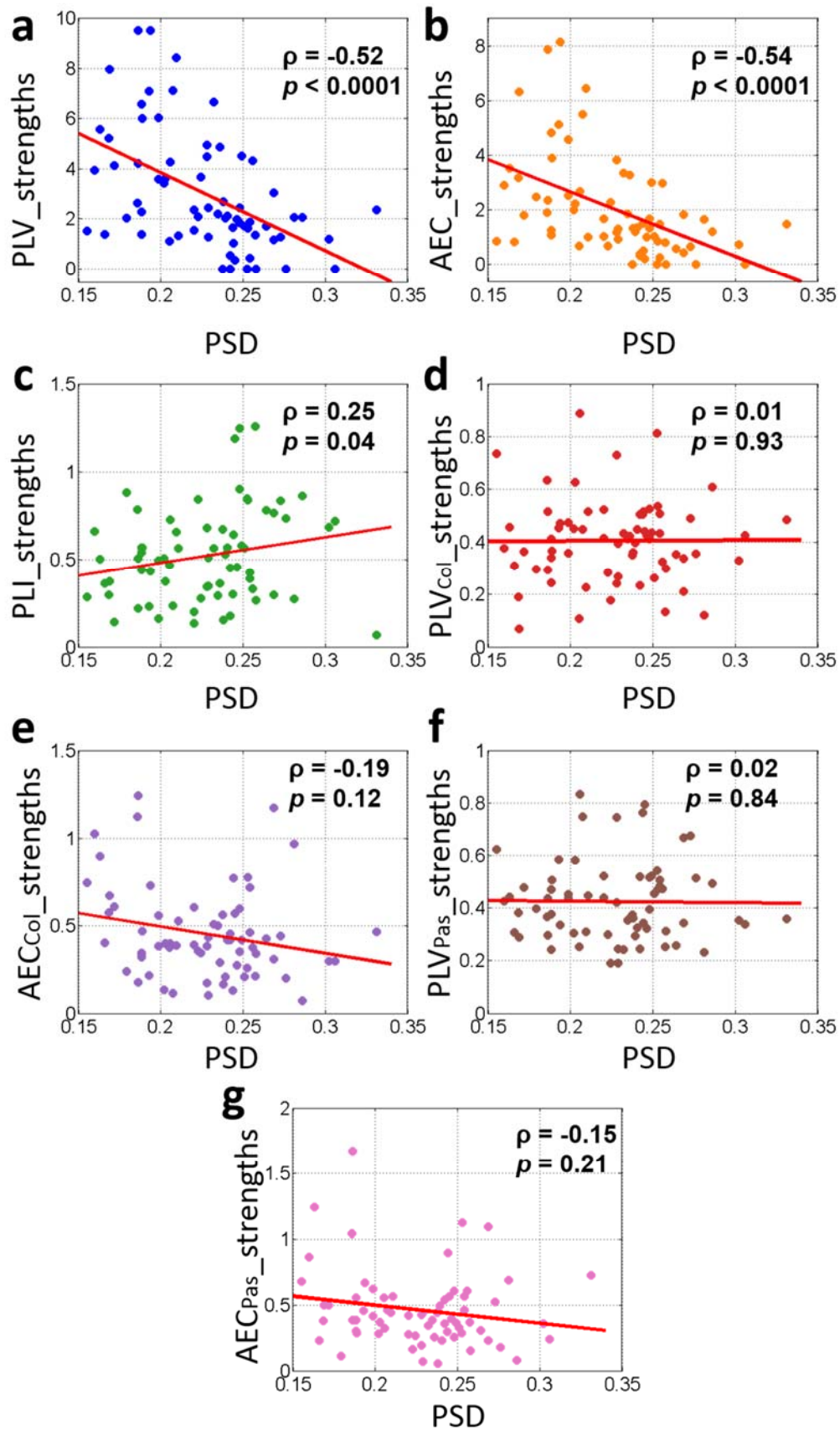


Fig S11: Spearman correlation between the beta relative power spectral density (PSD) and the MEG networks strengths.

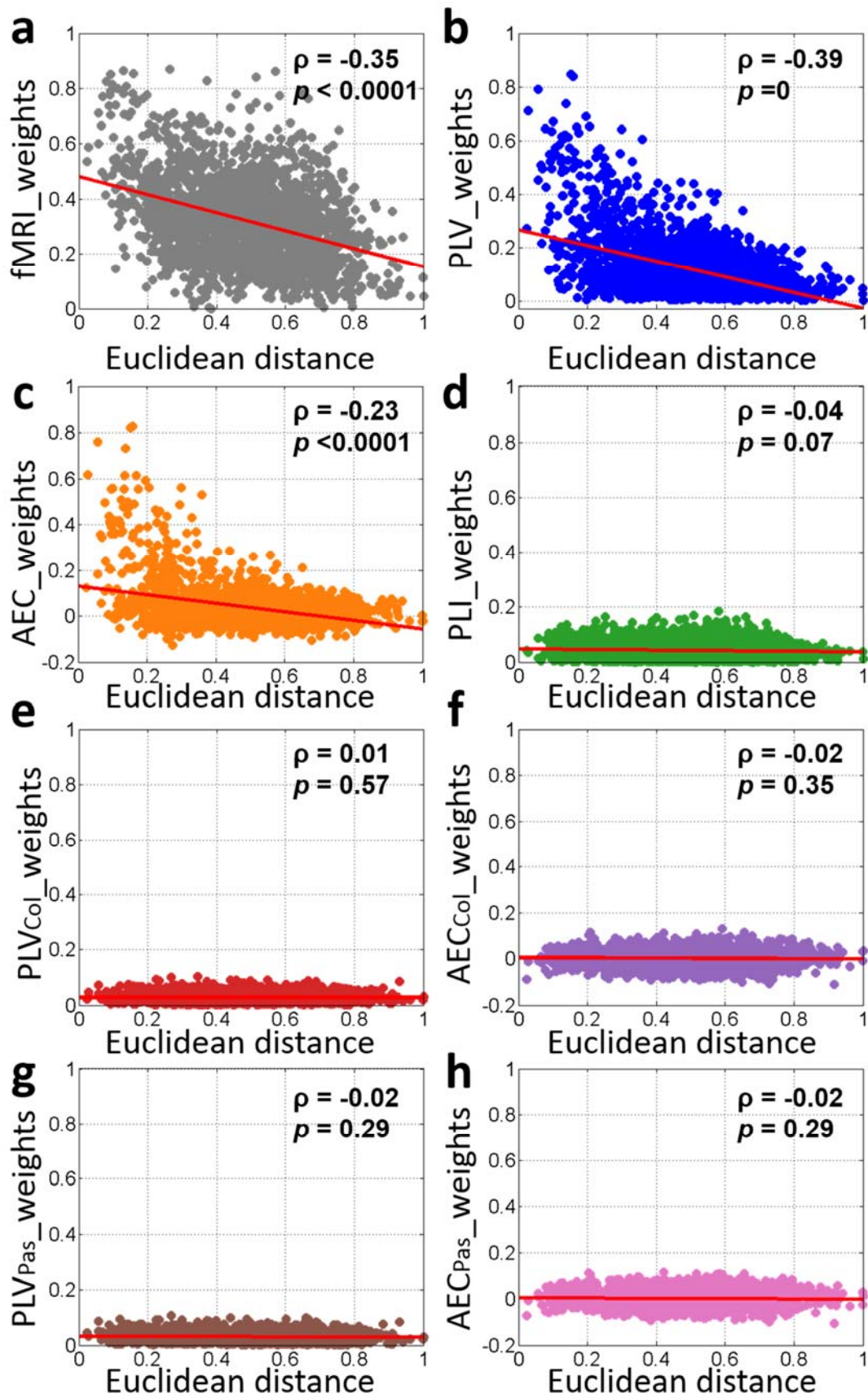


Fig S12: Spearman correlation between the normalized Euclidean distance of the 68 ROIs and the averaged fMRI and EEG networks weights in beta band.

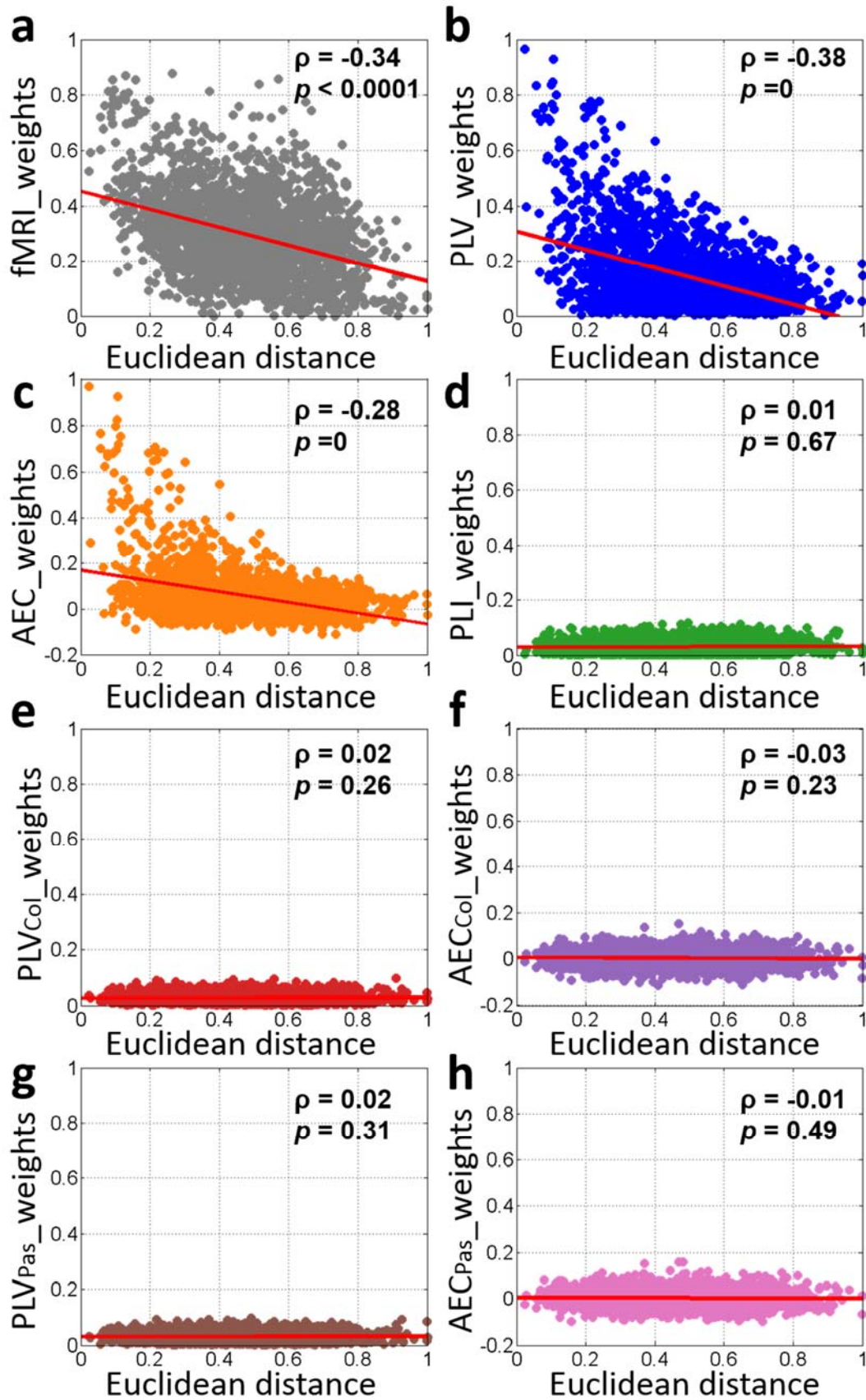


Fig S13: Spearman correlation between the normalized Euclidean distance of the 68 ROIs and the averaged fMRI and MEG networks weights in beta band.

Study 3: Decreased integration of EEG source-space networks in disorders of consciousness

J. Rizkallah, J. Annen, J. Modolo, O. Gosseries, P. Benquet, S. Mortaheb, H. Amoud, H. Cassol, A. Mheich, A. Thibaut, C. Chatelle, M. Hassan, R. Panda, F. Wendling, S. Laureys

Published in: Neuroimage Clinical (2019)

Objectives: Increasing evidence showed that disorders of consciousness (DoC) are linked with disruptions in functional connectivity between distant brain areas. However, to which extent the balance of brain network segregation and integration is modified in DoC patients remains unclear. Our objectives were to track alterations in functional connectivity measures reflecting cortical brain networks as a function of clinical consciousness levels and to identify the brain regions that were involved between groups.

Methods: Resting state high-density-electroencephalography (EEG) data were collected and analyzed from 82 participants: 61 DoC patients recovering from coma with various levels of consciousness (EMCS (n=6), MCS+ (n=29), MCS- (n=17) and UWS (n=9)), and 21 healthy subjects. Functional brain networks in five different EEG frequency bands and the broadband signal were estimated using EEG source connectivity method. Graph theory-based analyses were used to evaluate their relationship with decreasing levels of consciousness as well as group differences between healthy volunteers and DoC patient groups.

Results: Networks in DoC patients were characterized by impaired global information processing (network integration) and increased local information processing (network segregation) as compared to controls. The large-scale functional brain networks had integration decreasing with lower level of consciousness. Two common anatomical regions were identified with decreased integration when comparing the control group with any of the patient groups: the left precuneus and the left orbitofrontal cortex.

Key words: disorders of consciousness, high-density electroencephalography, functional brain networks, unresponsive wakefulness syndrome, minimally conscious state



Decreased integration of EEG source-space networks in disorders of consciousness

Jennifer Rizkallah^{a,b}, Jitka Annen^{c,d}, Julien Modolo^{a,*}, Olivia Gosseries^{c,d}, Pascal Benquet^a, Sepehr Mortaheb^c, Hassan Amoud^b, Helena Cassol^{c,d}, Ahmad Mheich^a, Aurore Thibaut^{c,d}, Camille Chatelle^{c,d}, Mahmoud Hassan^a, Rajanikant Panda^c, Fabrice Wendling^{a,1}, Steven Laureys^{c,d,1}

^a Univ Rennes, LTSI, F-35000 Rennes, France

^b Azm Center for Research in Biotechnology and its Applications, EDST, Lebanese University, Lebanon

^c GIGA Consciousness, University of Liège, Liège, Belgium

^d Coma Science Group, University Hospital of Liège, Liège, Belgium

ARTICLE INFO

Keywords:

Disorders of consciousness
High-density electroencephalography
Functional brain networks
Unresponsive wakefulness syndrome
Minimally conscious state

ABSTRACT

Increasing evidence links disorders of consciousness (DOC) with disruptions in functional connectivity between distant brain areas. However, to which extent the balance of brain network segregation and integration is modified in DOC patients remains unclear. Using high-density electroencephalography (EEG), the objective of our study was to characterize the local and global topological changes of DOC patients' functional brain networks.

Resting state high-density-EEG data were collected and analyzed from 82 participants: 61 DOC patients recovering from coma with various levels of consciousness (EMCS ($n = 6$), MCS+ ($n = 29$), MCS- ($n = 17$) and UWS ($n = 9$)), and 21 healthy subjects (i.e., controls). Functional brain networks in five different EEG frequency bands and the broadband signal were estimated using an EEG connectivity approach at the source level. Graph theory-based analyses were used to evaluate their relationship with decreasing levels of consciousness as well as group differences between healthy volunteers and DOC patient groups.

Results showed that networks in DOC patients are characterized by impaired global information processing (network integration) and increased local information processing (network segregation) as compared to controls. The large-scale functional brain networks had integration decreasing with lower level of consciousness.

1. Introduction

Severe brain damages may lead to various disorders of consciousness (DOC; (Giacino et al., 2014)). Emerging evidence associates DOC with alterations in functional and/or structural brain networks, mainly those sustaining arousal and awareness (Amico et al., 2017; Annen et al., 2016; Annen et al., 2018; Bodien et al., 2017; Boly et al., 2012; Fernández-Espejo et al., 2012; Owen et al., 2009). Therefore, network-based EEG methods enabling the identification of these pathological alterations in brain networks are valuable. More specifically, new 'neuromarkers' able to identify network characteristics associated with DOC could improve diagnosis and optimize patient-specific clinical follow-up. This is important, since DOC encompass a variety of consciousness states, such as the unresponsive wakefulness syndrome

(UWS; wakefulness with only reflex movements) (Laureys et al., 2010; Monti et al., 2010), the minimally conscious state (MCS, reproducible and purposeful behavior; divided in MCS- and MCS+, the latter characterized by the presence of response to command, intentional communication and/or intelligible verbalization) (Giacino et al., 2002), and emergence from the minimally conscious state (EMCS, characterized by recovered functional communication and/or object use) (Giacino et al., 2002).

These different clinical diagnoses are defined by functional boundaries as measured with behavior, preferably using the Coma Recovery Scale-Revised (CRS-R; (Giacino et al., 2004)). However, there is a transition zone between the different states that marks the recovery from UWS to MCS or higher awareness levels (Giacino et al., 2009; Schiff and Fins, 2016), emphasizing that DOC are not a static

* Corresponding author.

E-mail address: julien.modolo@inserm.fr (J. Modolo).

¹ Equally contributed.

phenomenon but could be conceptualized as a continuum, with patients sometimes moving from UWS to MCS and back in a short time span. Indeed, diagnosis is most reliable in chronic patients after at least 5 behavioral assessments, accounting for arousal and awareness fluctuations (Wannez et al., 2017). Clinical diagnosis based on behavior is furthermore limited by misdiagnosis due to, for example, physical limitations such as spasticity, language impairments, and medical complications. UWS patients in which the neuroimaging shows results in line with the ability to sustain consciousness are not rare and may represent about 30% of the DOC population (Stender et al., 2014). This category of patients are termed non-behavioral MCS (MCS*, (Gosseries et al., 2014) or Cognitive Motor Dissociation (CMD), (Schiff, 2015). Even though clinical diagnosis based on these functional boundaries is important for prognosis and treatment (e.g., (Thibaut et al., 2014)), overlapping cognitive function as measured with neuroimaging/neurophysiology between diagnostic entities is expected to some extent.

Electroencephalography (EEG) records cortical electrical activity from scalp electrodes, and has major assets due to its non-invasiveness, easiness-of-use and clinical accessibility. Previous EEG network-based studies in the context of DOC have indeed reported the limitations of computing connectivity at the EEG scalp level (see for review (Hassan and Wendling, 2018; Schoffelen and Gross, 2009) even if this can be compensated by methods removing zero-lag components, (Chennu et al., 2017; Vinck et al., 2011). More essentially, scalp analysis does not allow making inferences about interacting brain regions. A potential solution is an emerging technique called “MEG/EEG source connectivity” (De Pasquale et al., 2010; Hassan et al., 2015; Hipp et al., 2012; Kabbara et al., 2017; Kabbara et al., 2018; Mehrkanoon et al., 2014; Mheich et al., 2017; Rizkallah et al., 2018), which reduces the aforementioned volume conduction. It is also conceptually attractive since networks can be directly identified at the cortical level with a high time/space resolution (for more details, see (Hassan and Wendling, 2018). Since conscious processing involves synchronization of locally generated oscillations between remote groups of neurons (Melloni et al., 2007), high-density EEG functional connectivity at the source level is a promising approach to track such synchronizations. In contrast, the time resolution of most fMRI techniques does not enable the detection of fast neural oscillations (e.g., 30–80 Hz range), which are involved in conscious perception and information transfer between regions (Fries, 2015), limiting the possibilities to study synchronization-based communication with fMRI.

Over the past decade, graph theory has become a well-established approach in the field of network neuroscience (Fornito et al., 2016). It provides complementary information to source connectivity methods by quantifying functional and/or statistical aspects of identified brain networks. Among the few studies using graph theory in DOC, a common finding is the identification of disturbances in overall network integration, usually computed by modularity-based approaches (Chennu et al., 2017; Crone et al., 2014; Demertzi et al., 2015). However, to what extent the balance between EEG frequency-dependent network segregation (local information processing) and integration (global information processing) is altered in DOC remains elusive, which is the main objective of this paper. More specifically, large-scale communication (integration) between brain regions appears to involve rather low-frequency oscillations such as the theta rhythm, while local information processing rather involves high-frequency oscillations such as the gamma rhythm (Lisman and Jensen, 2013) for a detailed review). Here, we tackle the issue of the integration/segregation balance and its relationship with low/high frequency neuronal oscillations in patients

with DOC. In this study, we combined EEG source connectivity with graph theory, applied to resting-state high-density-EEG (256 channels) data recorded from patients with DOC whose diagnosis has been established based on the Coma Recovery Scale-Revised (CRS-R; (Giacino et al., 2004)).

Our specific objectives were to i) track alterations in objective functional connectivity measures reflecting cortical brain networks as a function of clinical consciousness levels (ranging from patients diagnosed as unresponsive, through those who have emerged from minimally conscious and healthy control subjects) and ii) identify the brain regions that were differentially involved between groups by means of direct group comparisons.

2. Materials and methods

2.1. Participants

Sixty-one patients (24 females, mean age 40 ± 14.5) and twenty-one healthy subjects (i.e. controls; 8 females, mean age 41 years ± 15.4) were included in this study. Patients were diagnosed as EMCS ($n = 6$), MCS+ ($n = 29$), MCS- ($n = 17$) and UWS ($n = 9$). Etiology was traumatic in 28 patients and non-traumatic in 33 patients. Time since injury was on average three years and ranged from nine days to 19 years. The Ethics Committee of the University Hospital of Liège approved this study. All healthy subjects and patients' legal surrogates gave informed written consent for participation to the study.

Patients' level of consciousness was assessed using the CRS-R (Giacino et al., 2004) repeated at least 5 times to minimize clinical misdiagnosis (Wannez et al., 2017). Patient's diagnosis was based on the best behaviors/highest item obtained over the repeated CRS-R assessments during the week of hospitalization. The following demographic information (listed in Supplementary Table T1) was also collected for each patient: age, gender, traumatic or non-traumatic etiologies and best clinical diagnosis based on the CRS-R assessments.

2.2. Data acquisition and preprocessing

The full pipeline of the analysis is described in Fig. 1. A high-density EEG system (EGI, Electrical Geodesic Inc., 256 electrodes applied with a saline solution) was used to record resting state brain activity with a sampling rate of either 250 Hz or 500 Hz (which were down-sampled to 250 Hz for consistency). During data collection, patients were awake and had their eyes open (an examiner was present during the whole acquisition to ensure that the patients remained awake and eyes open in a silent and dark room, tactile or auditory stimuli were administered if patients were closing their eyes).

EEG data from 178 channels on the scalp were retained for analysis; neck, forehead and cheeks channels were discarded, since they are the most prone to muscular artifacts, as previously described (Hassan et al., 2016; Kabbara et al., 2017). EEG signals were filtered between 0.3 and 45 Hz and then re-referenced using the average reference (Tadel et al., 2011). Overall, out of 115 patients' recordings, we retained 61 datasets for further processing and analysis. The other recordings were excluded due to excessive contamination by artifacts (e.g., muscle artifacts).

All EEG epochs were visually inspected before Independent Components Analysis (ICA) was performed to remove eye blinking artifacts using EEGLAB (Delorme and Makeig, 2004). Electrodes with poor signal quality were interpolated in Brainstorm using signals recorded by surrounding electrodes (spherical spline interpolating method, with a maximal distance between neighbors of 5 cm). Segments that have > 20 electrodes interpolated have been excluded from the analysis. The MRI template “Colin27” (Holmes et al., 1998) and EEG signals were co-registered through identification of the same anatomical landmarks (left and right tragus and nasion) using Brainstorm (without digitalizing the electrodes). The lead field matrix was then computed for a cortical mesh of 15,000 vertices using openMEEG

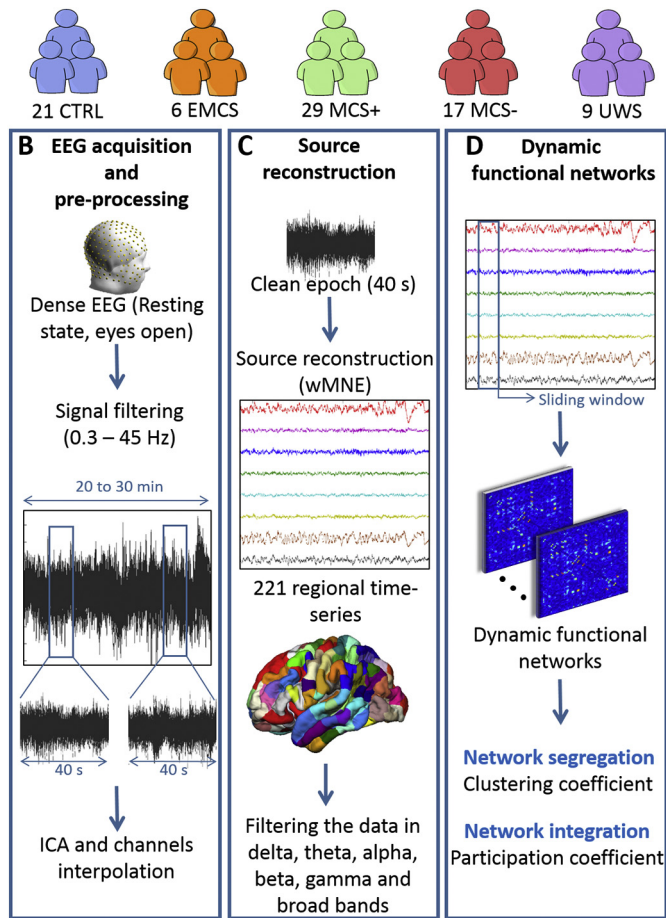


Fig. 1. Data processing pipeline. (A) Database: Patients were diagnosed according to repeated assessments with the CRS-R into EMCS, MCS+, MCS- and UWS. The demographic details are listed in Supplementary Table T1. (B) EEG acquisition and preprocessing: High-density-EEGs were recorded using 256 electrodes during resting-state (eyes open, in the dark) for 20 to 30 min. Signals were then filtered between 0.3 and 45 Hz and segmented into 40 s epochs. Independent Component Analysis (ICA) was applied and bad channels were interpolated. Finally, the first five clean epochs were kept for analysis. (C) Source reconstruction: EEG cortical sources were estimated using the weighted norm estimation method (wMNE). This step was followed by a projection of the source signals on an atlas based on Desikan-killiany and Hagmann atlases, using a template brain. Reconstructed regional time series were filtered in six different frequency bands: Delta (1–3 Hz), Theta (3–7 Hz), Alpha (7–13 Hz), Beta (14–25 Hz), Gamma (30–45 Hz) and Broadband (1–45 Hz). (D) Dynamic functional networks: Functional connectivity matrices were computed using the phase locking value (PLV) calculated using a sliding window technique. Networks were then characterized by their clustering coefficient (segregation) and participation coefficient (integration).

(Gramfort et al., 2010). The noise covariance matrix was calculated using a long segment of noisy EEG data at rest, as recommended in (Tadel et al., 2011). An atlas-based segmentation approach was used to project EEGs onto an anatomical framework consisting of 221 cortical regions identified by means of re-segmenting the Desikan-Killiany (Desikan et al., 2006) atlas using Freesurfer (Fischl, 2012). Time series within one region of interest were averaged after flipping the sign of sources with negative potentials.

2.3. Brain networks construction

Functional brain networks were constructed using the “high-density-EEG source connectivity” method (Hassan et al., 2014) which quantifies the functional connectivity between regional time series at

the source level. The EEG source connectivity method aims to bridge functional network at the level of cortical sources and the recorded scalp EEG signals, which involves solving an inverse problem (from the EEG to the sources). This is an ill-posed problem since we have a number of electrodes that is greatly inferior to the number of possible sources. Therefore, several physical (position and orientation of the sources) mathematical (amplitude) constraints have to be formulated to solve the inverse problem. Here, regarding the position of the sources, we used a segmented MRI image (template brain available in Brainstorm package), with the position of each source being a vertex on the brain mesh. Regarding the orientation of the sources, it was set as normal to the cortical surface for each vertex, which is plausible since the origin of EEG signals occurs from post-synaptic currents at the level of pyramidal cells, and that pyramidal cells are aligned “en palissade” and are normal to the cortical surface. In terms of mathematical constraints, we used the weighted minimum norm estimate (wMNE), which aims to identify sources with the smallest energy. For further details, see (Hassan and Wendling, 2018).

The EEG source connectivity method includes two main steps: i) reconstruction of the cortical regions (brain sources) temporal dynamics from the scalp EEG signals and ii) measurement of the functional connectivity between reconstructed regional time series. wMNE was used to reconstruct the cortical sources by introducing a weighting matrix:

$$\hat{S}_{wMNE} = (G^T W_X G + \lambda I)^{-1} G^T W_X X$$

where the diagonal matrix W_X is built from the lead field matrix G with non-zero terms inversely proportional to the norm of the lead field vectors. The regularization parameter λ is computed relatively to the signal to noise ratio ($\lambda = 0.1$ in our analysis). Reconstructed regional time series were filtered in six different frequency bands: Delta (1–3 Hz), Theta (3–7 Hz), Alpha (7–13 Hz), Beta (14–25 Hz), Gamma (30–45 Hz) and broadband (1–45 Hz). Then, we computed the functional connectivity between the reconstructed regional time series in each frequency band, using the phase locking value (PLV) (Lachaux et al., 1999) defined as:

$$PLV(t) = \left| \frac{1}{\delta} \int_{t-\delta/2}^{t+\delta/2} e^{j(\varphi_y(t) - \varphi_x(t))} d\tau \right|$$

where $\varphi_y(t)$ and $\varphi_x(t)$ are the phases of the signals x and y at time t extracted using the Hilbert transform. δ denotes the size of the window in which PLV is calculated. PLV values range between 0 (no phase locking) and 1 (full synchrony). Detailed methodological description and technical details of the high-density EEG source connectivity method as computed in this paper can be found in (Hassan et al., 2015).

We used a sliding window technique for each epoch to compute the dynamic functional connectivity matrices. The smallest window length recommended by (Lachaux et al., 2000) was used, equal to $\frac{\text{number of cycles}}{\text{central frequency}}$ where the number of cycles at the given frequency band is equal to six. Finally, we adopted a 10% (of the highest PLV values) threshold to retain only the ‘true’ functional connections, and remaining PLV values were set to zero.

2.4. Multi-slice networks modularity

Thresholded weighted connectivity matrices were split into time-varying modules using multi-slice networks modularity (Bassett et al., 2013; Mucha et al., 2010). This algorithm consists of linking nodes across network slices (time windows) via a coupling parameter before applying the modularity maximization method (Bassett et al., 2011; Bassett et al., 2015): each node is only connected to itself in the adjacent layers. This produces, for every brain region at every time window, a modular assignment reflecting the module allegiance.

Due to a degeneracy problem in the modularity algorithms (Good et al., 2010), i.e. running the same algorithm on the same connectivity

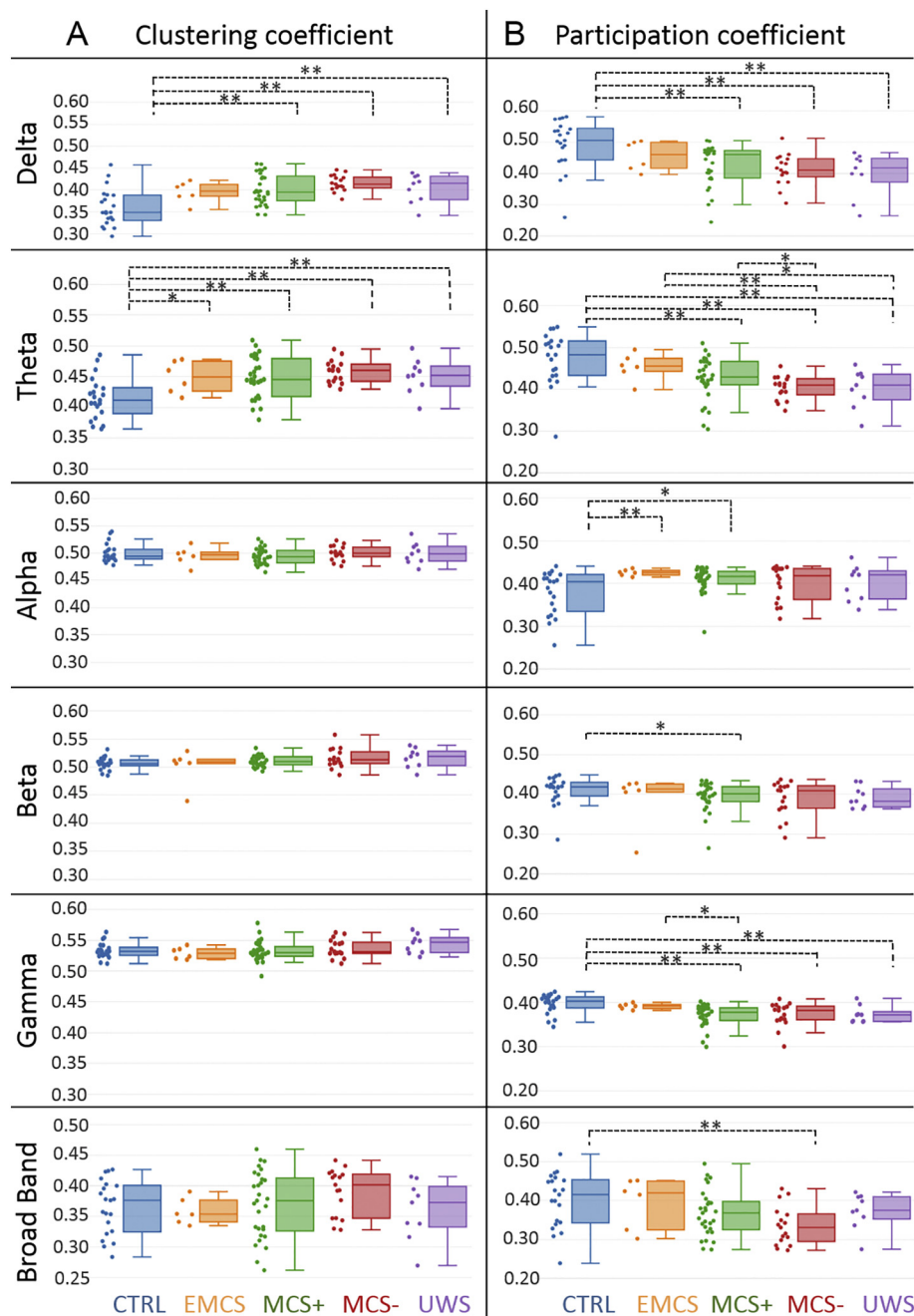


Fig. 2. Brain segregation and integration in control subjects and patients with decreasing levels of consciousness due to severe brain injury. A. The clustering (segregation) and B. participation (integration) coefficients are presented for all groups in delta (1–3 Hz), theta (3–7 Hz), alpha (7–13 Hz), beta (14–25 Hz), gamma (30–45 Hz) and broad band (3–45 Hz). Values were averaged over all brain regions. Individual patient metrics are shown in the scatter plot next to the box plot. Increase of clustering coefficient values and decrease of participation coefficient values with decreased consciousness level was found within all frequency bands. A Wilcoxon test was applied between groups. * denotes $p < .05$ without correction and ** with correction.

matrix can result in slightly different outputs, the multilayer network modularity was computed 100 times and a 221 by 221 association matrix was generated (Bassett et al., 2013; Fornito et al., 2016; Lancichinetti and Fortunato, 2012). The association matrix elements indicate the number of times each node was assigned to the same module with the other nodes across these 100 partitions. The association matrix was then compared to a null-model generated from 100 random permutation from the originals partitions, and only significant values ($p < .05$) were kept (Bassett et al., 2011). Finally, the Louvain algorithm (Blondel et al., 2008) was applied on the association matrix to cluster the network, resulting in a partition that is the most representative of network modularity.

2.5. Network measures

Our main intent was to explore two important properties related to

information processing in the human brain network:

- *Network segregation*, which reflects local information processing. For this reason, the clustering coefficient ‘C’ was computed and considered as a direct measure of network segregation (Bullmore and Sporns, 2009). In brief, C represents how close a node’s neighbors tend to cluster together (Watts and Strogatz, 1998).

$$C_i = \frac{2t_i}{k_i(k_i - 1)}$$

where t_i denotes the number of triangles around the node i and k_i represents the number of edges connected to the node i . This coefficient is the proportion of connections among a node’s neighbors, divided by the number of connections that could possibly exist between them, which is 0 if no connections exist and 1 if all neighbors are connected. The average clustering coefficient of a network was calculated for each epoch by averaging the clustering coefficient values over all the 221

regions.

- *Network integration*, which reflects global information processing. The participation coefficient was computed to measure the diversity of a node inter-modular connections (Guimerà and Amaral, 2005).

$$P_i = 1 - \sum_{s=1}^{N_m} \left(\frac{k_{is}}{k_i} \right)^2$$

where N_m is the number of modules, k_{is} is the number of edges between node i and other nodes in module s , and k_i is the total degree of node i . The participation coefficient of a node is close to 1 if its links are uniformly distributed among all the modules and 0 if all of its links are within its own module. Nodes with high participation coefficients interconnect multiple modules together, and hence can be seen connectivity hubs. The average participation coefficient of a network is calculated for each epoch by averaging the participation coefficient values over all 221 regions.

2.6. Statistical analysis

The Jonckheere-Terpstra (JT) test (Jonckheere, 1954; Terpstra, 1952), a non-parametric and rank-based trend test, was used to test the trends of network metrics as a function of the continuum of clinical levels of consciousness. Regional-level differences were analyzed between the groups, with the exception of the EMCS group due to its very small sample size ($N = 6$).

To statistically assess whether group differences between brain integration and segregation and clinical levels of consciousness exist (healthy volunteers versus all patient groups and between patient groups) we used the Mann-Whitney U Test. In order to address the family-wise error rate, statistical tests were corrected for multiple comparisons using the Bonferroni method. In the global-wise analysis, $p_{\text{bonf}} = 0.05/N_g$, where $N_g = 5$ denotes the number of groups. In the region-wise analysis, $p_{\text{bonf}} = 0.05/N_r$, where $N_r = 221$ denotes the number of regions of interest.

Data availability. The data used in the present study is available upon reasonable request.

3. Results

There were no differences between patients and controls in terms of gender ($p = .6$) or age ($p = .2$) and between patient groups for time since injury ($p = .12$).

3.1. Network segregation/integration as a function of clinical levels of consciousness

The results in Fig. 2A illustrate a trend towards increased clustering coefficient values with decreased consciousness level in the delta (JT trend statistic = 4.2, $p < .0001$), theta (JT trend statistic = 3.67, $p = .0001$), beta (JT trend statistic = 2.24, $p = .01$) and gamma (JT trend statistic = 1.66, $p = .04$) bands. In the delta band, controls had lower clustering coefficients than patients in MCS+ ($p = .0007$, $U = 133$, $r = 0.47$, corrected), MCS- ($p < .0001$, $U = 43$, $r = 0.62$, corrected) and UWS ($p = .01$, $U = 39$, $r = 0.485$ corrected). In the theta band, the clustering coefficient was also lower in controls as compared to MCS+ ($p = .001$, $U = 146$, $r = 0.43$, corrected), MCS- ($p = .0001$, $U = 47$, $r = 0.62$, corrected) and UWS ($p = .01$, $U = 38$, $r = 0.46$, corrected).

The results in Fig. 2B illustrate decreased participation coefficient values with decreased consciousness level in the delta (JT trend statistic = 4.5, $p < .0001$), theta (JT trend statistic = 4.9, $p < .0001$), beta (JT trend statistic = 2.2, $p = .01$), gamma (JT trend statistic = 3.9, $p < .0001$) and broad bands (JT trend statistic = 2.7, $p = .0034$). In the delta band, the participation coefficient was higher

in controls as compared to MCS+ ($p = .0005$, $U = 480$, $r = 0.48$, corrected), MCS- ($p = .0007$, $U = 294$, $r = 0.54$, corrected) and UWS ($p = .005$, $U = 156$, $r = 0.5$ corrected).

In the theta band, the participation coefficient was higher in controls as compared to MCS+ ($p = .003$, $U = 457$, $r = 0.42$, corrected), MCS- ($p < .0001$, $U = 317$, $r = 0.65$, corrected), and UWS ($p = .003$, $U = 159$, $r = 0.52$, corrected). The participation coefficient in the theta band was also higher in EMCS as compared to MCS- ($p = .007$, $U = 90$, $r = 0.56$, corrected).

In the alpha band, the participation coefficient showed lower values in controls than in EMCS ($p = .009$, $U = 18$, $r = 0.49$, corrected). However, in the gamma band, the participation coefficient showed a decrease in MCS+ patients ($p = .0002$, $U = 492$, $r = 0.52$, corrected), MCS- patients ($p = .002$, $U = 282$, $r = 0.49$, corrected), and UWS patients ($p = .01$, $U = 150$, $r = 0.45$, corrected) as compared to controls. Additionally, we performed the JT tests excluding the controls to confirm that our results were not solely driven by this group, and all trends remained significant in theta, delta and gamma bands.

3.2. Regional-wise differences between groups

We present below results for the participation coefficient in the theta (Fig. 3) and gamma (Fig. 4) bands.

All patient groups had brain regions with significantly (Bonferroni-corrected) decreased integration as compared to the control group and no regions with higher integration values were identified. As expected, a wider network was involved in the decreased integration in MCS-patients than in MCS+ patients, as compared to the controls. However, the differences between the control group and the UWS group were much less pronounced than between the control group and the MCS-group, which might originate from the small sample size of the UWS group ($N = 9$). Regions that resisted the Bonferroni correction were mainly located in the left precuneus and left/right orbitofrontal area for the comparison of controls > UWS ($p < .0002$). A large number of brain regions had decreased integration in the MCS- group as compared to the control group (exhaustive list in Supplementary Material), including the right orbitofrontal ($p < .0002$), left inferior temporal ($p < .0002$) and left superior parietal ($p < .0002$). The left precuneus, left/right orbitofrontal, left/right fusiform, left superior temporal, right precentral ($p < .0002$) showed a higher participation coefficient in the theta band for controls than MCS+ patients.

The results regarding the participation coefficient for the reconstructed functional networks in the gamma band are presented in Fig. 4. No significant differences were observed between patient groups. The comparison between control and MCS- groups revealed a decrease in participation coefficient in MCS- patients mainly in the left fusiform, left postcentral and right dorso-lateral frontal cortex ($p < .0002$). A much wider network of regions had a decreased participation coefficient between control and MCS+ groups, mainly located in the left/right lateral frontal cortex and right central cortex ($p < .0002$). Again, as in the case of the theta band, the UWS group had a lower number of regions with decreased integration than MCS groups, as compared to the control group. The exact labels of the regions with a significant difference in the participation coefficient (in theta and gamma bands), along with Bonferroni corrections, are available in the Supplementary Materials Tables T2 and T3.

4. Discussion

Emerging evidence supports that DOC are characterized by disruptions of brain networks that sustain arousal and awareness, as reviewed by (Bodien et al., 2017). Therefore, identifying alterations in whole-brain functional networks from non-invasive techniques, along with their relationships with varying consciousness levels, is a crucial and challenging issue. In this study, based on scalp high-density EEG recordings, we identified alterations in resting-state functional networks

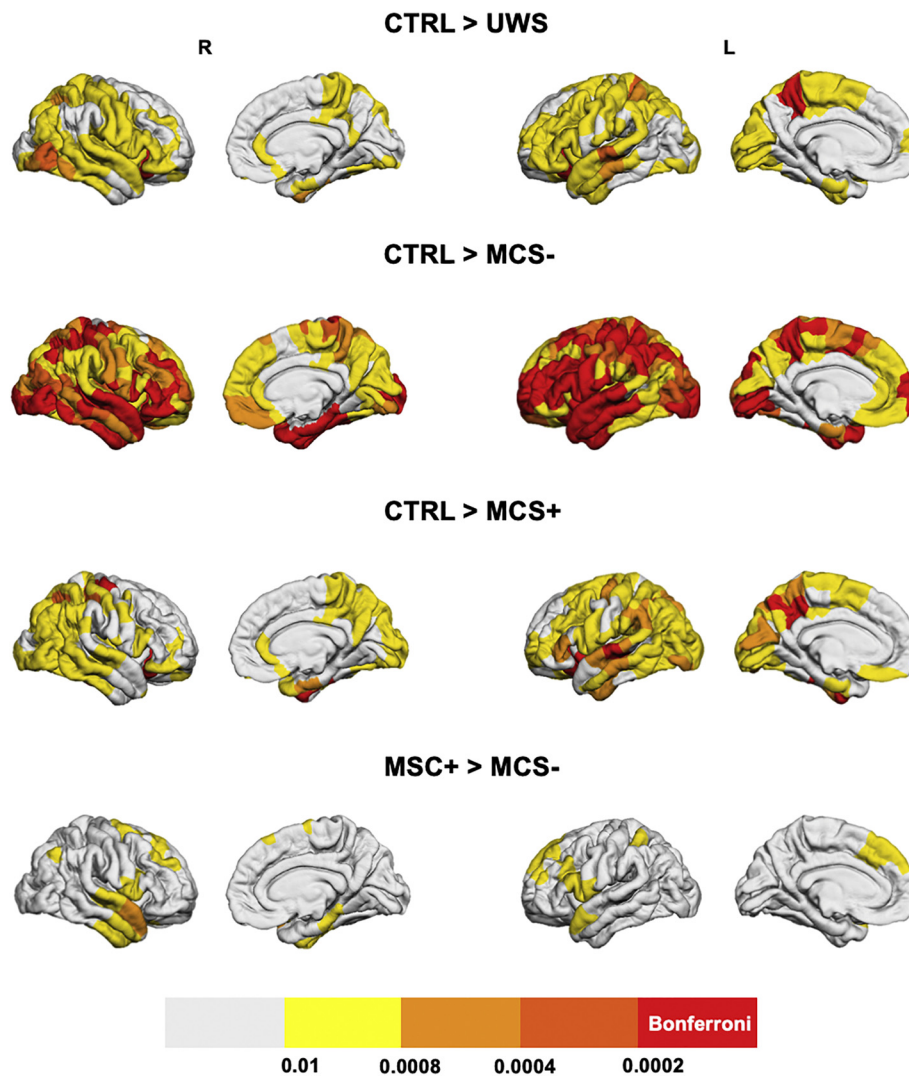


Fig. 3. Between-group comparison of regional decreases in theta band integration. Brain regions that have significantly lower integration in UWS, MCS- and MCS+ as compared to the control group and in MCS- patients compared to MCS+ patients are presented. Brain regions having a p -value lower than $0.05/221 = 0.0002$ (Bonferroni-corrected) are presented in the red color, regions with $0.0002 < p < .0004$ are presented in dark orange, if $0.0004 < p < .0008$ the light orange color was used, for $0.0008 < p < .01$ the yellow color was used and if $p > .01$ the regions are presented in white.

associated with DOC. Interestingly, a gradual reconfiguration of functional brain networks was observed in line with the consciousness level. Our findings also pointed at a decrease in brain network integration (communication between distant brain modules) and an increase in brain network segregation (communication within the same brain module) in DOC patients as compared to healthy controls. A decrease in brain integration with decreasing consciousness is especially relevant from a fundamental point of view. Indeed, one of the most prevalent theories, namely the Integrated Information Theory (IIT), describes the generation of conscious experiences as a result of a sufficiently complex integration of information between brain regions (Tononi, 2004; Tononi et al., 2016).

Although using EEG to identify markers in DOC is not novel in itself. The originality of the present work is that, as opposed to most previous studies, functional brain networks were estimated at the cortical level using high-density EEG data, which enabled making inferences about interacting regions. For example, we explored alterations of functional brain networks in two key aspects of human brain information processing: segregation and integration. These findings indicate that functional connectivity between distant areas (network integration) decreases with decreased level of consciousness.

4.1. Low network integration in DOC patients

The main finding of the present study is a decreasing trend in the integration of resting-state functional brain networks with the consciousness level. This finding is consistent with the conclusions from several studies (Chennu et al., 2017; Crone et al., 2014), including those investigating transcranial magnetic stimulation (TMS)-evoked EEG responses in patients with DOC (Casali et al., 2013; Casarotto et al., 2016). An important contribution of the present study is that, as opposed to complexity-based indexes computing using TMS-evoked responses, the computation of integration is based only on resting-state functional networks. It does not require any brain stimulation hardware, which could have a potential clinical and practical value, even if in this study we were not able to identify a difference between MCS and UWS groups.

Two common anatomical regions were identified with decreased integration when comparing the control group with any of the patient groups. The first is the left precuneus, a key hub structure from the default mode network (DMN). The precuneus is engaged in self-related processing (Zhang and Chiang-shan, 2012), episodic memory (Ren et al., 2018), awareness and conscious information processing (Kjaer et al., 2001; Long et al., 2016; Vogt and Laureys, 2005). Also, it has

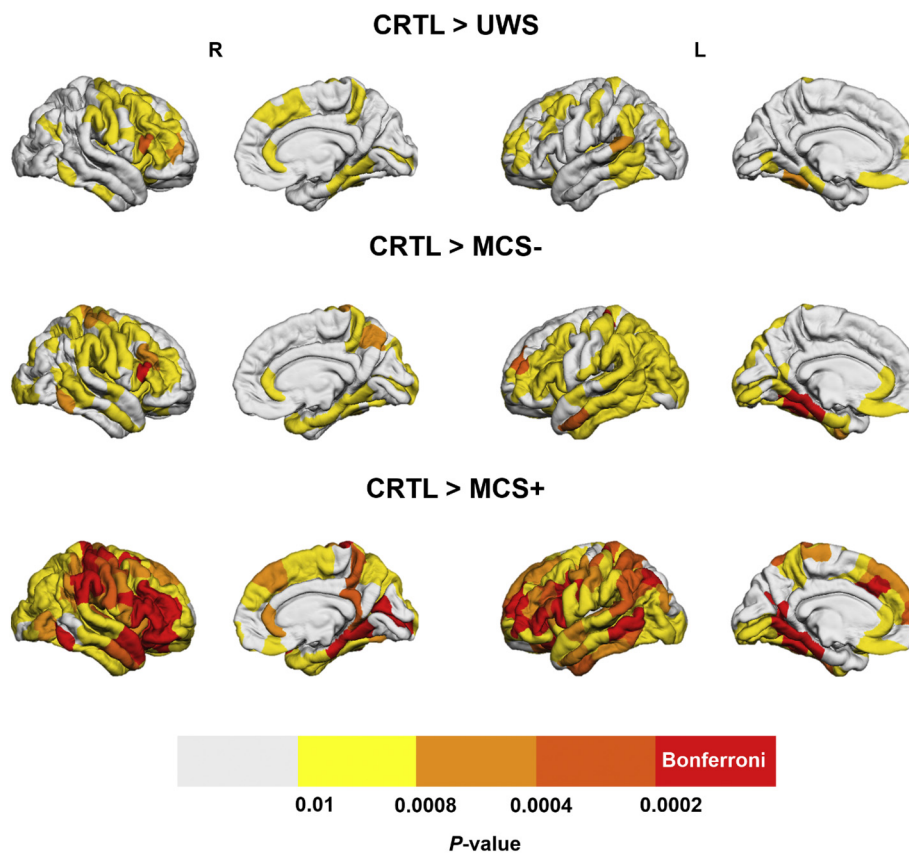


Fig. 4. Between-group comparison of regional decreases in gamma band integration. Brain regions that have significantly lower integration in UWS, MCS- and MCS+ as compared to the control group are presented. Brain regions having a p -value lower than $0.05/221 = 0.0002$ (Bonferroni-corrected) are presented in the red color, regions with $0.0002 < p < .0004$ are presented in dark orange, if $0.0004 < p < .0008$ the light orange color was used, for $0.0008 < p < .01$ the yellow color was used and if $p > .01$ the regions are presented in white. (For interpretation of the references to color in this figure legend, the reader is referred to the web version of this article.)

been shown that patients with UWS having residual functional connectivity of DMN and external awareness networks might be misdiagnosed, since such functional connectivity is an indicator of covert consciousness (Naro et al., 2017). Second a part of the left orbitofrontal cortex is affected, this region is believed to encode predicted values of potential rewards (Gottfried et al., 2003). It is also thought to play a major role in the evaluation of specific behavioral outcomes to influence action selection, depending on emotional and sensory contexts (Rudebeck and Murray, 2014) and in pain perception (Naro et al., 2015). As mentioned previously, the network of regions with decreased integration in the theta band is wider in MCS- patients than in MCS+ patients, which is consistent with their respective clinical CRS-R diagnosis. It remains unclear why the UWS group had fewer involved brain regions with decreased integration when compared to controls than the MCS+ and MCS- groups.

Two main factors may explain the absence of group differences between UWS and MCS patients. First, the limited sample size ($N = 9$) of the UWS group, which decreases statistical power for the group comparison, especially given the high heterogeneity in DOC patients' structural and functional brain lesions. Second, clinical diagnoses might represent overlapping brain functioning (Schiff and Fins, 2016). In line with this notion, previous studies identifying functional and structural differences between patient groups have sometimes failed to identify group differences between UWS and MCS, but found a difference between DOC and healthy controls' groups (e.g., (Demertzi et al., 2014; Di Perri et al., 2016)). The identification of group differences still remains a key objective for clinical applications and should be addressed in larger multicenter studies.

Regarding the increased network segregation, results were less pronounced between groups as compared to network integration. This could explain discrepancies between previous studies, some referring to an increase in network segregation (using the clustering coefficient for instance) (Chennu et al., 2014), while others reported the opposite (Chennu et al., 2017). It is worth mentioning that, in our study and the

one conducted by (Chennu et al., 2017), segregation results have opposite trends. A possible explanation is that the study by (Chennu et al., 2017) performed functional connectivity in the electrode space, while the present study functional connectivity was computed in the source space. The relationship between scalp versus source space functional connectivity using EEG is indeed still an open question in the EEG community. A recent study that compared scalp- and source- reconstructed networks concluded that, not only the magnitude of network measures may change from scalp to source (EEG) analysis, but even the direction of the effect may be the opposite (still depending on the functional connectivity metric) between both methods (Lai et al., 2018). Therefore, even if further efforts need to be made in the comparison between source- and scalp- EEG-based networks, such discrepancies can be explained by the method of network reconstruction.

4.2. Methodological considerations and limitations

In this study, a proportional threshold of 10% was used to eliminate spurious connections from connectivity matrices. We chose using a proportional threshold instead of an absolute threshold to warrant equal density between groups, as recommended by (van den Heuvel et al., 2017). Moreover, Garisson et al. (Garrison et al., 2015) reported that network measures are stable across proportional thresholds, as opposed to absolute thresholds. A variety of thresholding methods are available, but no method is free of bias, it is therefore recommended to perform studies across different values of thresholds to ensure that findings are robust against this methodological factor. Therefore, we tested several threshold values, which did not have any impact on the main conclusions of the study, as illustrated in Supplementary Figs. S1 and S2.

Second, the muscle artifact in the gamma band is a serious methodological issue. Here, we have reduced the effect of the muscle artifacts by selecting only 178 channels for analysis (neck, forehead and cheeks channels were discarded, since they are the most prone to muscular

artifacts). Data with excessive movement artifact were removed by interpolating abnormally noisy channels and removing epochs with > 20 interpolated electrodes.

Third, the choice of wMNE/PLV was supported by two comparative analyses performed in (Hassan et al., 2014; Hassan et al., 2016) that reported the superiority of wMNE/PLV over other combinations of five inverse algorithms and five connectivity measures. Briefly, in (Hassan et al., 2016), the network identified by each inverse/connectivity combination used to identify cortical brain networks from scalp EEG was compared to a simulated network (ground truth). The combination that showed the highest similarity between the scalp-EEG-based network and reference network (using a network similarity algorithm) was considered as the optimal combination, which was found to be wMNE/PLV.

A persistent problem in the field of MEG/EEG source functional connectivity is the volume conduction effect (Brookes et al., 2012). Source level connectivity analysis has been shown to diminish the volume conduction problem, since connectivity metrics are estimated between 'local' regional time-series. However, these 'mixing effects' can also arise in the cortical source space, and ghost couplings can be produced by some connectivity methods when applied to mixed signals. To tackle this issue, a number of methods were developed mainly centered on the zero-lag correlation rejection. Un-mixing methods, called 'leakage correction', have been reported to force the reconstructed signals to have zero cross-correlation at lag zero (Colclough et al., 2015). Although handling this problem -theoretically- improves interpretation, a recent study showed that the estimated connectivity can be false and significantly different from the true connectivity (Palva et al., 2018; Pascual-Marqui et al., 2017).

In the present study, a template source space was used, instead of a subject-specific one. This might be problematic in severely brain-injured patients, since different brain regions are injured between patients. In the case of healthy subjects, (Douw et al., 2018) found that co-registration with a template brain yielded largely consistent connectivity and network estimates as compared to native MRI. However, in the case of severe brain damage, it remains unknown how a template instead of a native MRI co-registration affects results and their interpretability.

Although the significant trends in network integration decrease with the level of consciousness, the current approach failed to identify a significant difference, at the group level, between MCS and UWS groups. This absence of difference represents, at this stage, a limitation in terms of potential clinical translation. That being said, this represents a challenge and an opportunity to develop further EEG network-based markers of the consciousness level based solely on resting-state recordings, to improve the diagnosis of DOC patients using a limited and accessible hardware.

Competing interests

The authors have no competing financial interests to declare.

Declaration of authorship

Conceptualization: PB, MH, FW, SL. Data curation: JA, OG, SM, HC, AT, CC, RP, SL. Formal analysis: JR, JM, PB, MH, FW. Funding acquisition: FW, SL. Investigation: JR, JA, OG, JM, PB, MH. Methodology: JA, PB, MH, FW, SL. Project administration: FW, SL. Resources: FW, SL. Software: JR, MH. Supervision: FW, SL. Validation: FW, SL. Visualization: JR, JA, JM, MH. Writing (original draft): JR. Writing (review and editing): JR, JA, JM, OG, PB, SM, HA, HC, AM, AT, CC, MH, RP, FW, SL.

Acknowledgements

This study was supported by the Future Emerging Technologies

(H2020-FETOPEN-2014-2015-RIA under agreement No. 686764) as part of the European Union's Horizon 2020 research and training program 2014–2018; the University and University Hospital of Liège; the Belgian National Funds for Scientific Research (FRS-FNRS); the Human Brain Project (EU-H2020-fetflagship-hbp-sga1-ga720270); the French Speaking Community Concerted Research Action (ARC - 06/11 - 340); NSERC discovery grant, IAP research network P7/06 of the Belgian Government (Belgian Science Policy); the European Commission; the James McDonnell Foundation; Mind Science Foundation; the BIAL foundation; the European space agency (ESA); the Public Utility Foundation 'Université Européenne du Travail'. JR is a PhD student with a fellowship from the AZM and SAADE Association, Tripoli, Lebanon. OG is postdoctoral researcher at FRS-FNRS. OG is post-doctoral fellow, and SL is research director at the F.R.S.-FNRS. CC is a post-doctoral Marie Skłodowska-Curie fellow (H2020-MSCA-IF-2016-ADOC-752686).

Appendix A. Supplementary data

Supplementary data to this article can be found online at <https://doi.org/10.1016/j.nicl.2019.101841>.

References

- Amico, E., et al., 2017. Mapping the functional connectome traits of levels of consciousness. *NeuroImage* 148, 201–211.
- Annen, J., et al., 2016. Function–structure connectivity in patients with severe brain injury as measured by MRI-DWI and FDG-PET. *Hum. Brain Mapp.* 37, 3707–3720.
- Annen, J., et al., 2018. Regional brain volumetry and brain function in severely brain-injured patients. *Ann. Neurol.* 83, 842–853.
- Bassett, D.S., et al., 2011. Dynamic reconfiguration of human brain networks during learning. *Proc. Natl. Acad. Sci.* 108, 7641–7646.
- Bassett, D.S., et al., 2013. Robust detection of dynamic community structure in networks. *Chaos: Interdisc. J. Nonlinear Sci.* 23, 013142.
- Bassett, D.S., et al., 2015. Learning-induced autonomy of sensorimotor systems. *Nat. Neurosci.* 18, 744–751.
- Blondel, V.D., et al., 2008. Fast unfolding of communities in large networks. *J. Stat. Mech.: Theory Exp.* 2008 P10008.
- Bodien, Y.G., Chatelle, C., Edlow, B.L., 2017. Functional networks in disorders of consciousness. In: *Seminars in Neurology*. vol. 37. Thieme Medical Publishers, pp. 485–502.
- Boly, M., et al., 2012. Brain connectivity in disorders of consciousness. *Brain Connectivity* 2, 1–10.
- Brookes, M.J., Woolrich, M.W., Barnes, G.R., 2012. Measuring functional connectivity in MEG: a multivariate approach insensitive to linear source leakage. *Neuroimage* 63, 910–920.
- Brunner, C., et al., 2016. Volume conduction influences scalp-based connectivity estimates. *Front. Comput. Neurosci.* 10.
- Bullmore, E., Sporns, O., 2009. Complex brain networks: graph theoretical analysis of structural and functional systems. *Nat. Rev. Neurosci.* 10, 186–198.
- Casali, A.G., et al., 2013. A theoretically based index of consciousness independent of sensory processing and behavior. *Sci. Transl. Med.* 5, 198ra105.
- Casarotto, S., et al., 2016. Stratification of unresponsive patients by an independently validated index of brain complexity. *Ann. Neurol.* 80, 718–729.
- Chennu, S., et al., 2014. Spectral signatures of reorganised brain networks in disorders of consciousness. *PLoS Comput. Biol.* 10, e1003887.
- Chennu, S., et al., 2017. Brain networks predict metabolism, diagnosis and prognosis at the bedside in disorders of consciousness. *Brain* 140, 2120–2132.
- Colclough, G.L., et al., 2015. A symmetric multivariate leakage correction for MEG connectomes. *NeuroImage* 117, 439–448.
- Crone, J.S., et al., 2014. Altered network properties of the fronto-parietal network and the thalamus in impaired consciousness. *NeuroImage: Clinical* 4, 240–248.
- De Pasquale, F., et al., 2010. Temporal dynamics of spontaneous MEG activity in brain networks. *Proc. Natl. Acad. Sci.* 107, 6040–6045.
- Delorme, A., Makeig, S., 2004. EEGLAB: an open source toolbox for analysis of single-trial EEG dynamics including independent component analysis. *J. Neurosci. Methods* 134, 9–21.
- Demertzi, A., et al., 2014. Multiple fMRI system-level baseline connectivity is disrupted in patients with consciousness alterations. *Cortex* 52, 35–46.
- Demertzi, A., et al., 2015. Intrinsic functional connectivity differentiates minimally conscious from unresponsive patients. *Brain* 138, 2619–2631.
- Desikan, R.S., et al., 2006. An automated labeling system for subdividing the human cerebral cortex on MRI scans into gyral based regions of interest. *Neuroimage* 31, 968–980.
- Di Perri, C., et al., 2016. Neural correlates of consciousness in patients who have emerged from a minimally conscious state: a cross-sectional multimodal imaging study. *Lancet Neurol.* 15, 830–842.
- Douw, L., et al., 2018. Consistency of magnetoencephalographic functional connectivity

- and network reconstruction using a template versus native MRI for co-registration. *Hum. Brain Mapp.* 39, 104–119.
- Engemann, D.A., et al., 2018. Robust EEG-based cross-site and cross-protocol classification of states of consciousness. *Brain* 141, 3179–3192.
- Fernández-Espejo, D., et al., 2012. A role for the default mode network in the bases of disorders of consciousness. *Ann. Neurol.* 72, 335–343.
- Fischl, B., 2012. FreeSurfer. *Neuroimage* 62, 774–781.
- Fornito, A., Zalesky, A., Bullmore, E., 2016. Fundamentals of Brain Network Analysis.
- Fries, P., 2015. Rhythms for cognition: communication through coherence. *Neuron* 88, 220–235.
- Garrison, K.A., et al., 2015. The (in) stability of functional brain network measures across thresholds. *Neuroimage* 118, 651–661.
- Giacino, J.T., et al., 2002. The minimally conscious state definition and diagnostic criteria. *Neurology* 58, 349–353.
- Giacino, J.T., Kalmar, K., Whyte, J., 2004. The JFK coma recovery scale-revised: measurement characteristics and diagnostic utility. *Arch. Phys. Med. Rehabil.* 85, 2020–2029.
- Giacino, J.T., et al., 2009. Behavioral assessment in patients with disorders of consciousness: gold standard or fool's gold? *Prog. Brain Res.* 177, 33–48.
- Giacino, J.T., et al., 2014. Disorders of consciousness after acquired brain injury: the state of the science. *Nat. Rev. Neurol.* 10, 99–114.
- Good, B.H., de Montjoye, Y.-A., Clauset, A., 2010. Performance of modularity maximization in practical contexts. *Phys. Rev. E* 81, 046106.
- Gosseries, O., Zasler, N.D., Laureys, S., 2014. Recent advances in disorders of consciousness: focus on the diagnosis. *Brain Inj.* 28, 1141–1150.
- Gottfried, J.A., O'Doherty, J., Dolan, R.J., 2003. Encoding predictive reward value in human amygdala and orbitofrontal cortex. *Science* 301, 1104–1107.
- Gramfort, A., et al., 2010. OpenMEEG: opensource software for quasistatic bioelectromagnetics. *Biomed. Eng. Online* 9, 45.
- Guimera, R., Amaral, L.A.N., 2005. Functional cartography of complex metabolic networks. *Nature* 433, 895–900.
- Hassan, M., Wendling, F., 2018. Electroencephalography source connectivity: aiming for high resolution of brain networks in time and space. *IEEE Signal Process. Mag.* 35, 81–96.
- Hassan, M., et al., 2014. EEG source connectivity analysis: from dense array recordings to brain networks. *PLoS One* 9, e105041.
- Hassan, M., et al., 2015. Dynamic reorganization of functional brain networks during picture naming. *Cortex* 73, 276–288.
- Hassan, M., et al., 2016. Identification of interictal epileptic networks from dense-EEG. *Brain Topogr.* 1–17.
- Hipp, J.F., et al., 2012. Large-scale cortical correlation structure of spontaneous oscillatory activity. *Nat. Neurosci.* 15, 884.
- Holmes, C.J., et al., 1998. Enhancement of MR images using registration for signal averaging. *J. Comput. Assist. Tomogr.* 22, 324–333.
- Jonckheere, A.R., 1954. A distribution-free k-sample test against ordered alternatives. *Biometrika* 41, 133–145.
- Kabbara, A., et al., 2017. The dynamic functional core network of the human brain at rest. *Sci. Rep.* 7.
- Kabbara, A., et al., 2018. Reduced integration and improved segregation of functional brain networks in Alzheimer's disease. *J. Neural Eng.* 15, 026023.
- Kjaer, T., et al., 2001. Precuneus–prefrontal activity during awareness of visual verbal stimuli. *Conscious. Cogn.* 10, 356–365.
- Lachaux, J.-P., et al., 1999. Measuring phase synchrony in brain signals. *Hum. Brain Mapp.* 8, 194–208.
- Lachaux, J.-P., et al., 2000. Studying single-trials of phase synchronous activity in the brain. *Int. J. Bifurcation Chaos* 10, 2429–2439.
- Lai, M., et al., 2018. A comparison between scalp-and source-reconstructed EEG networks. *Sci. Rep.* 8, 12269.
- Lancichinetti, A., Fortunato, S., 2012. Consensus clustering in complex networks. *Sci. Rep.* 2, 336.
- Laureys, S., et al., 2010. Unresponsive wakefulness syndrome: a new name for the vegetative state or apallic syndrome. *BMC Med.* 8, 68.
- Lisman, J.E., Jensen, O., 2013. The theta-gamma neural code. *Neuron* 77, 1002–1016.
- Long, J., et al., 2016. Distinct interactions between fronto-parietal and default mode networks in impaired consciousness. *Sci. Rep.* 6, 38866.
- Mehrkanoon, S., Breakspear, M., Boonstra, T.W., 2014. Low-dimensional dynamics of resting-state cortical activity. *Brain Topogr.* 27, 338–352.
- Melloni, L., et al., 2007. Synchronization of neural activity across cortical areas correlates with conscious perception. *J. Neurosci.* 27, 2858–2865.
- Mheich, A., et al., 2017. SimiNet: a novel method for quantifying brain network similarity. *IEEE Trans. Pattern Anal. Mach. Intell.* 40, 2238–2249.
- Monti, M.M., Laureys, S., Owen, A.M., 2010. The vegetative state. *Bmj* 341, c3765.
- Mucha, P.J., et al., 2010. Community structure in time-dependent, multiscale, and multiplex networks. *Science* 328, 876–878.
- Naro, A., et al., 2015. Moving toward conscious pain processing detection in chronic disorders of consciousness: anterior cingulate cortex neuromodulation. *J. Pain* 16, 1022–1031.
- Naro, A., et al., 2017. How far can we go in chronic disorders of consciousness differential diagnosis? The use of neuromodulation in detecting internal and external awareness. *Neuroscience* 349, 165–173.
- Owen, A.M., Schiff, N.D., Laureys, S., 2009. A new era of coma and consciousness science. *Prog. Brain Res.* 177, 399–411.
- Palva, J.M., et al., 2018. Ghost interactions in MEG/EEG source space: a note of caution on inter-areal coupling measures. *Neuroimage* 173, 632–643.
- Pascual-Marqui, R.D., et al., 2017. Innovations Orthogonalization: A Solution to the Major Pitfalls of EEG/MEG "Leakage Correction". *arXiv preprint arXiv:1708.05931*.
- Ren, Y., et al., 2018. Effective connectivity of the anterior hippocampus predicts recollection confidence during natural memory retrieval. *Nat. Commun.* 9, 4875.
- Rizkallah, J., et al., 2018. Dynamic reshaping of functional brain networks during visual object recognition. *J. Neural Eng.* 15, 056022.
- Rudebeck, P.H., Murray, E.A., 2014. The orbitofrontal oracle: cortical mechanisms for the prediction and evaluation of specific behavioral outcomes. *Neuron* 84, 1143–1156.
- Schiff, N.D., 2015. Cognitive motor dissociation following severe brain injuries. *JAMA Neurol.* 72, 1413–1415.
- Schiff, N.D., Fins, J.J., 2016. Brain death and disorders of consciousness. *Curr. Biol.* 26, R572–R576.
- Schoffelen, J.M., Gross, J., 2009. Source connectivity analysis with MEG and EEG. *Hum. Brain Mapp.* 30, 1857–1865.
- Sitt, J.D., et al., 2014. Large scale screening of neural signatures of consciousness in patients in a vegetative or minimally conscious state. *Brain* 137, 2258–2270.
- Stender, J., et al., 2014. Diagnostic precision of PET imaging and functional MRI in disorders of consciousness: a clinical validation study. *Lancet* 384, 514–522.
- Tadel, F., et al., 2011. Brainstorm: a user-friendly application for MEG/EEG analysis. *Comput. Intell. Neurosci.* 2011, 8.
- Terpstra, T., 1952. The asymptotic normality and consistency of Kendall's test against trend, when ties are present in one ranking. *Proc. Kon. Ned. Akad. v. Wetensch. A* 55, 327–333 [Terpstra32755Proc](#).
- Thibaut, A., et al., 2014. tDCS in patients with disorders of consciousness: sham-controlled randomized double-blind study. *Neurology* 82, 1112–1118.
- Tononi, G., 2004. An information integration theory of consciousness. *BMC Neurosci.* 5, 42.
- Tononi, G., et al., 2016. Integrated information theory: from consciousness to its physical substrate. *Nat. Rev. Neurosci.* 17, 450.
- Van de Steen, F., et al., 2016. Critical comments on EEG sensor space dynamical connectivity analysis. *Brain Topogr.* 1–12.
- van den Heuvel, M.P., et al., 2017. Proportional thresholding in resting-state fMRI functional connectivity networks and consequences for patient-control connectome studies: issues and recommendations. *Neuroimage* 152, 437–449.
- Vinck, M., et al., 2011. An improved index of phase-synchronization for electrophysiological data in the presence of volume-conduction, noise and sample-size bias. *Neuroimage* 55, 1548–1565.
- Vogt, B.A., Laureys, S., 2005. Posterior cingulate, precuneal and retrosplenial cortices: cytology and components of the neural network correlates of consciousness. *Prog. Brain Res.* 150, 205–217.
- Wannez, S., et al., 2017. The repetition of behavioral assessments in diagnosis of disorders of consciousness. *Ann. Neurol.* 81, 883–889.
- Watts, D.J., Strogatz, S.H., 1998. Collective dynamics of 'small-world' networks. *Nature* 393, 440–442.
- Zhang, S., Chiang-shan, R.L., 2012. Functional connectivity mapping of the human precuneus by resting state fMRI. *Neuroimage* 59, 3548–3562.

Study 3 Supplementary Materials: Decreased integration of EEG source-space networks in disorders of consciousness

Decreased integration of EEG source-space networks in disorders of consciousness

Jennifer Rizkallah^{1,2}, Jitka Annen^{3,4}, Julien Modolo^{1,*}, Olivia Gosseries^{3,4},
Pascal Benquet¹, Sepehr Mortaheb³, Hassan Amoud², Helena Cassol^{3,4}, Ahmad
Mheich¹, Aurore Thibaut^{3,4}, Camille Chatelle^{3,4}, Mahmoud Hassan¹, Rajanikant
Panda³, Fabrice Wendling¹, Steven Laureys^{3,4}

¹ Univ Rennes, LTSI, F-35000 Rennes, France

² Azm Center for Research in Biotechnology and its Application, EDST, Lebanese University,
Lebanon

³ GIGA Consciousness, University of Liège, Liège, Belgium

⁴ Coma Science Group, University Hospital of Liège, Liège, Belgium

* Corresponding author: julien.modolo@inserm.fr

Name	Age	Gender	Days since injury	Etiology	Best diagnosis
P1	27	F	1570	NT	MCS+
P2	27	M	1542	T	MCS+
P3	35	M	6950	NT	UWS
P4	60	M	9	NT	MCS-
P5	24	M	319	T	MCS-
P6	30	F	2406	NT	MCS-
P7	30	F	563	T	MCS-
P8	30	M	583	T	MCS+
P9	50	M	-	T	MCS+
P10	30	F	-	T	MCS+
P11	46	M	528	T	MCS+
P12	48	F	-	NT	MCS-
P13	37	M	1869	NT	MCS-
P14	59	F	-	NT	MCS-
P15	5	F	-	T	MCS+
P16	24	M	2681	NT	MCS+
P17	30	M	33	NT	MCS+
P18	43	M	3139	T	MCS-
P19	45	F	491	NT	UWS
P20	57	M	390	NT	MCS+
P21	25	F	308	NT	MCS+
P22	23	M	421	T	MCS+
P23	28	M	66	NT	MCS-
P24	53	M	1235	NT	MCS-
P25	24	M	-	T	MCS+
P26	36	F	-	NT	UWS
P27	22	M	2972	T	MCS-
P28	23	M	2035	T	MCS+
P29	73	M	28	NT	MCS-
P30	30	M	3337	T	MCS+
P31	47	F	-	NT	MCS-
P32	65	M	674	T	MCS+
P33	55	M	-	NT	MCS+
P34	19	M	426	T	MCS+
P35	39	F	1437	T	MCS-
P36	34	F	375	T	EMCS
P37	61	F	858	NT	MCS+
P38	14	M	185	NT	EMCS
P39	26	F	112	NT	UWS
P40	35	M	4154	NT	MCS+
P41	60	M	406	NT	EMCS
P42	62	M	672	NT	UWS
P43	67	F	1464	NT	MCS+
P44	23	M	456	NT	UWS
P45	42	F	220	NT	MCS-
P46	72	M	3062	NT	MCS+
P47	21	M	257	T	UWS
P48	30	M	402	T	MCS-
P49	28	M	2423	T	EMCS

P50	59	F	709	T	MCS+
P51	51	F	347	NT	UWS
P52	25	M	1283	T	MCS+
P53	42	M	1186	T	EMCS
P54	24	F	333	NT	MCS-
P55	43	F	40	T	UWS
P56	55	F	669	T	MCS+
P57	54	M	387	NT	MCS+
P58	38	M	541	T	MCS+
P59	43	F	98	NT	MCS+
P60	22	M	423	T	MCS+
P61	33	F	308	NT	EMCS

Table T1: Patients demographic information: age, gender, days since injury, traumatic (T) or non-traumatic (NT) etiology and clinical best diagnosis.

CTRL>UWS	CTRL>MCS-	CTRL>MCS+	MCS+>MCS-
Lateralorbitofrontal R	Lateralorbitofrontal R	Fusiform R	
Lateralorbitofrontal L	Lateralorbitofrontal L	Fusiform L	
Precuneus L	Postcentral R	Lateralorbitofrontal R	
	Inferiortemporal R		
	Parahippocampal R	Lateralorbitofrontal L	
	Fusiform R		
	Superiortemporal R	Precentral R	
	Superiortemporal L	Precuneus L	
	Precentral R	Insula L	
	Lateraloccipital R	Superiortemporal L	
	Lateraloccipital L		
	Parsobitalis R		
	Rostralmiddlefrontal R		
	Rostralmiddlefrontal L		
	Inferiorparietal R		
	Bankssts R		
	Superiorparietal R		
	Middletemporal R		
	Middletemporal L		
	Supramarginal R		
	Temporalpole R		
	Parsopercularis R		
	Parsopercularis L		
	Pericalcarine R		
	Entorhinal R		
	Postriangularis R		
	Caudalmiddlefrontal L		
	Transvertemporal L		

Table T2: Brain regions that have significantly lower integration in theta band in UWS, MCS- and MCS+ as compared to the control group and in MCS- patients compared to MCS+ patients with p-value lower than 0.05/221=0.0002 (Bonferroni-corrected)

CTRL>UWS	CTRL>MCS-	CTRL>MCS+
	Parsopercularis R	Parsopercularis R
	Fusiform L	Rostralmiddlefrontal R
	Parahippocampal L	Rostralmiddlefrontal L
	Lingual L	Parstriangularis R
	Postcentral L	Parstriangularis L
		Lateralorbitofrontal R
		Lateralorbitofrontal L
		Parsopercularis R
		Postcentral R
		Postcentral L
		Parsobitalis R
		Superiortemporal R
		Lingual R
		Lingual L
		Inferiortemporal R
		Precentral R
		Precentral L
		Pericalcarine
		Superiorfrontal R
		Superiorfrontal L
		Supramarginal R
		Parahippocampal R
		Parahippocampal L
		Fusiform L
		Caudalmiddlefrontal L
		Precuneus L
		Middletemporal L
		Parsopercularis L
		Inferiorparietal L

Table T3: Brain regions that have significantly lower integration in gamma band in UWS, MCS- and MCS+ as compared to the control group and in MCS- patients compared to MCS+ patients with p-value lower than 0.05/221=0.0002 (Bonferroni-corrected)

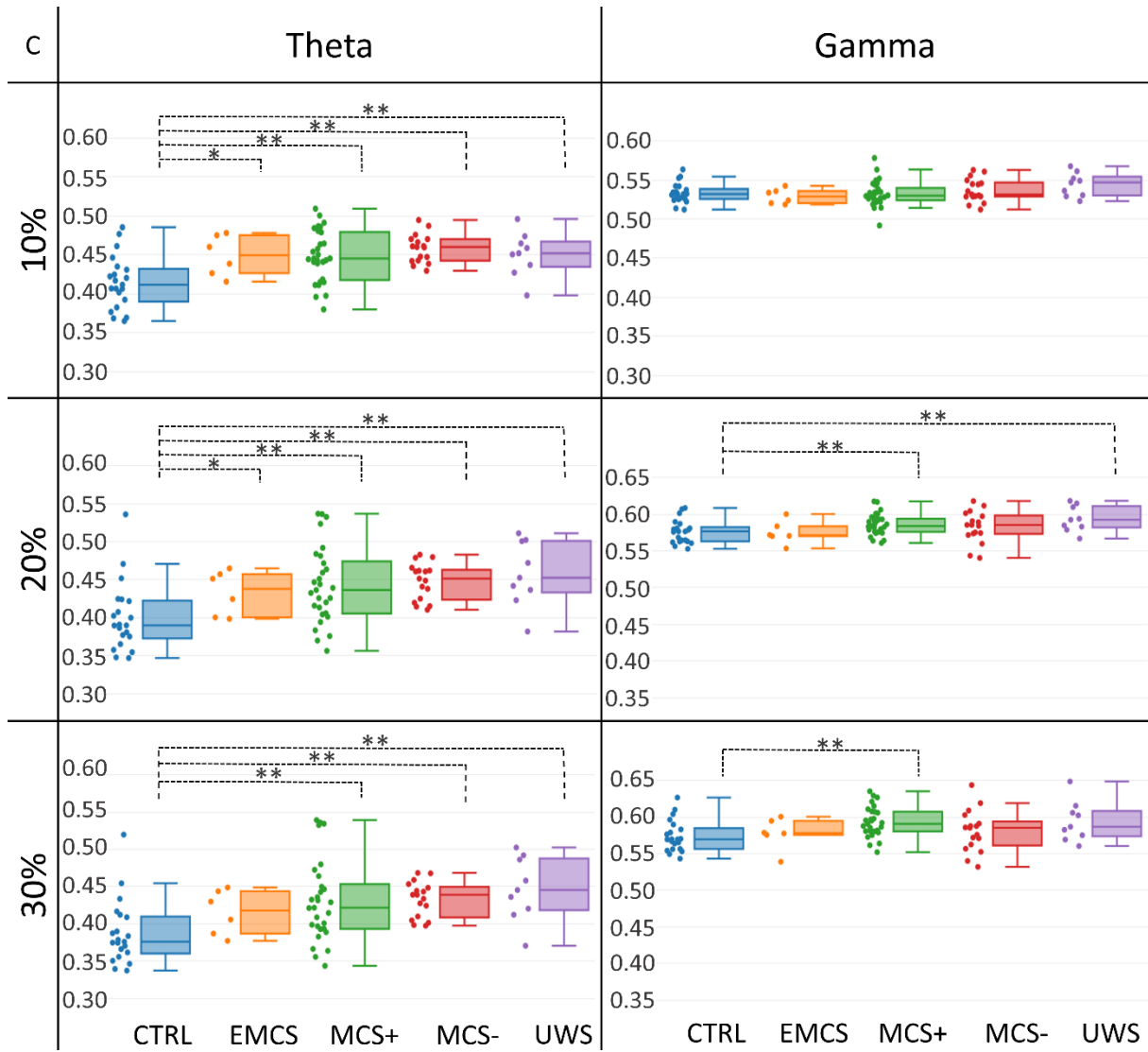


Figure S1: Clustering coefficient values for different thresholds (10%, 20% and 30%) in the theta and gamma bands. Significant differences are presented by * if $p < 0.05$ without correction and ** if corrected (Bonferroni correction $p < 0.05/5$).

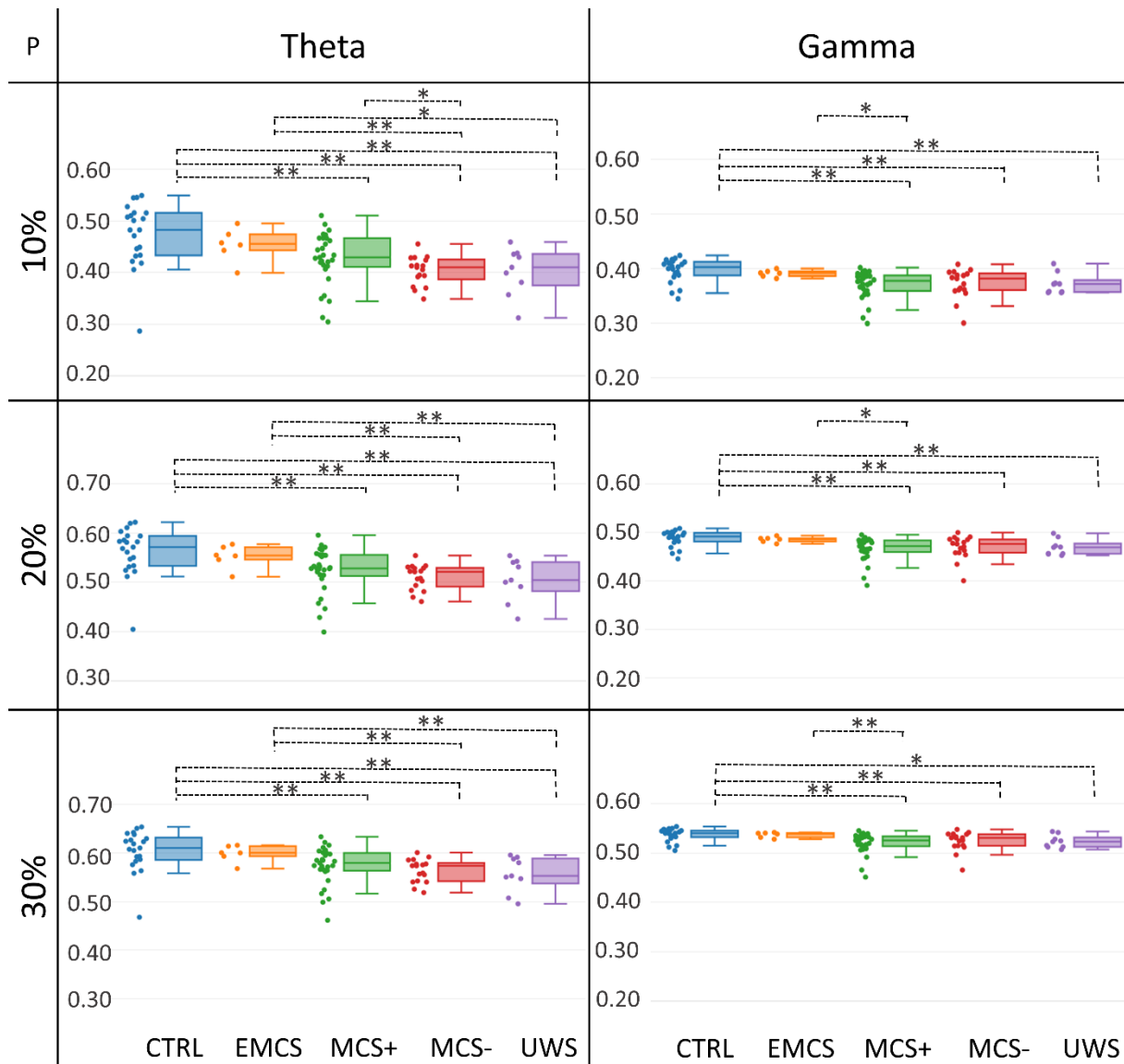


Figure S2: Participation coefficient values for different thresholds (10%, 20% and 30%) in the theta and gamma bands. Significant differences are presented by * if $p < 0.05$ without correction and ** if corrected (Bonferroni correction $p < 0.05/5$)

CHAPTER 5. DISCUSSION AND FUTURE WORK

There is an emerging consensus that the human brain is a dynamic complex network of structurally and functionally interconnected regions (Sporns et al., 2004; Stam and Reijneveld, 2007), that reconfigure during resting state (Damaraju et al., 2014; De Pasquale et al., 2016; Vink et al., 2019) and task (Medaglia et al., 2018; O’neill et al., 2017; Wang et al., 2019). The progress in the network neuroscience field showed the importance of studying brain network alterations in the case of brain disorders as they are related to large-scale network disruptions (Fornito et al., 2015; Monti et al., 2010b; Stam, 2014). Hence, there is an urgent need for easy-to-use, non-invasive techniques, to characterize the pathological networks.

The main contributions provided by this thesis can be summarized as follows:

- Track the fast brain network dynamics during the recognition of different category of visual object, meaningful and meaningless. We proposed a new metric, called “occurrence”, which presents the probability of any two nodes to fall in the same module over time and reflects the importance of strong or weak temporal interactions between any two brain regions during time. Our results showed i) greater integration and occurrence values for meaningless compared to meaningful images and ii) the occurrence within the right frontal and the left occipito-temporal regions can predict the ability of the brain to rapidly recognize and name visual stimuli.
- Evaluate the effect of the FC methods’ choice on EEG-source space networks at rest by testing two main families of FC methods: FC methods that do not remove zero-lag connectivity and FC methods that remove zero-lag connections. Networks obtained by each FC method were compared with fMRI networks (from the Human Connectome Project). Results show low correlations for all the FC methods. However, *PLV* and *AEC* networks are significantly correlated with fMRI networks ($\rho = 0.12$, $p = 1.93 \times 10^{-8}$ and $\rho = 0.06$, $p = 0.007$, respectively), while other methods are not.
- Reveal alterations in functional connectivity networks in DoC as a function of clinical consciousness levels. Results showed that networks in DoC patients were characterized by impaired global information processing (network integration) as compared to

controls. Furthermore, we were able to identify the brain regions with decreased integration that were involved between groups: the left precuneus (engaged in self-related processing, awareness and conscious information processing) and the left orbitofrontal cortex (engaged in action selection depending on emotional and sensory contexts and in pain perception).

- Track the dynamic modular states changes between healthy control and DoC groups and between MCS and UWS patients. Results showed that no emotions, cognitive, motor or language networks were extracted in the case of UWS patients. However, these networks were found in healthy participants and MCS patients. Moreover, the fronto-parietal connections were also only found in the MCS and healthy participants.

5.1. Dynamic functional networks at rest and task

Following the brain network dynamics has a great interest in network neuroscience since it helps to understand how the human brain reconfigures during cognitive tasks and to define the altered networks in neurological diseases. Brain network reshaping includes slow changes across the lifetime (due to long-term processes like learning or aging) which can be studied in a longitudinal way. Brain network changes include, as well, evoked and fast fluctuations during tasks or in response to external stimuli. Tracking these fast fluctuations is a key challenge in cognitive and clinical neuroscience (Allen et al., 2014; Hutchison et al., 2013).

In this thesis, we used EEG recordings, known for their high temporal resolution, and adopted a sliding window technique to compute the FC matrices at short time windows in two studies: the cognitive task in healthy with meaningful vs. meaningless object recognition, and the clinical study performed during resting state. In addition, we combined the sliding window technique with the categorical version of the modular states algorithm developed in our team (Kabbara et al., 2019) in order to reveal the modular structures over time for different groups of DOC patients.

For the cognitive task, higher integration and occurrence values were found for meaningless compared to meaningful images. We were also able to define the most involved brain regions: the right lingual and right fusiform regions known for their essential role in visual processing (Cai et al., 2015; Perani et al., 1999) and the left isthmus known for its role in the regulation of

the focus of attention (Leech and Sharp, 2013) had higher integration values, while the occipito-frontal connections, known for their role in object identification and decision making in case of unclear choice, had higher occurrence values, which provided a measure of the communication duration between these two regions.

As for the clinical study, results revealed a decrease in brain network integration (communications between distant brain modules) in DOC patients as compared to healthy controls, which is consistent with the findings of several previous studies (Chennu et al., 2017; Tononi et al., 2016). Networks obtained in healthy participants and MCS patients, which were not present in UWS, were mainly located in the cingulate, frontal and central cortex, known to play a key role in emotions, cognitive, memory and motor processes (Berger and Davelaar, 2018; Bush et al., 2000; Klimesch, 1999; Lustenberger et al., 2015). Moreover, fronto-parietal connections have been previously demonstrated to be a neural marker of behaviorally evidenced consciousness, not only in patients with disorders of consciousness (Chennu et al., 2014; Stender et al., 2014), but also during propofol sedation to normal subjects (Chennu et al., 2016).

Despite the good results we obtained, sliding window technique faces several difficulties such as the length of the window, since short windows may underlie errors in the generated networks and large windows may fail to capture the fast network changes and alterations in the brain. Moreover, it also requires a huge memory to save the reconstructed matrices and a large amount of time to compute the multislice modularity technique. Therefore, dimensionality reduction algorithms may be used to reduce the size of the matrices and the computing time. Other approaches proposed to track fast network transitions can also be tested, such as Hidden Markov model approaches (Baker et al., 2014; Vidaurre et al., 2018), K-means clustering (Allen et al., 2018; Mheich et al., 2015), principal components analysis (Leonardi et al., 2013), independent components analysis (Kiviniemi et al., 2011; O’neill et al., 2017) or tensor-based approach (Ozdemir et al., 2017).

5.2. EEG source connectivity

As stated before, the accurate identification of brain networks, from scalp EEG, is a major challenge due to volume conduction problem. In this scope, EEG source connectivity method has considerably developed over the past decades and offers the advantage to track the network dynamics with high space/time resolution (Hassan et al., 2015; Schoffelen and Gross, 2009).

However, the EEG source connectivity is still an immature method (Palva and Palva, 2012; Schoffelen and Gross, 2009; Song et al., 2015; Van Diessen et al., 2015) with the need to study the effect of the leakage correction (removing spurious connections between adjacent regions by removing zero-lag connections) on the reconstructed networks.

Hence, we compared M/EEG FC matrices (obtained from different FC methods – PLV, AEC, PLI, PLV_{Col}, AEC_{Col}, PLV_{Pas} and AEC_{Pas} – and different EEG montages) to those obtained using fMRI (collected from HCP databases) to explore the effect of the above-mentioned methodological considerations. FC matrices estimated using PLV and AEC (methods that keep the zero-lag correlations) correlated significantly with fMRI network (considered as ground truth) as compared to the other methods (methods that remove zero-lag connections) that did not. This can be explained by the fact that not all zero-lag connections are spurious (Gollo et al., 2014; Roelfsema et al., 1997) and by removing zero lag connections, false and significantly different estimated connectivity from the true connectivity can be revealed (Palva et al., 2018).

5.3. Methodological considerations

5.3.1. Ill-posed inverse problem solution

Different methods have been proposed to resolve the inverse problem. The most popular algorithms include low resolution brain electromagnetic tomography (LORETA) (Pascual-Marqui et al., 1994), standardized low resolution brain electromagnetic tomography (sLORETA) (Pascual-Marqui, 2002), beamforming (Brookes et al., 2004), Minimum Norm Estimate (MNE) (Hämäläinen and Ilmoniemi, 1994) and weight Minimum Norm Estimate (wMNE) (Lin et al., 2004).

It is likely that the selection of a source imaging method to solve the inverse problem has a remarkable effect on the accuracy of the reconstructed source signals, and ultimately on the brain networks obtained (a detailed comparison between different methods was reported by (Becker et al., 2015)). In this thesis, we used the weighted minimum norm estimate (wMNE) as an inverse solution since it implies relatively few hypotheses and presents acceptable distance of localization error and CPU runtime (Becker et al., 2015) which can be explained by the brain low energy cost during information processing. Moreover, the choice of wMNE was supported by two comparative analyses (Hassan et al., 2014; Hassan et al., 2016) that reported

the superiority of wMNE/PLV over other combinations of five inverse algorithms and five connectivity measures.

5.3.2. Template brain

In studies 2, 3 and 4, a template source space was used, instead of a subject-specific one as was done in study 1. In the case of healthy subjects, co-registration with a template brain yielded largely consistent connectivity and network estimates as compared to native MRI (Douw et al., 2018). This strategy was widely used in several studies (Lai et al., 2018; López et al., 2014; Mullen et al., 2013). However, in the case of severe brain damage, it remains unknown how a template instead of a native MRI co-registration affects results and their interpretability. Hence, we believe that comparing results of DOC study using subject-specific can positively affect the results and help differentiate between MCS and UWS patients.

5.3.3. Number of Regions of interests

In this thesis we used Desikan-Killiany atlas to parcellate the brain into regions of interest (ROIs). However, EEG source connectivity method can be used with other cortical parcellations such as Destrieux atlas composed of 148 ROIs (Destrieux et al., 2010) or Automated Anatomical Labelling (AAL) atlas composed of 90 ROIs (Tzourio-Mazoyer et al., 2002), provided that the number of regions is sufficiently low, and that regions are well separated to ensure that the windowed data matrices are of full rank which is a requirement of the orthogonalisation procedure (Colclough et al., 2015). We can then study the effect of brain parcellations on the efficiency of the reconstructed functional networks.

5.3.4. Sliding window length

To reconstruct dynamic functional connectivity matrices, we adopted in this thesis the sliding window technique. The ideal window length depends on which frequency band is used to process the signals since it should guarantee a sufficient number of data points over which the connectivity is calculated.

Here, we adopted the smallest window length recommendation by (Lachaux et al., 1999):

$$W = \frac{\textit{number of cycles}}{\textit{central frequency}}$$

where the number of cycles is equal to 6. However, future studies may

need to address how to dynamically regulate the sliding window length instead of predefining it. Other approaches, such as the use of graph signal processing (GSP) or the very recently

approach to estimate instantaneous phase difference of instantaneous amplitude correlation (Tewarie et al., 2019), can also be used to estimate dynamic networks without using the sliding window approach.

5.3.5. Connectivity matrix threshold

Usually, a threshold is applied on the obtained connectivity matrix to remove the spurious connections (very low connections weight). There is no consensus on the best thresholding technique (Fornito et al., 2016; Sporns, 2011). Many types of thresholds can be used such as empirical, proportional or statistical thresholds. The simplest approach is to apply a global threshold, which consist on setting a value for the connectivity matrix. The connections that are higher than this value are used and the lower connections removed and set to zero. However, absolute thresholds may remove significant connections in low-average connectivity networks, or keep weak connections in connectivity networks with high-average (Van Wijk et al., 2010). Proportional thresholds keep a percentage of the strongest connections of the connectivity matrix. Statistical thresholds are based on controlling the false discovery rate (FDR) used in many recent brain network studies (Bassett et al., 2011; Bassett et al., 2013). It requires converting the connectivity matrix to a p-value map and retaining only the connectivity values whose p-values passed the statistical FDR threshold (Achard et al., 2006; Genovese et al., 2002). Such thresholds are beneficial as they perform multiple testing to adjust thresholds by controlling false-positive rate.

However, choosing the right threshold is an open issue and depends on the analysis assessed. It is recommended to choose a proportional threshold when comparing connectivity between groups (van den Heuvel et al., 2017), and to choose a statistical threshold in other cases (Genovese et al., 2002). Network measures are shown to be stable across statistical and proportional thresholds contrary to absolute thresholds (Garrison et al., 2015).

5.4. Future directions

In this thesis, we investigated the capability of “EEG source connectivity” to track the fast dynamic changes of brain networks at very short time scale during a visual object recognition task and to identify the pathological alterations in disorders of consciousness as a clinical application. This investigation was performed by extracting dynamic characteristics and topologies of networks using graph theory. We also tested the effect of removing zero-lag

connections as a solution to the source leakage problem on the reconstructed networks using wMNE as a solution to the ill-posed inverse problem and several functional connectivity methods.

In a future work, other methods used to resolve the inverse problem such as beamforming combined with other functional and effective connectivity methods should be also studied. The number of regions of interest and the effect of the number of channels using EEG and fMRI recordings for the same subjects should also be considered.

In the case of DOC, using subject specific source space will be indeed of interest to explore how the brain lesions can affect and perhaps improve the obtained results. Results also showed significant differences between DOC groups at specific frequency bands (mainly theta and gamma). The cross coupling between these two frequency bands could also be an interesting direction to explore.

Finally, most existing approaches have focused on analyzing structural and functional brain graphs separately. However, graph signal processing (GSP) is an emerging area of research, where signals recorded at the nodes of the graph are studied atop the underlying graph structure, allowing to analyze the signals from a new viewpoint. GSP allows the decomposition of a graph signal into pieces that represent different levels of variability: low graph frequency components, which represent alignment with structural connectivity (brain regions that are physically wired and activate together), and high graph frequency components, which describe liberality (brain regions that exhibit high signal variability with respect to the underlying graph structure). This decomposition can indeed be important for the analysis of neurological disease and behavior (Garrett et al., 2012; Heisz et al., 2012) as in the case of DOC patients.

LIST OF PUBLICATIONS

Journals:

1. **J. Rizkallah**, P. Benquet, A. Kabbara, O. Dufor, F. Wendling, M. Hassan (2018). “Dynamic reshaping of functional brain networks during visual object recognition.” **Journal of neural engineering**.
2. **J. Rizkallah**, J. Annen, J. Modolo, O. Gosseries, P. Benquet, S. Mortaheb, H. Amoud, H. Cassol, A. Mheich, A. Thibaut, C. Chatelle, M. Hassan, R. Panda, F. Wendling, S. Laureys (2019). “Decreased integration of EEG source-space networks in disorders of consciousness.” **Neuroimage Clinical**.
3. **J. Rizkallah**, H. Amoud, M. Fraschini, F. Wendling, M. Hassan (2019). “Removing zero-lag functional connections can alter EEG-source space networks at rest.” **Submitted to Brain Topography**.
4. “Detecting modular brain states in disorders of consciousness.” **In preparation**.

Conferences:

1. **J. Rizkallah**, P. Benquet, F. Wendling, M. Khalil, A. Mheich, O. Dufor, M. Hassan (2016). “Brain network modules of meaningful and meaningless objects.” **Third Middle East Conference on Biomedical Engineering, Lebanon**.
2. **J. Rizkallah**, H. Amoud, F. Wendling, M. Hassan (2019). “Effect of connectivity measures on the identification of brain functional core network at rest.” **41st International Engineering in Medicine and Biology Conference, Berlin**.
3. S. Al-Ali, M. Youssf, **J. Rizkallah**, M. Hassan, A. Karfoul (2019). “An efficient graph structure inference strategy based on random walk model on graph: Application to functional brain networks.” **Fifth International Conference on Advances in Biomedical Engineering, Lebanon**.

Public speaking:

1. **3rd price**: My thesis in 3 minutes, Rennes, 2019.

REFERENCES

- Achard, S., et al., 2006. A resilient, low-frequency, small-world human brain functional network with highly connected association cortical hubs. *Journal of Neuroscience*. 26, 63-72.
- Akaike, H., 1974. A new look at the statistical model identification. In: *Selected Papers of Hirotugu Akaike*. Vol., ed.^eds. Springer, pp. 215-222.
- Alario, F.X., Ferrand, L., 1999. A set of 400 pictures standardized for French: Norms for name agreement, image agreement, familiarity, visual complexity, image variability, and age of acquisition. *Behavior Research Methods*. 31, 531-552.
- Alexander-Bloch, A.F., et al., 2010. Disrupted modularity and local connectivity of brain functional networks in childhood-onset schizophrenia. *Frontiers in systems neuroscience*. 4, 147.
- Allen, E., et al., 2018. EEG signatures of dynamic functional network connectivity states. *Brain topography*. 31, 101-116.
- Allen, E.A., et al., 2014. Tracking whole-brain connectivity dynamics in the resting state. *Cerebral cortex*. 24, 663-676.
- Amico, E., et al., 2017. Mapping the functional connectome traits of levels of consciousness. *NeuroImage*. 148, 201-211.
- Annen, J., et al., 2016. Function–structure connectivity in patients with severe brain injury as measured by MRI-DWI and FDG-PET. *Human brain mapping*. 37, 3707-3720.
- Annen, J., et al., 2018. Regional brain volumetry and brain function in severely brain-injured patients. *Ann Neurol*. 83, 842-853.
- Babiloni, F., et al., 2005. Estimation of the cortical functional connectivity with the multimodal integration of high-resolution EEG and fMRI data by directed transfer function. *Neuroimage*. 24, 118-131.
- Baggio, H.C., et al., 2015. Cognitive impairment and resting-state network connectivity in Parkinson's disease. *Human brain mapping*. 36, 199-212.
- Bagnato, S., et al., 2010. Prognostic value of standard EEG in traumatic and non-traumatic disorders of consciousness following coma. *Clinical Neurophysiology*. 121, 274-280.
- Baker, A.P., et al., 2014. Fast transient networks in spontaneous human brain activity. *Elife*. 3, e01867.
- Bardin, J.C., Schiff, N.D., Voss, H.U., 2012. Pattern classification of volitional functional magnetic resonance imaging responses in patients with severe brain injury. *Archives of neurology*. 69, 176-181.

- Bassett, D.S., et al., 2008. Hierarchical organization of human cortical networks in health and schizophrenia. *Journal of Neuroscience*. 28, 9239-9248.
- Bassett, D.S., et al., 2011. Dynamic reconfiguration of human brain networks during learning. *Proceedings of the National Academy of Sciences*. 108, 7641-7646.
- Bassett, D.S., et al., 2013. Robust detection of dynamic community structure in networks. *Chaos: An Interdisciplinary Journal of Nonlinear Science*. 23, 013142.
- Bassett, D.S., et al., 2015. Learning-induced autonomy of sensorimotor systems. *Nature neuroscience*. 18, 744-751.
- Bassett, D.S., Sporns, O., 2017. Network neuroscience. *Nature neuroscience*. 20, 353.
- Becker, H., et al., 2015. Brain-source imaging: From sparse to tensor models. *IEEE Signal Processing Magazine*. 32, 100-112.
- Berger, A.M., Davelaar, E.J., 2018. Frontal alpha oscillations and attentional control: a virtual reality neurofeedback study. *Neuroscience*. 378, 189-197.
- Bernat, J.L., 2009. Chronic consciousness disorders. *Annual review of medicine*. 60, 381-392.
- Blondel, V.D., et al., 2008. Fast unfolding of communities in large networks. *Journal of statistical mechanics: theory and experiment*. 2008, P10008.
- Bodien, Y.G., Chatelle, C., Edlow, B.L., 2017. Functional Networks in Disorders of Consciousness. In: *Seminars in neurology*. Vol. 37, ed.^eds. Thieme Medical Publishers, pp. 485-502.
- Bola, M., Sabel, B.A., 2015. Dynamic reorganization of brain functional networks during cognition. *Neuroimage*. 114, 398-413.
- Boly, M., et al., 2012. Brain connectivity in disorders of consciousness. *Brain connectivity*. 2, 1-10.
- Braun, U., et al., 2015. Dynamic reconfiguration of frontal brain networks during executive cognition in humans. *Proceedings of the National Academy of Sciences*. 112, 11678-11683.
- Brookes, M.J., et al., 2004. A general linear model for MEG beamformer imaging. *NeuroImage*. 23, 936-946.
- Brookes, M.J., Woolrich, M.W., Barnes, G.R., 2012. Measuring functional connectivity in MEG: a multivariate approach insensitive to linear source leakage. *Neuroimage*. 63, 910-920.
- Brookes, M.J., et al., 2014. Measuring temporal, spectral and spatial changes in electrophysiological brain network connectivity. *Neuroimage*. 91, 282-299.
- Brunner, C., et al., 2016. Volume conduction influences scalp-based connectivity estimates. *Frontiers in computational neuroscience*. 10.

- Bruno, M.-A., et al., 2010. Disorders of consciousness: moving from passive to resting state and active paradigms. *Cognitive neuroscience*. 1, 193-203.
- Bruno, M.-A., et al., 2011. From unresponsive wakefulness to minimally conscious PLUS and functional locked-in syndromes: recent advances in our understanding of disorders of consciousness. *Journal of neurology*. 258, 1373-1384.
- Bruno, M.-A., et al., 2012. Functional neuroanatomy underlying the clinical subcategorization of minimally conscious state patients. *Journal of neurology*. 259, 1087-1098.
- Bullmore, E., Sporns, O., 2009. Complex brain networks: graph theoretical analysis of structural and functional systems. *Nature Reviews Neuroscience*. 10, 186-198.
- Bush, G., Luu, P., Posner, M.I., 2000. Cognitive and emotional influences in anterior cingulate cortex. *Trends in cognitive sciences*. 4, 215-222.
- Buzsaki, G., Anastassiou, C.A., Koch, C., 2012. The origin of extracellular fields and currents-EEG, ECoG, LFP and spikes. *Nat Rev Neurosci*. 13, 407-20.
- Cai, S., et al., 2015. Altered functional connectivity of fusiform gyrus in subjects with amnesic mild cognitive impairment: a resting-state fMRI study. *Frontiers in human neuroscience*. 9, 471.
- Chennu, S., et al., 2014. Spectral signatures of reorganised brain networks in disorders of consciousness. *PLoS computational biology*. 10, e1003887.
- Chennu, S., et al., 2016. Brain connectivity dissociates responsiveness from drug exposure during propofol-induced transitions of consciousness. *PLoS computational biology*. 12, e1004669.
- Chennu, S., et al., 2017. Brain networks predict metabolism, diagnosis and prognosis at the bedside in disorders of consciousness. *Brain*. 140, 2120-2132.
- Colclough, G.L., et al., 2015. A symmetric multivariate leakage correction for MEG connectomes. *NeuroImage*. 117, 439-448.
- Cruse, D., et al., 2012. Bedside detection of awareness in the vegetative state: a cohort study. *The Lancet*. 378, 2088-2094.
- Damaraju, E., et al., 2014. Dynamic functional connectivity analysis reveals transient states of dysconnectivity in schizophrenia. *NeuroImage: Clinical*. 5, 298-308.
- De Pasquale, F., et al., 2010. Temporal dynamics of spontaneous MEG activity in brain networks. *Proceedings of the National Academy of Sciences*. 107, 6040-6045.
- de Pasquale, F., et al., 2012. A cortical core for dynamic integration of functional networks in the resting human brain. *Neuron*. 74, 753-764.
- De Pasquale, F., et al., 2016. A dynamic core network and global efficiency in the resting human brain. *Cerebral Cortex*. 26, 4015-4033.

- Delorme, A., Makeig, S., 2004. EEGLAB: an open source toolbox for analysis of single-trial EEG dynamics including independent component analysis. *Journal of neuroscience methods*. 134, 9-21.
- Demertzi, A., et al., 2015. Intrinsic functional connectivity differentiates minimally conscious from unresponsive patients. *Brain*. 138, 2619-2631.
- Dennis, E.L., et al., 2013. Development of brain structural connectivity between ages 12 and 30: a 4-Tesla diffusion imaging study in 439 adolescents and adults. *Neuroimage*. 64, 671-684.
- Desikan, R.S., et al., 2006. An automated labeling system for subdividing the human cerebral cortex on MRI scans into gyral based regions of interest. *Neuroimage*. 31, 968-980.
- Destrieux, C., et al., 2010. Automatic parcellation of human cortical gyri and sulci using standard anatomical nomenclature. *Neuroimage*. 53, 1-15.
- Di Perri, C., et al., 2014. Functional neuroanatomy of disorders of consciousness. *Epilepsy & Behavior*. 30, 28-32.
- Di Perri, C., et al., 2016. Measuring Consciousness Through Imaging. In: *Brain Function and Responsiveness in Disorders of Consciousness*. Vol., ed. eds. Springer, pp. 51-65.
- Di Perri, C., et al., 2017. Multifaceted brain networks reconfiguration in disorders of consciousness uncovered by co-activation patterns. *Human brain mapping*.
- DiCarlo, J.J., Zoccolan, D., Rust, N.C., 2012. How does the brain solve visual object recognition? *Neuron*. 73, 415-434.
- Douw, L., et al., 2018. Consistency of magnetoencephalographic functional connectivity and network reconstruction using a template versus native MRI for co-registration. *Hum Brain Mapp*. 39, 104-119.
- Drakesmith, M., et al., 2015. Overcoming the effects of false positives and threshold bias in graph theoretical analyses of neuroimaging data. *NeuroImage*. 118, 313-333.
- Edelman, B.J., Baxter, B., He, B., 2015. EEG source imaging enhances the decoding of complex right-hand motor imagery tasks. *IEEE Transactions on Biomedical Engineering*. 63, 4-14.
- Engels, M., et al., 2017. Alzheimer's disease: the state of the art in resting-state magnetoencephalography. *Clinical Neurophysiology*. 128, 1426-1437.
- Engemann, D.A., et al., 2018. Robust EEG-based cross-site and cross-protocol classification of states of consciousness. *Brain*. 141, 3179-3192.
- Estraneo, A., et al., 2013. Predictors of recovery of responsiveness in prolonged anoxic vegetative state. *Neurology*. 80, 464-470.
- Estraneo, A., et al., 2016. Standard EEG in diagnostic process of prolonged disorders of consciousness. *Clinical Neurophysiology*. 127, 2379-2385.

- Fernández-Espejo, D., et al., 2012. A role for the default mode network in the bases of disorders of consciousness. *Annals of neurology*. 72, 335-343.
- Fiedler, M., 1973. Algebraic connectivity of graphs. *Czechoslovak mathematical journal*. 23, 298-305.
- Finger, H., et al., 2016. Modeling of Large-Scale Functional Brain Networks Based on Structural Connectivity from DTI: Comparison with EEG Derived Phase Coupling Networks and Evaluation of Alternative Methods along the Modeling Path. *PLoS Comput Biol*. 12, e1005025.
- Fischl, B., 2012. FreeSurfer. *Neuroimage*. 62, 774-781.
- Fornito, A., Bullmore, E.T., 2015. Connectomics: a new paradigm for understanding brain disease. *European Neuropsychopharmacology*. 25, 733-748.
- Fornito, A., Zalesky, A., Breakspear, M., 2015. The connectomics of brain disorders. *Nature Reviews Neuroscience*. 16, 159.
- Fornito, A., Zalesky, A., Bullmore, E., 2016. Fundamentals of brain network analysis.
- Freeman, L.C., 1977. A set of measures of centrality based on betweenness. *Sociometry*. 35-41.
- Friston, K.J., Harrison, L., Penny, W., 2003. Dynamic causal modelling. *Neuroimage*. 19, 1273-1302.
- Fuchs, M., et al., 1998. An improved boundary element method for realistic volume-conductor modeling. *IEEE Transactions on Biomedical Engineering*. 45, 980-997.
- Gallen, C.C., Hirschkoﬀ, E.C., Buchanan, D.S., 1995. Magnetoencephalography and magnetic source imaging. Capabilities and limitations. *Neuroimaging Clin N Am*. 5, 227-49.
- Gantner, I.S., et al., 2013. Our rapidly changing understanding of acute and chronic disorders of consciousness: challenges for neurologists. *Future Neurology*. 8, 43-54.
- Garrett, D.D., et al., 2012. The modulation of BOLD variability between cognitive states varies by age and processing speed. *Cerebral cortex*. 23, 684-693.
- Garrison, K.A., et al., 2015. The (in) stability of functional brain network measures across thresholds. *Neuroimage*. 118, 651-661.
- Genovese, C.R., Lazar, N.A., Nichols, T., 2002. Thresholding of statistical maps in functional neuroimaging using the false discovery rate. *Neuroimage*. 15, 870-878.
- Giacino, J.T., et al., 1991. Monitoring rate of recovery to predict outcome in minimally responsive patients. *Archives of physical medicine and rehabilitation*. 72, 897-901.
- Giacino, J.T., et al., 2002. The minimally conscious state definition and diagnostic criteria. *Neurology*. 58, 349-353.

- Giacino, J.T., Kalmar, K., Whyte, J., 2004. The JFK Coma Recovery Scale-Revised: measurement characteristics and diagnostic utility. *Archives of physical medicine and rehabilitation*. 85, 2020-2029.
- Giacino, J.T., et al., 2014. Disorders of consciousness after acquired brain injury: the state of the science. *Nature Reviews Neurology*. 10, 99-114.
- Goldfine, A.M., et al., 2011. Determination of awareness in patients with severe brain injury using EEG power spectral analysis. *Clinical Neurophysiology*. 122, 2157-2168.
- Gollo, L.L., et al., 2014. Mechanisms of zero-lag synchronization in cortical motifs. *PLoS computational biology*. 10, e1003548.
- Goñi, J., et al., 2014. Resting-brain functional connectivity predicted by analytic measures of network communication. *Proceedings of the National Academy of Sciences*. 111, 833-838.
- Good, B.H., de Montjoye, Y.-A., Clauset, A., 2010. Performance of modularity maximization in practical contexts. *Physical Review E*. 81, 046106.
- Gosseries, O., Zasler, N.D., Laureys, S., 2014. Recent advances in disorders of consciousness: focus on the diagnosis. *Brain injury*. 28, 1141-1150.
- Gramfort, A., et al., 2010. OpenMEEG: opensource software for quasistatic bioelectromagnetics. *Biomedical engineering online*. 9, 45.
- Granger, C.W., 1969. Investigating causal relations by econometric models and cross-spectral methods. *Econometrica: Journal of the Econometric Society*. 424-438.
- Guimera, R., Amaral, L.A.N., 2005. Functional cartography of complex metabolic networks. *Nature*. 433, 895-900.
- Hagmann, P., et al., 2008. Mapping the structural core of human cerebral cortex. *PLoS biology*. 6, e159.
- Hagmann, P., et al., 2010. White matter maturation reshapes structural connectivity in the late developing human brain. *Proceedings of the National Academy of Sciences*. 107, 19067-19072.
- Hämäläinen, M.S., Ilmoniemi, R.J., 1994. Interpreting magnetic fields of the brain: minimum norm estimates. *Medical and biological engineering and computing*. 32, 35-42.
- Harrison, A.H., Connolly, J.F., 2013. Finding a way in: a review and practical evaluation of fMRI and EEG for detection and assessment in disorders of consciousness. *Neurosci Biobehav Rev*. 37, 1403-19.
- Hassan, M., et al., 2014. EEG source connectivity analysis: from dense array recordings to brain networks. *PloS one*. 9, e105041.
- Hassan, M., et al., 2015. Dynamic reorganization of functional brain networks during picture naming. *Cortex*. 73, 276-288.

- Hassan, M., et al., 2016. Identification of interictal epileptic networks from dense-EEG. *Brain Topography*. 1-17.
- Hassan, M., et al., 2017. Functional connectivity disruptions correlate with cognitive phenotypes in Parkinson's disease. *NeuroImage: Clinical*. 14, 591-601.
- Hassan, M., Wendling, F., 2018. Electroencephalography Source Connectivity: Aiming for High Resolution of Brain Networks in Time and Space. *IEEE Signal Processing Magazine*. 35, 81-96.
- Hata, M., et al., 2016. Functional connectivity assessed by resting state EEG correlates with cognitive decline of Alzheimer's disease—An eLORETA study. *Clinical Neurophysiology*. 127, 1269-1278.
- Heisz, J.J., Shedden, J.M., McIntosh, A.R., 2012. Relating brain signal variability to knowledge representation. *Neuroimage*. 63, 1384-1392.
- Hipp, J.F., et al., 2012. Large-scale cortical correlation structure of spontaneous oscillatory activity. *Nature neuroscience*. 15, 884.
- Holmes, C.J., et al., 1998. Enhancement of MR images using registration for signal averaging. *Journal of computer assisted tomography*. 22, 324-333.
- Hu, S., et al., 2018. How do reference montage and electrodes setup affect the measured scalp EEG potentials? *Journal of neural engineering*. 15, 026013.
- Huettel, S.A., Song, A.W., McCarthy, G., 2004. *Functional magnetic resonance imaging*, Vol. 1, Sinauer Associates Sunderland, MA.
- Hutchison, R.M., et al., 2013. Dynamic functional connectivity: promise, issues, and interpretations. *Neuroimage*. 80, 360-378.
- Jmail, N., et al., 2016. Comparison of brain networks during interictal oscillations and spikes on magnetoencephalography and intracerebral EEG. *Brain topography*. 29, 752-765.
- Jones, C., 1979. *Glasgow coma scale*. Vol., ed.^eds. LWW.
- Kabbara, A., et al., 2017. The dynamic functional core network of the human brain at rest. *Scientific Reports*. 7.
- Kabbara, A., et al., 2018. Reduced integration and improved segregation of functional brain networks in Alzheimer's disease. *Journal of neural engineering*. 15, 026023.
- Kabbara, A., et al., 2019. Detecting modular brain states in rest and task. *Network Neuroscience*. 1-41.
- Kiviniemi, V., et al., 2011. A sliding time-window ICA reveals spatial variability of the default mode network in time. *Brain connectivity*. 1, 339-347.
- Klimesch, W., 1999. EEG alpha and theta oscillations reflect cognitive and memory performance: a review and analysis. *Brain research reviews*. 29, 169-195.

- Koch, C., et al., 2016. Neural correlates of consciousness: progress and problems. *Nature Reviews Neuroscience*. 17, 307-321.
- Lachaux, J.-P., et al., 1999. Measuring phase synchrony in brain signals. *Human brain mapping*. 8, 194-208.
- Lachaux, J.-P., et al., 2000. Studying single-trials of phase synchronous activity in the brain. *International Journal of Bifurcation and Chaos*. 10, 2429-2439.
- Lai, M., et al., 2018. A comparison between scalp-and source-reconstructed EEG networks. *Scientific reports*. 8, 12269.
- Lancichinetti, A., Fortunato, S., 2012. Consensus clustering in complex networks. *Scientific reports*. 2, 336.
- Latora, V., Marchiori, M., 2001. Efficient behavior of small-world networks. *Physical review letters*. 87, 198701.
- Laureys, S., Owen, A.M., Schiff, N.D., 2004. Brain function in coma, vegetative state, and related disorders. *The Lancet Neurology*. 3, 537-546.
- Laureys, S., 2005. The neural correlate of (un) awareness: lessons from the vegetative state. *Trends in cognitive sciences*. 9, 556-559.
- Laureys, S., et al., 2010. Unresponsive wakefulness syndrome: a new name for the vegetative state or apallic syndrome. *BMC medicine*. 8, 68.
- Laureys, S., Gosseries, O., Tononi, G., 2015. *The neurology of consciousness: cognitive neuroscience and neuropathology*, Vol., Academic Press.
- Leech, R., Sharp, D.J., 2013. The role of the posterior cingulate cortex in cognition and disease. *Brain*. 137, 12-32.
- Leonardi, N., et al., 2013. Principal components of functional connectivity: a new approach to study dynamic brain connectivity during rest. *NeuroImage*. 83, 937-950.
- Li, L., et al., 2013. Mapping putative hubs in human, chimpanzee and rhesus macaque connectomes via diffusion tractography. *Neuroimage*. 80, 462-474.
- Lin, F.-H., et al., 2004. Spectral spatiotemporal imaging of cortical oscillations and interactions in the human brain. *Neuroimage*. 23, 582-595.
- Liu, M., et al., 2014. Disrupted anatomic white matter network in left mesial temporal lobe epilepsy. *Epilepsia*. 55, 674-682.
- Liu, Q., et al., 2015. Estimating a neutral reference for electroencephalographic recordings: the importance of using a high-density montage and a realistic head model. *Journal of neural engineering*. 12, 056012.
- Liu, Q., et al., 2018. Detecting large-scale brain networks using EEG: impact of electrode density, head modeling and source localization. *Frontiers in neuroinformatics*. 12, 4.

- Logothetis, N.K., et al., 2001. Neurophysiological investigation of the basis of the fMRI signal. *Nature*. 412, 150-7.
- López, M.E., et al., 2014. Alpha-band hypersynchronization in progressive mild cognitive impairment: a magnetoencephalography study. *Journal of Neuroscience*. 34, 14551-14559.
- Lu, Q., et al., 2013. Predicting depression based on dynamic regional connectivity: a windowed Granger causality analysis of MEG recordings. *Brain research*. 1535, 52-60.
- Lustenberger, C., et al., 2015. Functional role of frontal alpha oscillations in creativity. *Cortex*. 67, 74-82.
- Mallio, C.A., et al., 2015. Epicentral disruption of structural connectivity in Alzheimer's disease. *CNS neuroscience & therapeutics*. 21, 837-845.
- Medaglia, J.D., et al., 2018. Functional alignment with anatomical networks is associated with cognitive flexibility. *Nature human behaviour*. 2, 156.
- Mehrkanoon, S., Breakspear, M., Boonstra, T.W., 2014. Low-dimensional dynamics of resting-state cortical activity. *Brain topography*. 27, 338-352.
- Melloni, L., et al., 2007. Synchronization of neural activity across cortical areas correlates with conscious perception. *Journal of neuroscience*. 27, 2858-2865.
- Mheich, A., et al., 2015. A new algorithm for spatiotemporal analysis of brain functional connectivity. *Journal of neuroscience methods*. 242, 77-81.
- Monti, M.M., Laureys, S., Owen, A.M., 2010a. The vegetative state. *Bmj*. 341, c3765.
- Monti, M.M., et al., 2010b. Willful modulation of brain activity in disorders of consciousness. *New England Journal of Medicine*. 362, 579-589.
- Mucha, P.J., et al., 2010. Community structure in time-dependent, multiscale, and multiplex networks. *science*. 328, 876-878.
- Mullen, T., et al., 2013. Real-time modeling and 3D visualization of source dynamics and connectivity using wearable EEG. In: 2013 35th annual international conference of the IEEE engineering in medicine and biology society (EMBC). Vol., ed.^eds. IEEE, pp. 2184-2187.
- Nissen, I.A., et al., 2017. Identifying the epileptogenic zone in interictal resting-state MEG source-space networks. *Epilepsia*. 58, 137-148.
- Nolte, G., et al., 2004. Identifying true brain interaction from EEG data using the imaginary part of coherency. *Clinical neurophysiology*. 115, 2292-2307.
- O'Neill, G.C., et al., 2018. Dynamics of large-scale electrophysiological networks: a technical review. *Neuroimage*. 180, 559-576.

- O'Neill, G.C., et al., 2017. Measurement of dynamic task related functional networks using MEG. *NeuroImage*. 146, 667-678.
- Oostenveld, R., Oostendorp, T.F., 2002. Validating the boundary element method for forward and inverse EEG computations in the presence of a hole in the skull. *Human brain mapping*. 17, 179-192.
- Owen, A.M., et al., 2006. Detecting awareness in the vegetative state. *science*. 313, 1402-1402.
- Owen, A.M., Schiff, N.D., Laureys, S., 2009. A new era of coma and consciousness science. *Progress in brain research*. 177, 399-411.
- Ozdemir, A., Bernat, E.M., Aviyente, S., 2017. Recursive tensor subspace tracking for dynamic brain network analysis. *IEEE Transactions on Signal and Information Processing over Networks*. 3, 669-682.
- Palva, J.M., et al., 2018. Ghost interactions in MEG/EEG source space: A note of caution on inter-areal coupling measures. *Neuroimage*. 173, 632-643.
- Palva, S., Palva, J.M., 2012. Discovering oscillatory interaction networks with M/EEG: challenges and breakthroughs. *Trends in cognitive sciences*. 16, 219-230.
- Pascual-Marqui, R.D., Michel, C.M., Lehmann, D., 1994. Low resolution electromagnetic tomography: a new method for localizing electrical activity in the brain. *International Journal of psychophysiology*. 18, 49-65.
- Pascual-Marqui, R.D., 2002. Standardized low-resolution brain electromagnetic tomography (sLORETA): technical details. *Methods Find Exp Clin Pharmacol*. 24, 5-12.
- Pascual-Marqui, R.D., et al., 2017. Innovations orthogonalization: a solution to the major pitfalls of EEG/MEG "leakage correction". *arXiv preprint arXiv:1708.05931*.
- Perani, D., et al., 1999. Word and picture matching: a PET study of semantic category effects. *Neuropsychologia*. 37, 293-306.
- Rizkallah, J., et al., 2018. Dynamic reshaping of functional brain networks during visual object recognition. *Journal of neural engineering*. 15, 056022.
- Rizkallah, J., et al., 2019a. Removing zero-lag functional connections can alter EEG source space networks at rest. *bioRxiv*. 617118.
- Rizkallah, J., et al., 2019b. Decreased integration of EEG source-space networks in disorders of consciousness. *NeuroImage: Clinical*. 101841.
- Roelfsema, P.R., et al., 1997. Visuomotor integration is associated with zero time-lag synchronization among cortical areas. *Nature*. 385, 157.
- Rogers, B.P., et al., 2007. Assessing functional connectivity in the human brain by fMRI. *Magnetic resonance imaging*. 25, 1347-1357.

- Rubinov, M., Sporns, O., 2010. Complex network measures of brain connectivity: uses and interpretations. *Neuroimage*. 52, 1059-1069.
- Sanders, R.D., et al., 2012. Unresponsiveness \neq unconsciousness. *Anesthesiology: The Journal of the American Society of Anesthesiologists*. 116, 946-959.
- Schiff, N.D., Fins, J.J., 2016. Brain death and disorders of consciousness. *Current biology*. 26, R572-R576.
- Schnakers, C., et al., 2009. Diagnostic accuracy of the vegetative and minimally conscious state: clinical consensus versus standardized neurobehavioral assessment. *BMC neurology*. 9, 35.
- Schoffelen, J.M., Gross, J., 2009. Source connectivity analysis with MEG and EEG. *Human brain mapping*. 30, 1857-1865.
- Scholz, J., et al., 2009. Training induces changes in white-matter architecture. *Nature neuroscience*. 12, 1370.
- Sitt, J.D., et al., 2014. Large scale screening of neural signatures of consciousness in patients in a vegetative or minimally conscious state. *Brain*. 137, 2258-2270.
- Song, J., et al., 2015. EEG source localization: sensor density and head surface coverage. *Journal of neuroscience methods*. 256, 9-21.
- Sporns, O., et al., 2004. Organization, development and function of complex brain networks. *Trends in cognitive sciences*. 8, 418-425.
- Sporns, O., 2011. *Networks of the Brain*, Vol., MIT press.
- Sporns, O., Betzel, R.F., 2016. Modular brain networks. *Annual review of psychology*. 67, 613-640.
- Stam, C.J., et al., 2006. Small-world networks and functional connectivity in Alzheimer's disease. *Cerebral cortex*. 17, 92-99.
- Stam, C.J., Nolte, G., Daffertshofer, A., 2007. Phase lag index: assessment of functional connectivity from multi channel EEG and MEG with diminished bias from common sources. *Human brain mapping*. 28, 1178-1193.
- Stam, C.J., Reijneveld, J.C., 2007. Graph theoretical analysis of complex networks in the brain. *Nonlinear biomedical physics*. 1, 3.
- Stam, C.J., 2014. Modern network science of neurological disorders. *Nature Reviews Neuroscience*. 15, 683.
- Stender, J., et al., 2014. Diagnostic precision of PET imaging and functional MRI in disorders of consciousness: a clinical validation study. *The Lancet*. 384, 514-522.
- Tadel, F., et al., 2011. *Brainstorm: a user-friendly application for MEG/EEG analysis*. *Computational intelligence and neuroscience*. 2011, 8.

- Tewarie, P., et al., 2019. Tracking dynamic brain networks using high temporal resolution MEG measures of functional connectivity. *NeuroImage*.
- Thibaut, A., et al., 2012. Metabolic activity in external and internal awareness networks in severely brain-damaged patients. *Journal of rehabilitation medicine*. 44, 487-94.
- Tijms, B.M., et al., 2013. Alzheimer's disease: connecting findings from graph theoretical studies of brain networks. *Neurobiology of aging*. 34, 2023-2036.
- Tononi, G., et al., 2016. Integrated information theory: from consciousness to its physical substrate. *Nature Reviews Neuroscience*. 17, 450.
- Tzourio-Mazoyer, N., et al., 2002. Automated anatomical labeling of activations in SPM using a macroscopic anatomical parcellation of the MNI MRI single-subject brain. *Neuroimage*. 15, 273-289.
- Van de Steen, F., et al., 2016. Critical comments on EEG sensor space dynamical connectivity analysis. *Brain topography*. 1-12.
- Van Den Heuvel, M.P., Sporns, O., 2011. Rich-club organization of the human connectome. *Journal of Neuroscience*. 31, 15775-15786.
- van den Heuvel, M.P., Sporns, O., 2013. Network hubs in the human brain. *Trends in cognitive sciences*. 17, 683-696.
- van den Heuvel, M.P., et al., 2017. Proportional thresholding in resting-state fMRI functional connectivity networks and consequences for patient-control connectome studies: Issues and recommendations. *Neuroimage*. 152, 437-449.
- Van Diessen, E., et al., 2015. Opportunities and methodological challenges in EEG and MEG resting state functional brain network research. *Clinical Neurophysiology*. 126, 1468-1481.
- Van Wijk, B.C., Stam, C.J., Daffertshofer, A., 2010. Comparing brain networks of different size and connectivity density using graph theory. *PloS one*. 5, e13701.
- Vidaurre, D., et al., 2018. Discovering dynamic brain networks from big data in rest and task. *Neuroimage*. 180, 646-656.
- Vink, J., et al., 2019. EEG functional connectivity predicts causal brain interactions. *Brain Stimulation: Basic, Translational, and Clinical Research in Neuromodulation*. 12, 449.
- Wang, P., et al., 2019. Long-range functional coupling predicts performance: Oscillatory EEG networks in multisensory processing. *Neuroimage*. 196, 114-125.
- Wang, S.H., et al., 2018. Hyperedge bundling: A practical solution to spurious interactions in MEG/EEG source connectivity analyses. *NeuroImage*. 173, 610-622.
- Wannez, S., et al., 2017. The repetition of behavioral assessments in diagnosis of disorders of consciousness. *Annals of neurology*.

- Watts, D.J., Strogatz, S.H., 1998. Collective dynamics of ‘small-world’ networks. *nature*. 393, 440-442.
- Yuan, H., et al., 2012. Spatiotemporal dynamics of the brain at rest—exploring EEG microstates as electrophysiological signatures of BOLD resting state networks. *Neuroimage*. 60, 2062-2072.
- Zhang, J., et al., 2011. Disrupted brain connectivity networks in drug-naive, first-episode major depressive disorder. *Biological psychiatry*. 70, 334-342.
- Zhang, Y., et al., 2006. A cortical potential imaging study from simultaneous extra-and intracranial electrical recordings by means of the finite element method. *NeuroImage*. 31, 1513-1524.